Dissertation

submitted to the

Combined Faculty of Natural Sciences and Mathematics

of the Ruperto Carola University Heidelberg, Germany

for the degree of

Doctor of Natural Sciences

Presented by

Hanke Gwendolyn Bauersachs

Born in: Berlin, Germany

Oral examination: 16.11.2021

Excitotoxicity and NMDA receptor-mediated acquired neuroprotection in human iPSC-derived brain organoids

Referees: **Prof. Dr. Hilmar Bading**

Prof. Dr. Christoph Schuster

Summary

Excitotoxic cell death, resulting from excess brain glutamate and mediated predominantly through NMDA receptors (NMDARs), is implicated in various acute and chronic pathological conditions of the human brain, such as stroke, traumatic brain injury and neurodegenerative diseases. In contrast, physiological NMDAR activation renders rodent neurons more resistant to potentially toxic stressors - a mechanism referred to as acquired neuroprotection. It is, however, not known whether such a dual action of NMDAR-signalling also exists human neurons.

This study employed human induced pluripotent stem cell-derived forebrain organoids to investigate NMDAR-mediated pro-death and pro-survival signalling in human neurons. Exposure of forebrain organoids to high concentrations of NMDA caused an excitotoxic cascade involving loss of plasma membrane potential, cessation of synaptic activity, shut-off of the transcription factor CREB, induction of death-promoting *P53* expression, structural disintegration and ultimately cell death. In contrast, treatment of brain organoids with low doses of NMDA triggered enhanced synaptic activity and survival-promoting signalling including the CREB phosphorylation and the expression of neuroprotective genes. This condition, if applied as a pre-treatment, protected organoids against excitotoxic insults within a defined time window. Surprisingly, the protective mechanism relied solely on the activation of NMDARs *per se* and occurred independently of the concomitant synaptic activation. Moreover, application of established as well as newly developed drugs to combat excitotoxicity protected human forebrain organoids against NMDA-induced cell death.

The findings presented here show that many aspects of the dual action of NMDAR-signalling, including NMDAR-mediated acquired neuroprotection, are preserved in human neurons. The forebrain organoid methodology established here may serve as a platform for the development and testing of drugs counteracting excitotoxic cell death arising, for example, from acute cerebrovascular ischaemia and neurodegenerative diseases in humans.

Zusammenfassung

Exzitotoxischer Zelltod, ausgelöst durch übermäßiges Hirnglutamat und hauptsächlich vermittelt durch NMDA-Rezeptoren (NMDARs), wird mit verschiedenen akut- sowie chronisch-pathologischen Zuständen des menschlichen Gehirns in Verbindung gebracht. Zu diesen zählen, unter anderem, Schlaganfälle, Schädel-Hirn-Traumata oder neurodegenerativen Erkrankungen. Im Gegensatz dazu bewirkt die physiologische Aktivierung von NMDARs in Nagetieren eine gewisse Resistenz gegenüber potenziell toxischen Stressoren. Dieser Mechanismus wird auch als „erworbene Neuroprotektion" bezeichnet. Ob die NMDAR-gesteuerte Signaltransduktion auch im Menschen eine ähnliche, duale Wirkung entfalten kann, ist allerdings nicht bekannt.

Diese Studie verwendete aus induzierten, pluripotenten humanen Stammzellen generierte Vorderhirnorganoide um die NMDAR-abhänge tödliche, beziehungsweise protektive Signalgebung in menschlichen Neuronen zu untersuchen. Die Stimulation von Organoiden mit hohen Konzentrationen an NMDA löste eine exzitotoxischen Kaskade aus, die den Verlust des Plasmamembranpotentials, eine Beendigung synaptischer Aktivität, eine Deaktivierung des Transkriptionsfaktors CREB, eine Induktion von todförderndem *P53*, einen strukturellen Zerfall und schließlich den Zelltod miteinschloss. Im Gegensatz dazu bewirkte eine Behandlung von Vorderhirnorganoiden mit niedrigen Mengen NMDA verstärkte synaptische Aktivität und induzierte über dies hinaus überlebensfördernde Signalwege, einschließlich der Phosphorylierung von CREB und der Expression neuroprotektiver Gene. Diese Bedingung, angewandt als Vorbehandlung, schützte Vorderhirnorganoide innerhalb eines definierten Zeitfensters vor exzitotoxischen Stimuli. Überraschenderweise beruhte dieser Schutzmechanismus ausschließlich auf der Aktivierung von NMDARs und manifestierte sich unabhängig von begleitend auftretender synaptischer Aktivität. Darüber hinaus schützte die Anwendung etablierter sowie neuentwickelter Pharmazeutika zur Bekämpfung von Exzitotoxizität die Organoide vor NMDA-induziertem Zelltod.

Die hier präsentierten Ergebnisse zeigen, dass viele Aspekte der dualen Wirkung der NMDAR-gesteuerten Signaltransduktion, einschließlich der NMDAR-vermittelten erworbenen Neuroprotektion, in menschlichen Neuronen konserviert sind. Die hier etablierte Vorderhirnorganoid-Methodik kann als Plattform für die Entwicklung und Erprobung von Medikamenten dienen, die darauf abzielen, exzitotoxischem Zelltod, wie beispielsweise nach akuter zerebrovaskulärer Ischämie und bei neurodegenerativen Erkrankungen entgegenzuwirken.

Abbreviations

2D	two dimensional
3D	three dimensional
aCSF	artificial cerebrospinal fluid
AD	Alzheimer´s disease
AID genes	activity-regulated inhibitor of death genes
AIF	apoptosis inducing factor
ALS	amyotrophic lateral sclerosis
AMPA	α-amino-3-hydroxy-5-methyl-4-isoxazolepropionic acid
APV	2-amino-5-phosphonovaleric acid
Ca^{2+}	Calcium ion
CaMKIV	Ca^{2+}/calmodulin-dependent protein kinase IV
Casp3	caspase 3
CBP	CREB binding protein
Cl^-	Chloride ion
CRE	cAMP response element
CREB	cAMP-responsive element binding protein
CTD	C-terminal domain
DCX	doublecortin
EAAT	excitatory amino acid transporter
ER	endoplasmic reticulum
ERK	extracellular signal-regulated kinase
ESC	embryonic stem cell
FACS	fluorescence activated cell sorting
$GABA_A$ receptor	γ-aminobutyric acid type A receptor
HD	Huntington´s disease
iGluR	ionotropic glutamate receptor
IN	inhibitory neuron
INHBA	inhibin-ß-A
IP_3R	inositol triphosphate receptors
iPSC	induced pluripotent stem cells

K^+	Potassium ion
KyMg	kynurenic acid/magnesium
LBD	ligand binding domain
LDH	lactate dehydrogenase
MEK	MAPK/ERK kinase
Mg^{2+}	Magnesium ion
mGLuR	metabotropic glutamate receptor
mPTP	mitochondrial permeability transition pore
Na^+	Sodium ion
NBQX	2,3-dioxo-6-nitro-7-sulfamoyl-benzo[f]quinoxaline
NKCC1	Na^+-K^+-Cl^- co-transporter 1
NMDA	N-Methyl-D-aspartate
NMDAR	NMDA receptor
PARP	poly (ADP-ribose) polymerase
PD	Parkinson´s disease
PI3K/AKT	phosphatidylinositol 3-kinase/ protein kinase B
PP1	protein phosphatase 1
PSC	postsynaptic currents
PSD95	postsynaptic density 95
PTEN	phosphatase and tensin homolog
RLU	relative light units
RT	room temperature
RyR	ryanodine receptors
scRNAseq	single cell RNA sequencing
SD	standard deviation
SEM	scanning electron microscopy
sEPSC	spontaneous excitatory postsynaptic current
sIPSC	spontaneous inhibitory postsynaptic current
snRNAseq	single nucleus RNA sequencing
sPSC	spontaneous postsynaptic current
TBP	TATA box binding protein

TEM	transmission electron microscopy
TrkB	tyrosine receptor kinase B
TRPM4	transient receptor potential cation channel subfamily M member 4
TTX	tetrodotoxin
UMI	unique molecular identifier

Table of contents

1. Introduction

1.1. Glutamate signalling

Glutamate is the most abundant excitatory neurotransmitter in the central nervous system and essential for every major brain function, as for example cognition, learning and memory (1). Upon arrival of an action potential in the axon terminal of a presynaptic neuron, glutamate is released into the synaptic cleft where it activates glutamate receptors on the postsynaptic neuron and thereby induces downstream signalling events. The nature of such events depends on the type of glutamate receptor: whereas metabotropic receptors (mGluRs) act via G-protein signalling cascades, activation of ionotropic receptors (iGluRs) results in ion influx and thereby evokes excitatory currents (2). The latter family of glutamate receptors can further be subdivided into α-amino-3-hydroxy-5-methyl-4-isoxazolepropionic acid (AMPA), kainate and N-Methyl-D-aspartate (3) receptors, named after the preferred chemical agonist for each subtype (4). While all iGluRs share several characteristics, such as their heterotetrameric assembly and a common ligand-gated ion channel function, they differ in their permeability for cations (4). AMPA and kainate receptors are predominantly permeable to sodium (Na^+) and potassium (K^+), thus leading to membrane depolarization when activated. In contrast, NMDA receptors (NMDARs), even though they are also permeable to Na^+ and K^+ to a certain degree, exert their main function via influx of calcium (Ca^{2+}) (5), which acts as an intracellular messenger and controls numerous cellular processes (6). Due to the enormous impact of glutamate signalling on cellular function, its activation needs to be tightly regulated. Thus, after its release into the synaptic cleft, glutamate is rapidly and actively removed to prevent continuous receptor activation. Glutamate clearance is mainly achieved via excitatory amino acid transporter (EAAT) uptake into neighbouring astrocytes, where it is metabolized to glutamine. Glutamine, in turn, is then released and taken up by neurons where it serves as a precursor for neurotransmitter synthesis (7).

Physiological glutamate neurotransmission is of fundamental importance for neuronal signalling and survival. The loss of functional glutamate receptors in rodents is associated with severe behaviour and health impairments including prenatal fatality, depending on which receptor subtype is affected (8-11). On the other hand, overactivation of glutamate receptors initiates a neurotoxic cascade – termed excitotoxicity -, eventually causing cell death (12). The main contributors to this dual, dichotomous role of glutamate signalling are NMDARs, whose hyper- and hypoactivation strongly affect neuronal health (13).

1.1.2. NMDA receptors (NMDARs)

NMDARs are heterotetrameric complexes composed of two obligatory GluN1 and two additional regulatory subunits, GluN2 and/or GluN3, that together assemble a central ion channel pore. There are four GluN2 (GluN2A-D) and two GluN3 subunit types (GluN3A-B) (14), whose expression is regulated in a temporal and spatial manner. Some subunits, for example GluN2B and GluN2D, exhibit high expression levels during development that decrease with ongoing neuronal maturation, whereas expression of other subunits, such as GluN2A and GluN2C, is initiated later in development (15, 16). In most brain regions, NMDARs predominantly contain GluN2A and GluN2B subunits, which are either organized as diheteromeric (GluN1/GluN2A or GluN1/GluN2B) or triheteromeric receptor complexes (GluN1/GluN2A/GluN2B) (17). Depending on their subunit composition, NMDARs have distinct functional properties, such as different channel kinetics or opening probabilities, thereby influencing neuronal activity (12). Additionally, NMDAR function is regulated by posttranslational modifications, protein-protein interactions (18, 19) and their subcellular localization. Aside from synapses, NMDARs are also present at perisynaptic and extrasynaptic sites. As for subunit composition, localization of NMDARs varies throughout development (20).

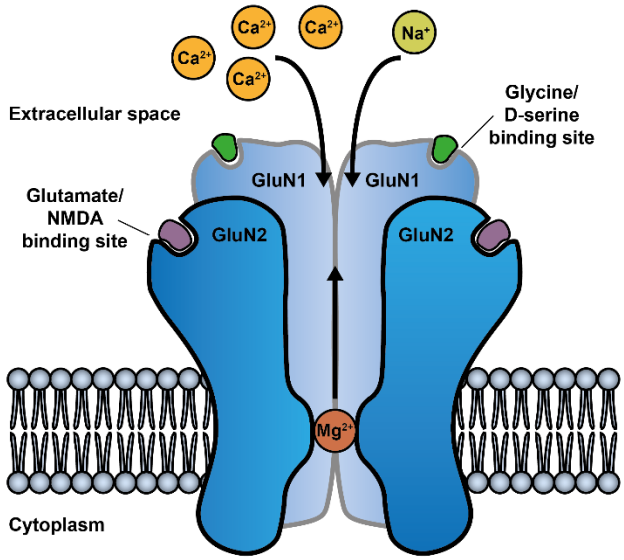

Figure 1: Schematic illustration of NMDAR subunit composition and function
NMDARs are heterotetramers composed of two GluN1 subunits with glycine / D-serine binding sites and two additional regulatory subunits, GluN2 and / or GluN3. In most brain regions, NMDARs are predominantly comprised of GluN1 / GluN2 subunits, the latter containing glutamate / NMDA binding sites. At resting membrane potential, the central ion channel is blocked by Mg^{2+}. Upon subtle depolarization, the Mg^{2+} block is relieved and thereby allows ions, mainly Ca^{2+} but also Na^{+}, to enter the cell.

Upon glutamate release into the synaptic cleft, the neurotransmitter binds to the ligand-binding domain (LBD) of GluN2. For maximal NMDAR activation, however, simultaneous binding of a co-agonist (glycine or D-serine) to the LBD of GluN1 subunits is required (21). Additionally, at resting membrane potential, the ion channel of NMDARs is blocked by magnesium (Mg^{2+}), whose extracellular concentrations are much higher than inside the cell,

thus resulting in a net inward driving force. Upon subtle depolarization, mediated for example by AMPA receptors, Mg^{2+} ions are repelled from the NMDAR pore, thus relieving the channel blockade and consequently allowing ion fluxes through the receptor (3, 14, 22).

In general, NMDARs are essential for proper brain development and function. During early development, glutamatergic synaptic transmission, synapse maturation and refinement of axonal and dendritic arbors are predominantly mediated by NMDARs (23-26). Consequently, knockout of GluN1 and GluN2B subunits in rodents results in neonatal death (27, 28). In adult animals, functional NMDARs are critical for the induction of activity-dependent synaptic modifications such as long-term potentiation and long-term depression (29-31). Thus, in mature rodents, depletion of NMDAR subunits or pharmacological blockade of the receptor is not lethal, but causes severe memory impairments and behavioural deficits (32-35).

1.2. Toxic glutamate signalling: Excitotoxicity

The observation that treatment with high concentrations of glutamate induces neuronal death in rodent dates back to studies in the retina in 1957 (36) and was further corroborated in the hypothalamus and hippocampus in 1969 (37). Based on the fact that overexcitation of neurons by high doses of glutamate results in neurotoxicity, the phenomenon was termed excitotoxicity.

1.2.1. Mechanisms of excitotoxicity

Since the discovery of excitotoxicity more than 60 years ago, countless studies investigated the underlying mechanisms that ultimately lead to neuronal cell death. Glutamate overactivation was found to induce a whole cascade of neurotoxic events, involving direct death signalling but also unspecific consequences due to cellular damage (38-41). The following section summarizes the main aspects of excitotoxicity induced neuronal cell death.

Excessive accumulation of extracellular glutamate leads to overactivation of all types of glutamate receptors, resulting in massive influx of Na^+ and Ca^{2+}. The resulting depolarization and the increase in intracellular Ca^{2+} levels activate voltage-gated- and Ca^{2+}-activated- Cl^- channels, respectively, thereby triggering Cl^- influx. Further, stimulation of glutamate receptors increases the activity of the Na^+-K^+-Cl^- co-transporter 1 (NKCC1) (42), thereby augmenting intracellular Cl^- concentrations. Together, the ion influx causes an osmotic imbalance that is accompanied by water influx, leading to cellular swelling and ultimately membrane rupture (43). In cell culture experiments, removal of Na^+ from the medium only slightly attenuates cell death, whereas elimination of Ca^{2+} markedly reduces neuronal loss (44). In line with these findings, pharmacological blockade of NMDARs, but not AMPA or kainate receptors, markedly ameliorates neuronal death induced by excitotoxicity in several

cell culture models (45-47). These results demonstrate the predominant role of NMDAR activation accompanied by Ca^{2+} influx in glutamate induced cell death. In neurons, similar to all eukaryotic cells, Ca^{2+} acts as a versatile intracellular messenger controlling a vast number of cellular functions and thus, needs to be tightly regulated. Under physiological conditions, glutamate release and subsequent receptor activation evokes an increase in intracellular Ca^{2+} levels that returns to basal levels within minutes (48).

Upon toxic glutamate exposure, however, massive amounts of Ca^{2+} enter the neurons, thereby altering a vast range of cellular functions and thus threatening neuronal viability. For example, Ca^{2+} is used as a co-factor by many enzymes such as lipases, proteases and endonucleases. Excessive accumulation of intracellular Ca^{2+}, however, results in unregulated activation of enzymes that consequently damage cellular components (49-51). Furthermore, Ca^{2+} overload

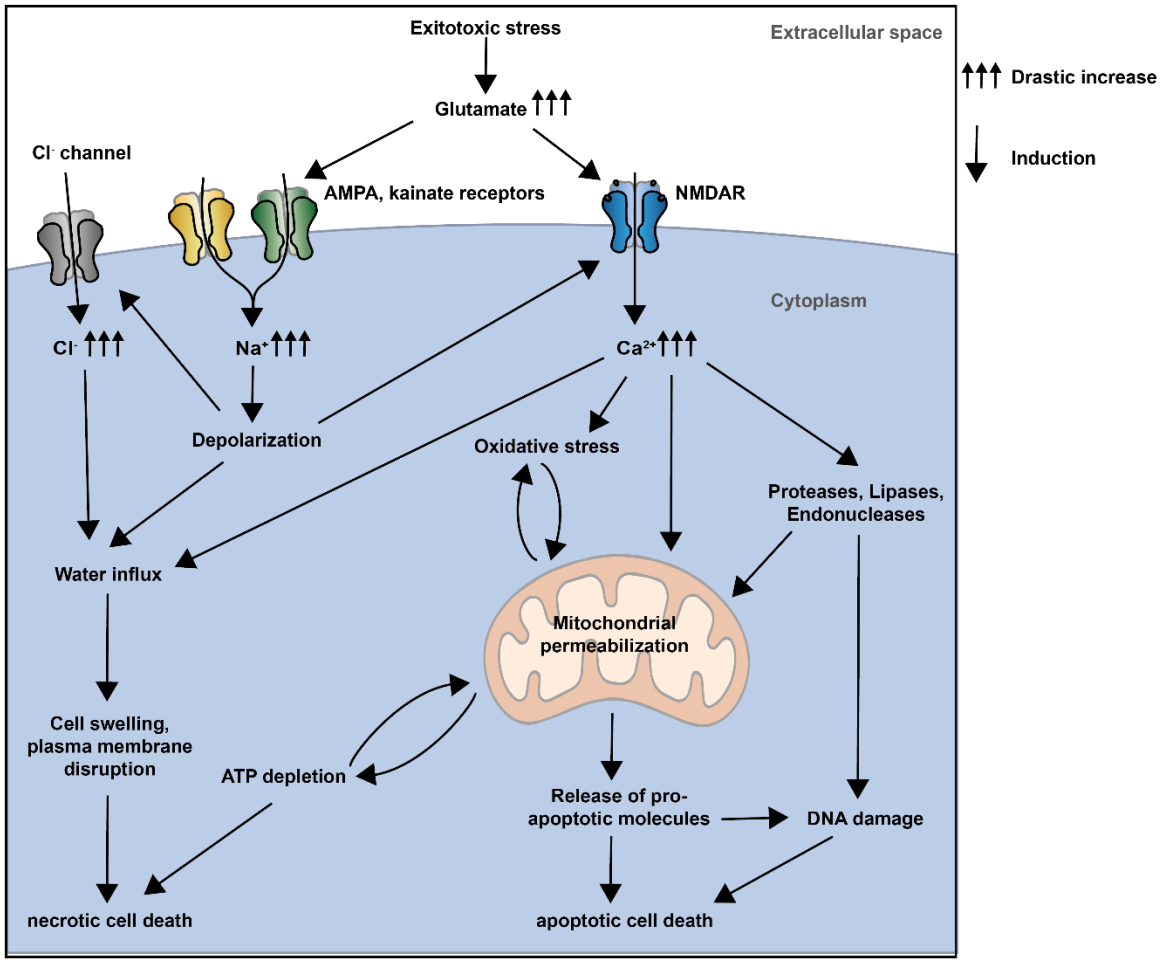

Figure 3: Schematic illustration of NMDAR-induced pro-death signalling
Excitotoxic stress triggers the accumulation of extracellular glutamate, thereby activating glutamate receptors, followed by massive influx of Na^+ and Ca^{2+} and subsequently also Cl^-. The resulting ionic imbalance is accompanied by water influx which leads to cellular swelling, plasma membrane disruption and ultimately necrotic cell death. Additionally, excess intracellular Ca^{2+} strongly impairs cellular health via several mechanisms: (1) mitochondrial permeabilization, either directly or via activation of Ca^{2+}-dependent enzymes, (2) induction of oxidative stress, which damages mitochondria and thereby further augments oxidative stress. Upon permeabilization, pro-apoptotic molecules are released from the mitochondria into the cytosol where they trigger apoptotic cell death via several mechanisms, including DNA damage. If the mitochondrial damage is too strong and energy supply is depleted, necrosis instead of ATP-dependent apoptosis takes place.

of mitochondria, that together with the endoplasmic reticulum (ER) control Ca^{2+} homeostasis by acting as intracellular stores, leads to the opening of permeability transition pores (mPTP) of the inner mitochondrial membrane (52). mPTP formation, in turn, results in the loss of the mitochondrial membrane potential. Consequently, mitochondria become incapable of ATP synthesis, which leads to energy depletion and oxidative stress. Additionally, opening of mPTPs allows water to enter and pro-apoptotic molecules, such as cytochrome c or apoptosis-inducing factor (AIF), to exit mitochondria, thereby leading to mitochondrial swelling and initiation of apoptotic cascades, respectively (53). Together, all these events caused by excessive glutamate exposure drastically impair neuronal function and ultimately result in cell death. Thereby, neurons can undergo regulated, apoptotic cell death, or, if the insult is too strong, die via necrosis (54).

1.2.2. Excitotoxicity in pathological conditions of the human brain

There is increasing evidence that NMDAR-mediated excitotoxicity is a central mechanism involved in a wide range of neurodegenerative pathologies. These include acute excitotoxic conditions such as ischemic stroke or traumatic brain injury as well as chronic conditions found in a variety of neurodegenerative diseases.

In ischemic stroke, blockade of blood vessels results in a loss of energy supply in the affected brain region, thereby leading to the breakdown of neuronal and glial membrane potential and subsequent massive release of glutamate (55). In rodent models of ischemia, glutamate accumulation is fortified by impairment or reversal of glial and neuronal glutamate uptake systems (56, 57). Further, in these models, injection of NMDA antagonists significantly reduced excitotoxic cell death (58, 59). Another example of a neurodegenerative condition involving acute excitotoxicity is traumatic brain injury, where high concentrations of extracellular glutamate were detected after mechanical damage (60, 61). Administration of the non-competitive NMDAR antagonist MK-801 immediately after induction of a brain injury decreased hippocampal cell loss and memory-related impairments in rats (62).

Although the origin and progression of neurodegenerative diseases such as amyotrophic lateral sclerosis (ALS), Alzheimer´s disease (AD), Huntington´s disease (HD) and Parkinson´s disease (PD) differ fundamentally, there is growing evidence that excitotoxicity is a shared cause for neuronal death (12, 63). In ALS and AD, glutamate levels in the cerebrospinal fluid are elevated for many patients (64, 65) and also in the blood plasma of PD patients, high glutamate concentrations can be observed (66). This increase of extracellular neurotransmitter can either be caused by enhanced glutamate release or by impaired uptake systems. Indeed, in rodent models of all the neurodegenerative disorders mentioned above, the function of the astroglial excitatory amino acid transporter 2 (EAAT2) is impaired (67-70).

Similar alterations could also be observed in post mortem brain samples of ALS, AD, and HD patients (71-73). Besides decreased operation of glutamate uptake mechanisms, neurodegenerative diseases were also shown to affect NMDAR function. For example, expression of mutant Huntingtin, the molecular trigger of HD, increased GluN2B-mediated currents in a rodent model (74). Additionally, GluN2B mRNA levels were found to be increased in brains of patients in early stages of HD (73). Further, amyloid beta oligomers that are related to AD pathogenesis, cause synaptic currents that can be blocked by NMDAR antagonists 2-amino-5-phosphonovaleric acid (APV), MK-801 and Memantine (75). While APV and MK-801 failed in clinical trials, Memantine is approved by the FDA to treat moderate-to-severe cases of AD (76).

1.3. Pro-survival glutamate signalling: Acquired neuroprotection

Based on the finding that excessive NMDAR activation is a common inducer of neuronal death in many neurodegenerative conditions, numerous therapeutics were developed that act on different parts of the receptor. Despite promising results in rodent, the vast majority of drugs failed in clinical trials in humans due to a lack of efficacy and/or the emergence of severe adverse effects (77, 78). The reasons for these translational failures are manifold and caused by, amongst others, the choice of the animal model, success criteria and limited therapeutic time windows (79). Additionally, physiological NMDAR signalling is not only non-toxic but even essential for neuronal survival, and triggers a mechanism referred to as acquired neuroprotection (80). In rodents, knockout of GluN1 and GluN2B causes neonatal death and blockade of NMDAR activity in developing neurons results in widespread apoptosis (27, 28, 81). In adult animals, elimination of NMDAR signalling does not directly kill neurons, but renders them more sensitive to subsequent insults. For example, treatment with NMDAR antagonists enhances neurodegeneration caused by mitochondrial toxins or mechanical damage in rats (82). Conversely, increasing synaptic activity and thereby NMDAR signalling promotes neuronal survival even under harmful conditions such as chemically induced apoptosis, growth factor withdrawal, excitotoxicity or hypoxia (83, 84). Thus, pharmacological interference with NMDAR function impairs not only toxic but also protective signalling and might therefore contribute to poor clinical outcomes. At the same time, augmenting the endogenous protective mechanism may offer new approaches to develop treatments against neurodegenerative conditions.

1.3.1. Mechanisms of acquired neuroprotection

Synaptic activity and concomitant glutamate release lead to NMDAR activation followed by Ca^{2+} and Na^{+} influx. Additionally, membrane depolarization by cation influx through other glutamate receptors triggers the activation of voltage-gated Ca^{2+} channels, thereby increasing intracellular Ca^{2+} concentrations (85). The Ca^{2+} levels are further amplified by Ca^{2+}-induced Ca^{2+} release from the endoplasmic reticulum via ryanodine receptors (RyR) and inositol triphosphate receptors (IP_3R) (86). As a versatile second messenger, Ca^{2+} can activate a multitude of enzymes and proteins, thereby regulating numerous cellular processes, including acquired neuroprotection. Ca^{2+} mediates the activation of the Ca^{2+}/calmodulin-dependent protein kinase IV (CaMKIV), which in turn phosphorylates cAMP-responsive element binding protein (CREB), thereby activating it (87). Additionally, CREB can get phosphorylated by the extracellular signal-regulated kinase 1/2 (ERK1/2), which also becomes activated by Ca^{2+} via Ras and MAPK/ERK kinase (MEK) (88). Upon activation, CREB is able to bind to cAMP response elements (CRE) of target gene promoters (87). To initiate gene transcription, CREB further recruits the transcriptional co-activator CREB binding protein (CBP), which is also

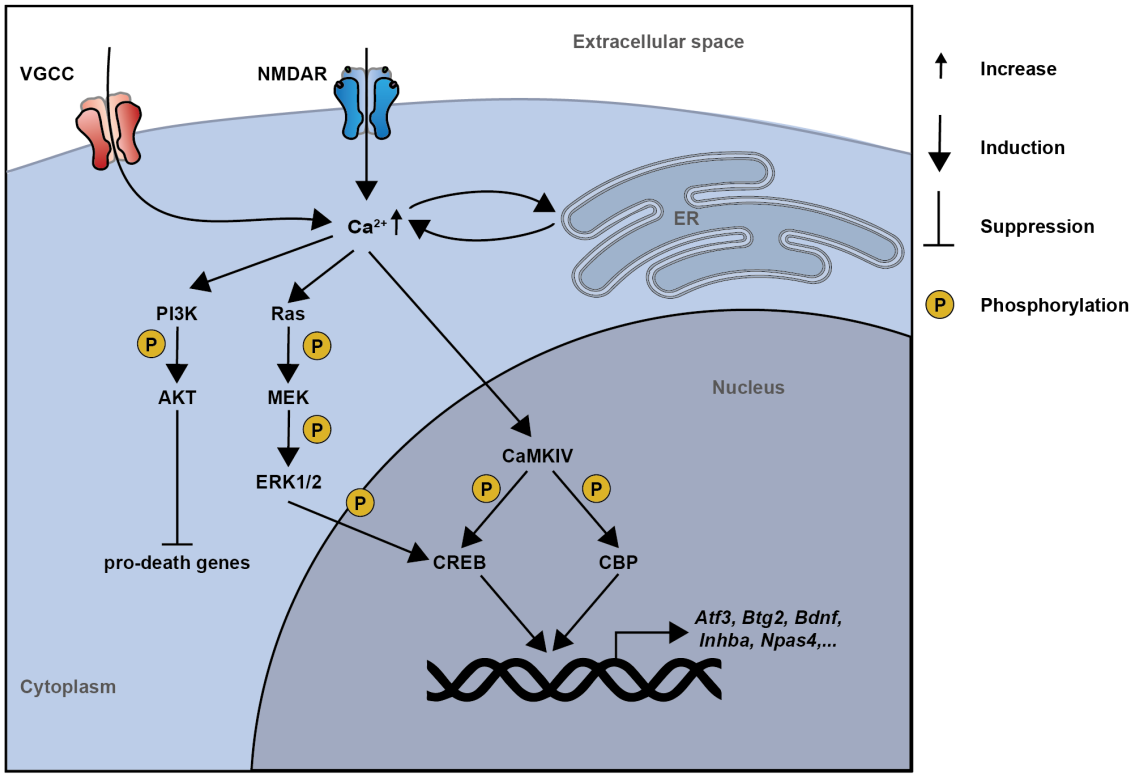

Figure 3: Schematic illustration of NMDAR-induced pro-survival signalling
NMDA receptor (NMDAR) activation elevates intracellular Ca^{2+} levels which are further increased via opening of voltage-gated Ca^{2+} channels (VGCCs). Additionally, Ca^{2+} concentrations are amplified by Ca^{2+}-induced Ca^{2+} release from the endoplasmic reticulum (ER). Intracellular Ca^{2+} induces cAMP-responsive element binding protein (CREB) signalling via Ca^{2+} / calmodulin-dependent protein kinase IV (CamKIV) or via the Ras-MEK-ERK1/2 pathway. Furthermore, CaMKIV activates CBP, which acts as a transcriptional co-activator and together with CREB initiates the transcription of various genes, including the neuroprotective genes *Atf3*, *Btg2*, *Bdnf*, *Inhba* and *Npas4*. Moreover, Ca^{2+} activates the PI3K-AKT pathway which suppresses the expression on pro-death genes.

activated through CaMKIV-mediated phosphorylation (89, 90). Besides it´s critical role in neuronal development and plasticity (91), CREB mediated transcription was shown to induce a set of genes that positively affects neuronal health (83). These so-called activity-regulated inhibitor of death (AID) genes include, amongst others, *Atf3*, *Btg2*, *Inhibin-ß-A* (*Inhba*) and *Npas4*. In addition, CREB also regulates the expression of *BDNF*, another gene promoting cellular survival via various mechanisms, such as increasing the expression of anti-apoptotic proteins and inhibiting cellular Ca^{2+} overload (92, 93).

Besides the induction of CREB-dependent transcriptional changes that mediate neuroprotection, NMDAR evoked Ca^{2+} influx further activates additional mechanisms that promote neuronal survival. For example, elevated Ca^{2+} levels lead to the activation of the phosphatidylinositol 3-kinase/ protein kinase B (PI3K/AKT) pathway, which in turn triggers nuclear export of the transcription factor FOXO3, thereby supressing the expression of pro-death genes (94, 95). Additionally, NMDAR activation was further shown to enhance intrinsic antioxidant defences by increasing thioredoxin activity and thereby reducing neuronal vulnerability towards oxidative stress (96).

1.4. Dual action of NMDARs: Subtype versus location hypothesis

Physiological NMDAR signalling is necessary for proper neuronal function, while excessive NMDAR activation results in neuronal death (see section 1.2 and 1.3). Several elements of the underlying mechanisms have been identified, however, it is still unknown, how stimuli with different intensities can lead to these drastically opposing outcomes. Various hypotheses have been formulated with the most established ones being the “subtype hypothesis” and the “location hypothesis” (13).

The subtype hypothesis suggests that the subunit composition determines the outcome of NMDAR stimulation (13). Accordingly, activation of GluN2B-containing NMDARs results in toxicity, while GluN2A-containing NMDARs mediate neuronal survival. Indeed, pharmacological blockade of GluN2B-containing NMDARs reduces excitotoxic cell death *in vitro* and *in vivo* (97, 98). Further, genetic deletion of GluN2B markedly attenuates cell death in response to a toxic NMDA treatment (97). In contrast, antagonizing GluN2A-containing NMDARs enhanced neuronal cell death in primary neuron cultures treated with NMDA and a rodent model of transient global ischemia (97, 98). These opposing effects on neuronal health may be caused by different downstream signalling complexes coupled to the large C-terminal domain (CTD) of the individual NMDAR subunits. Genetically replacing the CTD of GluN2B with that of GluN2A decreased neuronal vulnerability towards excitotoxic stress *in vitro* and *in vivo*. Vice versa, GluN2A subunits containing the GluN2B-CTD enhanced NMDA toxicity

(99). Besides GluN2A and GluN2B, also other NMDAR subunits were reported to influence neuronal health. For example, GluN2C and GluN3A were shown to have neuroprotective properties, whereas GluN2D mediates neurotoxicity (100-102). Compared to diheteromeric NMDARs, little is known about the impact of triheteromeric NMDARs due to the lack of pharmacological tools that specifically target such subunit compositions. However, depending on the brain region, GluN1/GluN2A/GluN2B triheteromeric receptors account for 15-50% of the total NMDAR population (103, 104).

In contrast, the location hypothesis assumes that the subcellular position of NMDARs is decisive for their functional outcome (13). More precisely, NMDARs located at the synapse are thought to mediate survival signalling pathways, whereas activation of receptors at extrasynaptic locations triggers a neurotoxic signalling cascade. In line with this hypothesis, stimulation of synaptic NMDARs was shown to activate the Ras-ERK pathway, thereby leading to CREB phosphorylation and subsequent induction of pro-survival genes (105, 106). In contrast, activation of extrasynaptic NMDARs triggers a CREB shut-off pathway and thus impede expression of neuroprotective genes (105). Similar to the subtype hypothesis, these differential effects could be mediated by the interaction between NMDARs and other proteins preferentially located at synaptic or extrasynaptic sites. Recently, NMDARs were shown to form a complex with the transient receptor potential cation channel subfamily M member 4 (TRPM4), which is absent from synapses. Disrupting the interaction between NMDAR and TRPM4 prevented transcriptional shut-off, mitochondrial dysfunction and neuronal cell death in response to an excitotoxic treatment i*n vitro* and *in vivo* (107). Paradoxically, NMDARs also form complexes with postsynaptic density 95 (PSD95), a synaptically located protein, and dissociating their interaction was demonstrated to be neuroprotective (108).

1.5. NMDAR signalling in human neurons

The vast majority of our knowledge about the dual action of NMDAR signalling is derived from experiments in rodent. For a long time, studies on human neurons were limited to post mortem observations. Using human brain tissue samples, it was demonstrated that the spatial and temporal NMDAR subunit expression is highly similar to that in rodents (109-112). Comparison of the amino acid sequences between rat and human NMDARs revealed an identity of 87.1 – 99.3 %, dependent on the subunit (113). Furthermore, when various NMDAR subtypes from rat and human were expressed in *Xenopus* oocytes, no differences in the pharmacological or functional properties of the receptors could be detected (113). Albeit all these similarities, knowledge about the underlying signalling pathways in human neurons was long lacking. This changed, however, with the development of new technologies such as the

generation of induced pluripotent stem cells (iPSCs) and subsequent neuronal differentiation in 2D and 3D culture, which now allow investigating neuronal function and molecular mechanisms in human neurons. Since then, many differentiation protocols were developed to generate human neurons that respond to NMDA application with inward currents or Ca^{2+} fluxes (114-120). However, in most studies high doses of NMDA are used (50 μM – 100 μM) to evoke a response, reflecting concentrations that would result in excitotoxic cell death in rodent neurons (121, 122). The requirement of these high doses might be caused by the immature NMDAR expression in young neurons (123). Although the presence of functional NMDARs in iPSC-derived neurons has been confirmed, it is not known if their activation induces similar signalling events as in rodent and if NMDAR-mediated neuroprotection exists in human neurons.

While NMDAR-induced excitotoxic cell death is well established in rodents, only few studies have investigated this phenomenon in human neurons (124, 125). They show that application of glutamate and/or NMDA leads to cell death in a dose-dependent manner in embryonic stem cell- (ESC) or iPSC-derived neuronal monolayer cultures. The presence of the NMDAR antagonist MK-801 reduced or even abolished glutamate-induced cell death, thus highlighting the role of NMDARs in human excitotoxicity. In iPSC-derived cortical neurons, excitotoxicity was further dependent on poly (ADP-ribose) polymerase (PARP) and resulted in parthanatos, a specific form of cell death distinct from apoptosis and necrosis (125). It is, however, not known if also other mechanisms are involved in excitotoxic cell death in human neurons, such as induction of pro-death genes and suppression of potential pro-survival signalling.

1.5.1. Human iPSC-derived brain organoids as a model system to investigate NMDAR signalling

In recent years, a multitude of protocols have been established that allow for the generation of iPSC-derived neurons either by inhibiting meso- and endodermal fate adoption or by overexpression of specific transcription factors, such as Neurogenin-2 (126, 127). Besides conventional monolayer cultures, iPSCs can also be differentiated into brain organoids, which are 3D neuronal structures that mimic one specific or several regions of the human brain (128-131). Within the organoids, cells can differentiate in a 3D environment, which, compared to planar cultures, allows for enhanced interaction with other cells and extracellular matrix components as well as spontaneous self-organization, thus better resembling the *in vivo* situation of the human brain. Indeed, transcriptome analyses comparing human fetal brain with organoids or monolayer cultures revealed a stronger correlation with the 3D approach (132). Furthermore, organoids contain various cell types, such as different neuron types in diverse developmental stages as well as glial cells, the latter being essential for neuronal

differentiation and synapse maturation (133). Another advantage of brain organoids is that they allow for long-term cultivation over several months, thus allowing the study of late-stage developmental features, such as certain electrophysiological and synaptic properties (134). Based on the aforementioned characteristics, brain organoids appear to be a well-suited model system to investigate NMDAR signalling in human neurons in a relatively physiological environment. Furthermore, prolonged culture times might enable enhanced expression of GluN2A-containing NMDARs, which emerge at later developmental stages and play an important role in NMDAR-mediated pro-survival signalling (97, 98, 135). Indeed, in long-term cultures of human cortical organoids, a switch in NMDAR subunit composition from GluN2B to GluN2A similar to the *in vivo* data could be observed between day 250 and 300 (136).

1.6. Aims

The aim of this thesis was to investigate the dual action of NMDAR signalling in human neurons using an iPSC-derived brain organoid system.
In order to establish a suitable model, we decided to pattern organoids towards forebrain identity, a complex brain region that gives rise to structures like the cerebral cortex, hypothalamus and hippocampus. That approach of guided differentiation is generating a more homogeneous and thus more reproducible organoid model compared to unguided protocols, which give rise to organoids featuring multiple regional identities (137). After establishing and characterizing the organoid model in terms of cell type composition, NMDAR expression and synaptic connectivity, the specific aims for this thesis were the following:

- Exploring conditions of NMDAR activation that induce either pro-death or pro-survival signalling
- Comparing these conditions in respect of electrophysiological and transcriptional responses
- Determining if NMDAR-mediated pro-survival signalling is sufficient to prevent excitotoxic cell death in the organoid model
- Investigating the potential of forebrain organoids to serve as a tool for drug testing against excitotoxic cell death in human neurons

Previous work and contribution by co-workers

The methodology for the generation of forebrain organoids has been largely established during my Master's Thesis. All data shown in this dissertation has been produced during the course of my PhD.

The majority of the data presented in this thesis are included in a manuscript that is currently in submission. This involves data presented in **Figure 4**, **5**, **6A**, **7A**, **7B**, **8**, **9**, **10**, **11**, **12**, **13**, **14**, **15**, **16**, **17**, **18A**, **18B** and **19**. Figure legends for these figures or individual panels were obtained and modified from Bauersachs et al. (currently in submission) and had been originally written by myself. Individual figures not created by myself were obtained as they are displayed in Bauersachs et al. (currently in submission). These include **Figure 6A**, **8**, **9D** and **9E** which were originally designed as stated below.

Single nucleus RNA sequencing (snRNAseq) was performed by the Kaessmann group (Heidelberg, Germany). Bastienne Zaremba performed the processing, analysis and visualization of the snRNAseq data (**Figure 6** and **8**). Ursula Weiss conducted the immunoblots (**Figure 9**, **10** and **17**). C. Peter Bengtson and Celia García-Vilela executed the electrophysiological recordings (**Figure 9**, **15** and **16**). C. Peter Bengtson performed the data analysis and generated the graphs shown in **Figure 9**, **15** and **16**. Andrea Hellwig performed the sample preparation and image acquisition for scanning and transmission electron microscopy (**Figure 9**, **12** and **13**).

Descriptions of methods that have not been performed by myself during the course of this project, namely the single nucleus RNA sequencing, the electrophysiology and the electron microscopy, were obtained from Bauersachs et al. (currently in submission), and had been originally written by Bastienne Zaremba, C. Peter Bengtson or Andrea Hellwig.

2. Results

2.1. Forebrain organoid generation and characterization

In order to investigate the dual action of NMDAR-signalling in human neurons, we sought to develop a protocol for the robust and reproducible generation of brain organoids from iPSCs. Therefore, a previously published protocol (129) was modified in several aspects. Briefly, aggregation of a defined number of hiPSCs was followed by dual SMAD inhibition (126) to promote neural fate adoption. After neural induction, organoids were cultured in proliferation-, differentiation- and maturation-media for up to six months. In order to reduce variability in cellular composition, forebrain patterning was performed for the first three weeks in culture using inhibitors of Wnt- and Shh-signalling (IWP-2 and Cyclopamine, respectively) that allow for robust induction of forebrain identity (138-141) (**Figure 4A**).

During development, organoids generated from two different hiPSC lines (D1 and HD6) grew similarly from a diameter of 500 µm to approximately 1500 µm over the course of 24 weeks (**Figure 4B**). While the pluripotency marker gene *OCT4* was rapidly downregulated in developing organoids, the neural stem cell marker *SOX1* was drastically increased, indicating neural fate adoption. Dorsal forebrain identity was confirmed by *FOXG1* and *PAX6* expression. A strong increase in *MYT1L* levels indicated the presence of post-mitotic neurons already after 6 weeks in culture, whereas gliogenesis, judged by *GFAP* expression, followed a more moderate but rather constant increase during development (**Figure 4C**). Next, for a more detailed insight into the cell type composition, we performed immunohistochemistry on cryosections of 5 months old D1 organoids. In line with the RT-qPCR results, organoids contained a dense neuronal network (TUJ1 and MAP2 expressing cells) with forebrain identity, as shown by PAX6 and FOXG1 expression (**Figure 5A** and **B**). By staining for VGLUT2 and GAD67, we could detect the presence of both, glutamatergic and GABAergic neurons, respectively (**Figure 5C**). As shown by GFAP and SOX2 / NESTIN expression, organoids also contain glial and neural stem cells (**Figure 5D** and **E**).

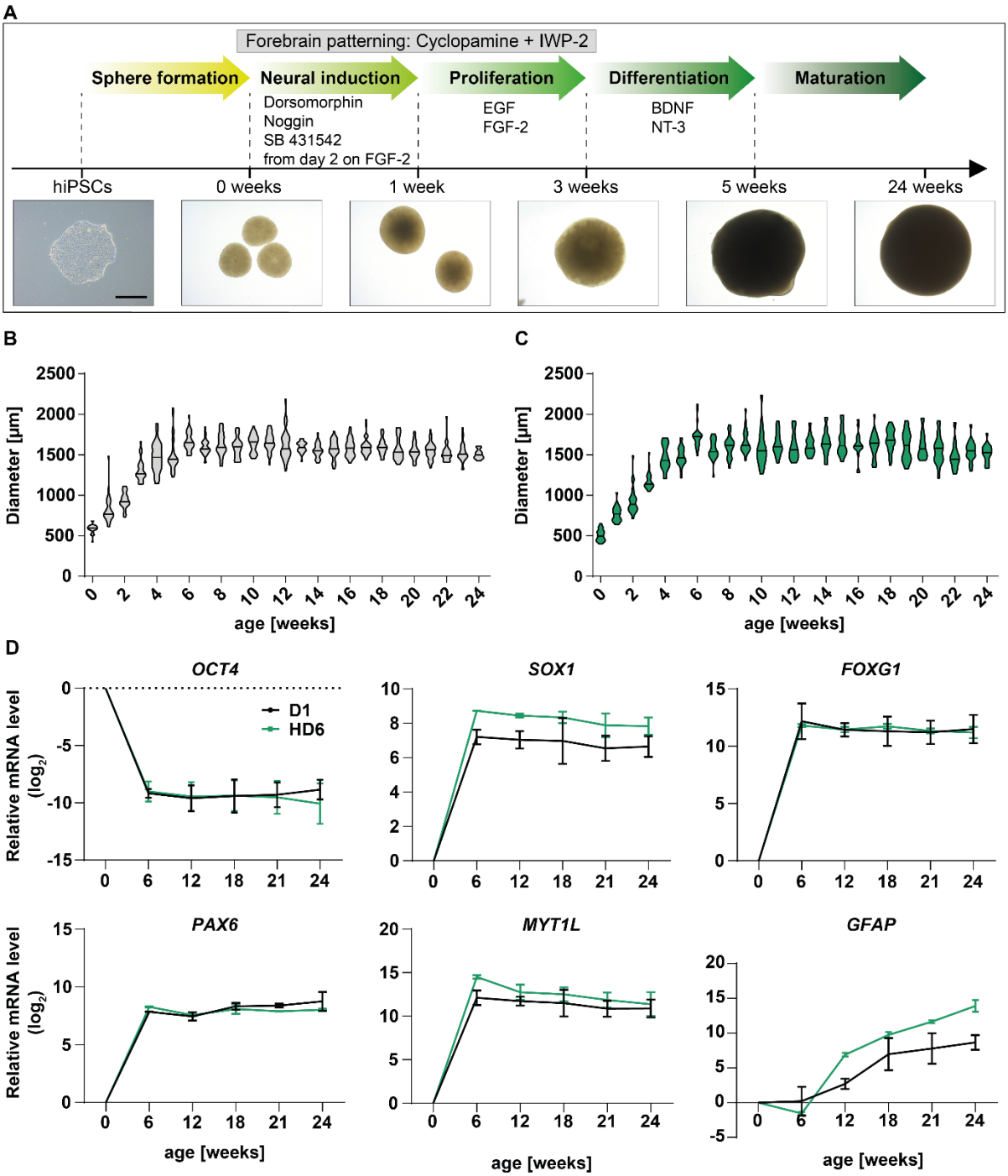

Figure 4: Characterization of forebrain organoid development
(**A**) Schematic illustration of forebrain organoid generation. Scale bar = 50 µm. (**B**, **C**) Size of forebrain organoids derived from two different iPSC lines during development. For each batch and time point, images of 2-8 organoids were acquired and Feret´s diameter was determined. Data is represented as violin plot. (**B**) D1: n = 4 batches. (**C**) HD6: n = 3 batches. (**D**) RT-qPCR analysis of relative mRNA expression levels of *OCT4* (pluripotent cells), *SOX1* (neural stem cells), *FOXG1* (dorsal forebrain), *PAX6* (rostral forebrain), *MYT1L* (post-mitotic neurons) and *GFAP* (glial cells) during development. D1: n = 3 batches, HD6: n = 2 batches. Data is represented as mean ± SD.

(Figure legends for **Figure 4** were obtained and modified from Bauersachs et al. (in submission) and had been originally written by myself.)

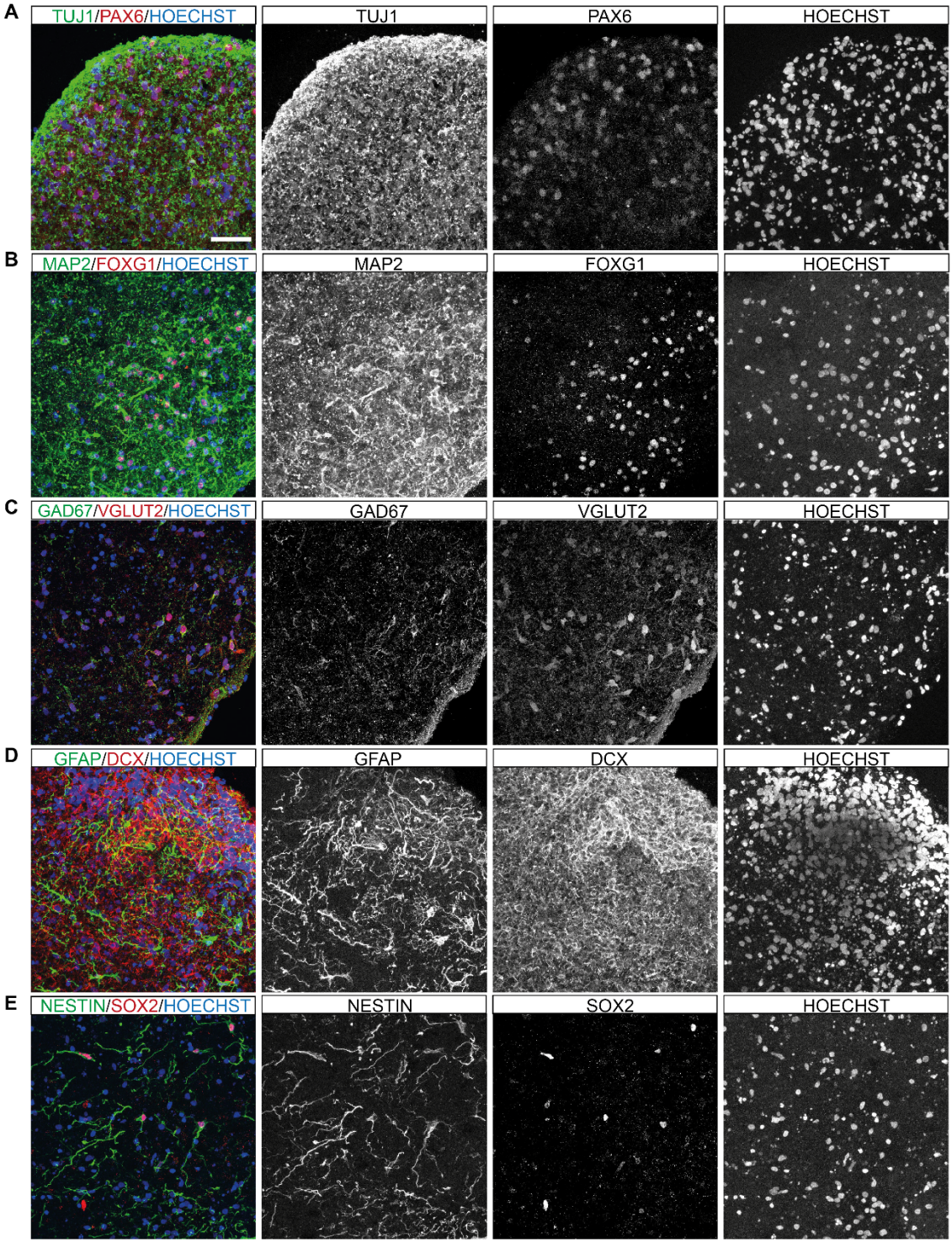

Figure 5: Cell type composition of 5 months old forebrain organoids
Representative immunofluorescence images of (**A**) TUJ1 (pre- and post-mitotic neurons), PAX6 (rostral forebrain), (**B**) MAP2 (post-mitotic neurons), FOXG1 (dorsal forebrain), (**C**) GAD67 (inhibitory neurons), VGLUT2 (excitatory neurons), (**D**) GFAP (glial cells), DCX (young neurons), (**E**) NESTIN and SOX2 (neural stem cells) in 5 months old D1 organoids. Scale bar = 50 µm.

(Figure legends for **Figure 5** were obtained and modified from Bauersachs et al. (in submission) and had been originally written by myself.)

For comprehensive analysis of cell type composition and regional identity, we performed single nucleus RNA sequencing (snRNAseq) from D1 organoids at an age of 21 weeks. Using dimensional reduction of the relative gene expression counts, three distinct cell populations were identified (**Figure 6A**). Based on marker gene expression analysis (**Figure 6B**), these clusters represent two inhibitory neuron populations (IN_1 and IN_2) and one glial cell population (Glia). Surprisingly, and in contrast to our results from immunohistochemistry (**Figure 5C**) and electrophysiology (**Figure 9**) barely any glutamatergic neurons, defined through expression of *SLC17A6* (VGLUT2) and *SLC17A7* (VGLUT1), were detected in our dataset.

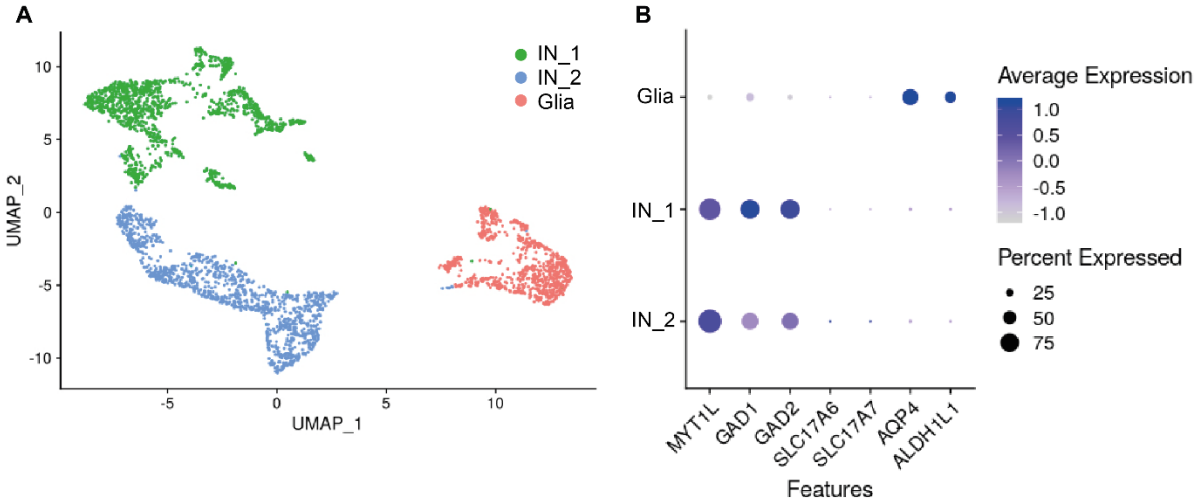

Figure 6: Cell type composition analysis of 21 week old organoids with snRNA-seq
(**A**) UMAP visualization of snRNAseq data from 21 week old D1 organoids. The distinct populations represent glia cells (Glia) and inhibitory neuron cluster 1 (IN_1) and 2 (IN_2). (**B**) Dot plot vizualization of relative expression of a subset of marker genes (MYT1L: postmitotic neurons; GAD1 and GAD2: inhibitory neurons; SLC17A7 and SLC17A6: exitatory neurons; AQP4 and ALDH1L1: glial cells) across clusters. Analysis performed by B. Zaremba.

(**Figure 6A** is presented in a similar way as in Bauersachs et al. (in submission). Figure legends for **Figure 6** were obtained and modified from Bauersachs et al. (in submission) and had been originally written by myself.)

To obtain an estimation of the real fraction of glutamatergic neurons, we quantified VGLUT2 positive cells within organoids via immunohistochemistry. This analysis revealed that glutamatergic neurons account on average for 33.72 % of all cells (**Figure 7A**). To exclude the possibility that the VGLUT2 antibody (Synaptic Systems) used for immunohistochemistry (**Figure 5C**) and subsequent quantification (**Figure 7A**) caused false positive labelling of cells, we further also tested an additional, different VGLUT2 (Sigma Aldrich) antibody. Similar to what was observed before, we detected a large fraction of VGLUT2 positive cells (**Figure 7B**). These results indicate that forebrain organoids indeed contain a substantial fraction of glutamatergic neurons that is drastically underrepresented in the snRNAseq dataset. It has been previously reported that different RNA sequencing methods may introduce cell type

composition biases, depending on the protocol used to dissociate single cells or nuclei (142). In order test if another sequencing method may prevent the loss of glutamatergic neurons, we performed single cell RNA sequencing (scRNAseq). Preliminary analysis of sequencing data from a fraction of cells, however, revealed similar results as those obtained by with snRNAseq, including the absence of glutamatergic neurons (data not shown). To verify the loss of certain cell populations, we dissociated forebrain organoids by the same protocol as used for scRNAseq and compared mRNA levels of cell type specific marker genes between dissociated and intact control organoids. Additionally, even though the dissociation kit used was optimized for neuronal tissue, we included a condition containing kynurenic acid and magnesium (KyMg), two components that are regularly added to dissociation medium for primary brain tissue to prevent neuronal cell death (143, 144).

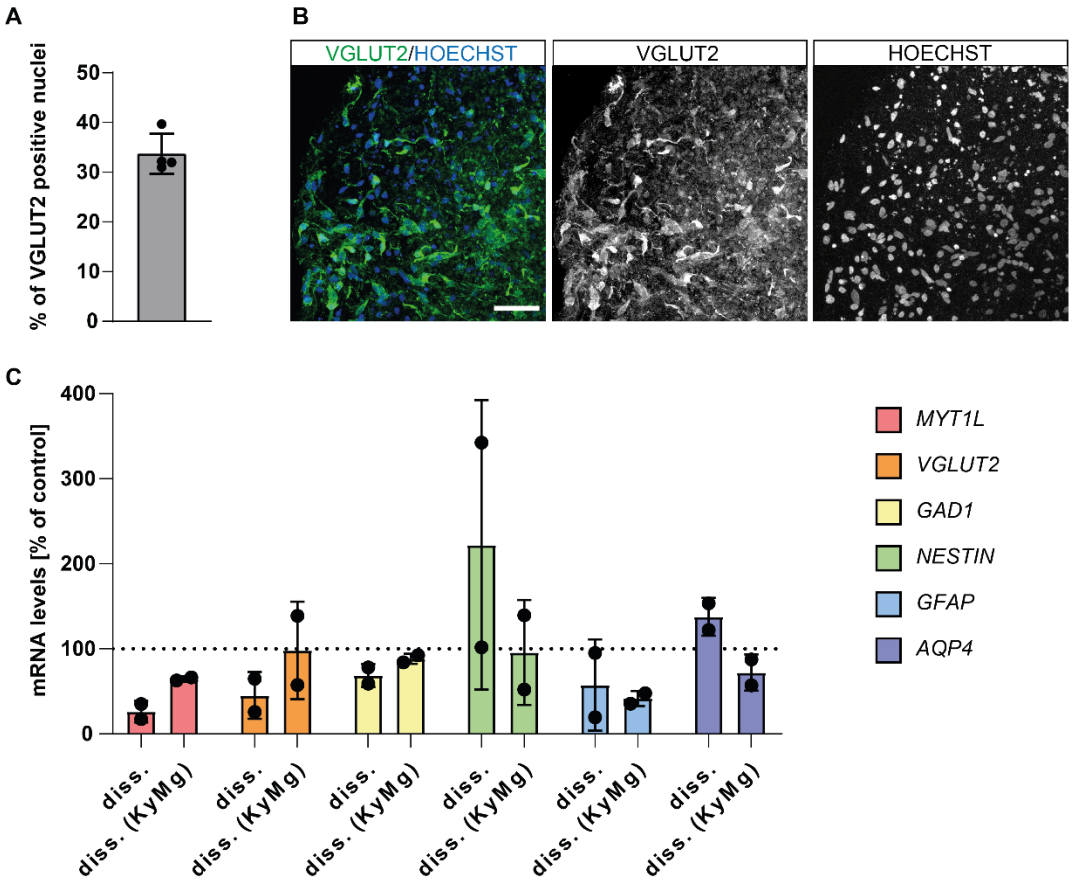

Figure 7: Validation of glutamatergic neuron loss during organoid dissociation
(**A**) Quantification of VGLUT2 positive cells in 21 week old D1 organoids. The average from 7 - 10 images per organoid is shown. n = 4 organoids from 3 batches. (**B**) Representative immunofluorescence image of VGLUT2 expression in 21 week old D1 organoids with an additional, different antibody. Scale bar = 50 µM. (**C**) RT-qPCR analysis of relative mRNA expression levels of *MYT1L* (post-mitotic neurons), *VGLUT2* (glutamatergic neurons), *GAD1* (GABAergic neurons), *NESTIN* (neural stem cells), *GFAP* and *AQP4* (glial cells) in D1 organoids dissociated in absence or presence of KyMg. mRNA level are shown as percentage of those in control organoids (dashed line). n = 2 batches. Data is represented as mean ± SD.

(Figure legends for **Figure 7** were obtained and modified from Bauersachs et al. (in submission) and had been originally written by myself.)

RT-qPCR analysis revealed a reduction in relative mRNA levels of *MYT1L*, *VGLUT2* and to a lesser extent also *GAD1* in dissociated organoids (**Figure 7C**), suggesting that neurons, specifically glutamatergic neurons, indeed may be lost during the dissociation process. Interestingly, the reduction of mRNA levels can be mitigated in by the presence of KyMg in the dissociation media (**Figure 7C**).

Taken together, there is strong evidence that the snRNAseq data do not represent the complete cellular diversity within the organoids and that further protocol optimization is required to enable a comprehensive analysis of cell type composition. Nevertheless, the snRNAseq data set allows for an unbiased analysis of the regional identity of the organoids. Transcriptome-wide 1-to-1 ortholog gene expression comparison of forebrain organoids and the developing mouse brain revealed the highest correlation with neurons of the forebrain (**Figure 8** and **Table 1**) (145).

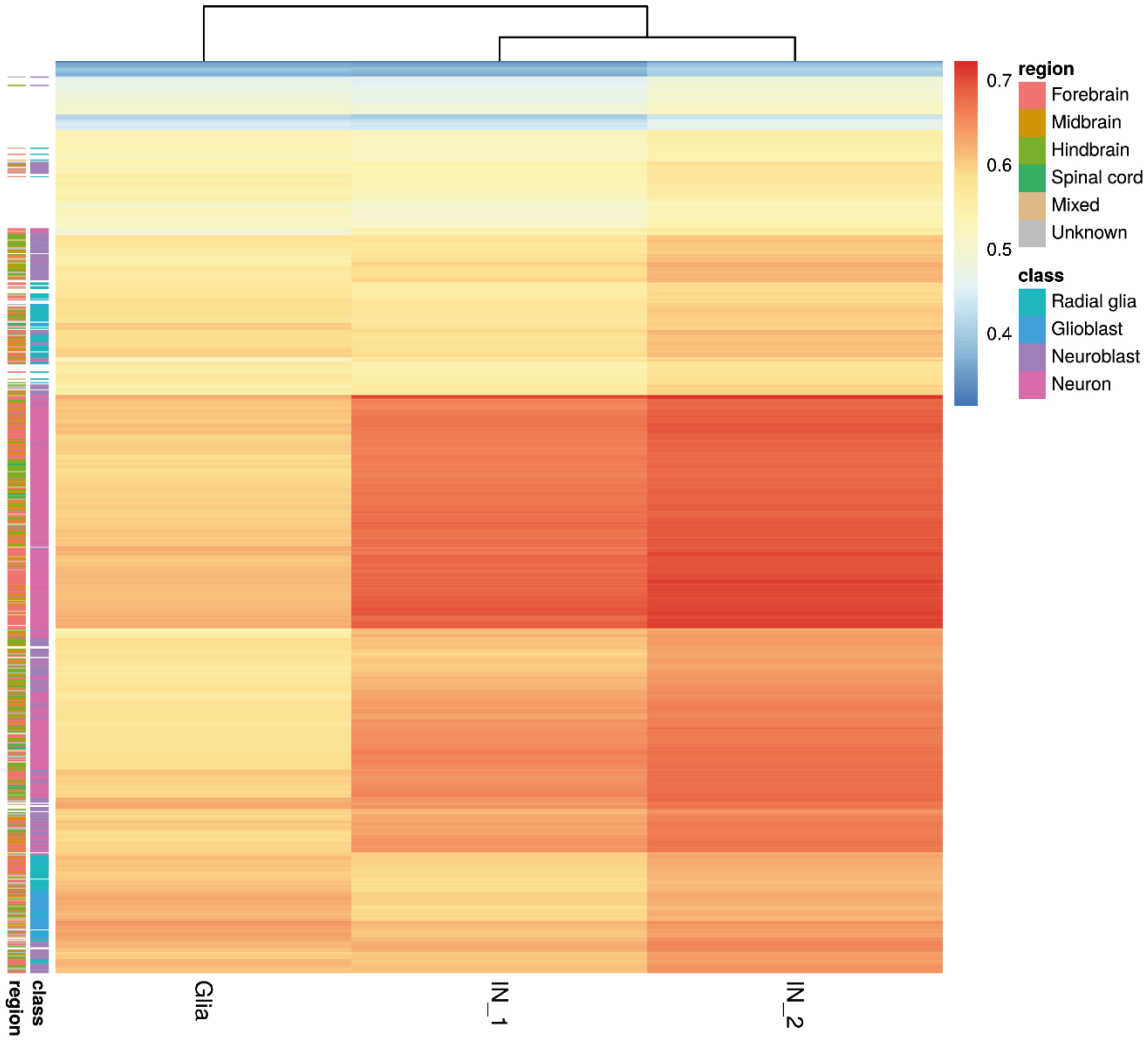

Figure 8: Cell type composition analysis of 21 week old D1 organoids with snRNA-seq
Heatmap visualization showing the Spearman correlation of relative gene expression between cell clusters (glia cells (Glia), Inhibitory neuron cluster 1 (IN_1) and 2 (IN_2)) and cells in the developing mouse brain. The regional identity of cells and cell classes are indicated on the left. Analysis performed by B. Zaremba.

(**Figure 8** is presented in a similar way as in Bauersachs et al. (in submission). Figure legends were obtained and modified from Bauersachs et al. (in submission) and had been originally written by myself.)

Glia			IN_1			IN_2		
Class	**Subclass**	**ρ**	**Class**	**Subclass**	**ρ**	**Class**	**Subclass**	**ρ**
GB	Forebrain astrocyte	0.653	N	Mixed region GABAergic	0.716	N	Mixed region GABAergic	0.724
GB	Midbrain	0.645	N	Forebrain GABAergic	0.704	N	Forebrain GABAergic	0.716
GB	PreOPC	0.644	N	Forebrain glutamatergic	0.700	N	Forebrain GABAergic	0.716
GB	Mixed region astrocytes	0.643	N	Forebrain GABAergic	0.700	N	Forebrain GABAergic	0.716
OGD	OGD precursor cell	0.641	N	Forebrain glutamatergic	0.699	N	Forebrain GABAergic	0.715
GB	Forebrain	0.639	N	Midbrain glutamatergic	0.698	N	Forebrain GABAergic	0.714
GB	Forebrain	0.638	N	Mixed region GABAergic	0.698	N	Forebrain GABAergic	0.713
N	Mixed region GABAergic	0.638	N	Forebrain GABAergic	0.697	N	Undefined	0.713
RG	Ependymal -like	0.638	N	Mixed region GABAergic	0.696	N	Forebrain GABAergic	0.713
GB	Forebrain	0.637	N	Forebrain GABAergic	0.694	N	Forebrain GABAergic	0.712

Table 1: **Developing mouse brain cell types with the highest gene expression correlation with each of the D1 forebrain organoid clusters.**
ρ: Spearman´s rank correlation coefficient; GB: glioblast; OGD: oligodendrocyte; N: neuron; RG: radial glia; OPC: pre-oligodendrocyte precursor cell; Glia: glia cells; IN_1: inhibitory neuron cluster 1; IN_2: inhibitory neuron cluster 2.

(Figure legends for **Table 1** were obtained and modified from Bauersachs et al. (in submission) and had been originally written by myself.)

One prerequisite for a functional neuronal network is the presence of synapses. To determine if neurons within organoids are able to form synapses, we first performed immunoblotting for the pre-synaptic marker SYNAPSIN-1 at various developmental stages. In both, D1- and HD6 iPSC-derived organoids, SYNAPSIN-1 expression was already detected after 6 weeks in culture (**Figure 9A**). With ongoing development, SYNAPSIN-1 was further upregulated, implying increased synaptic connectivity and functional maturation of neurons (**Figure 9B**). Using transmission electron microscopy (TEM), we confirmed the presence of structurally defined synapses, containing presynaptic vesicles and postsynaptic densities (**Figure 9C**). Single cell blind patch clamp recordings from the organoids verified the presence of glia cells and neurons, which were distinguished by their resting membrane potential as well as their ability to produce action potentials upon current injection (**Figure 9D** and **Table 2**).

Voltage clamp recording revealed spontaneous postsynaptic currents with both rapid (AMPA receptor-mediated) and slow ($GABA_A$ receptor-mediated) decay kinetics (verified with receptor selective antagonists, see below), which verifies the existence of both, glutamatergic and GABAergic neurons within the organoids as well as their synaptic connectivity.

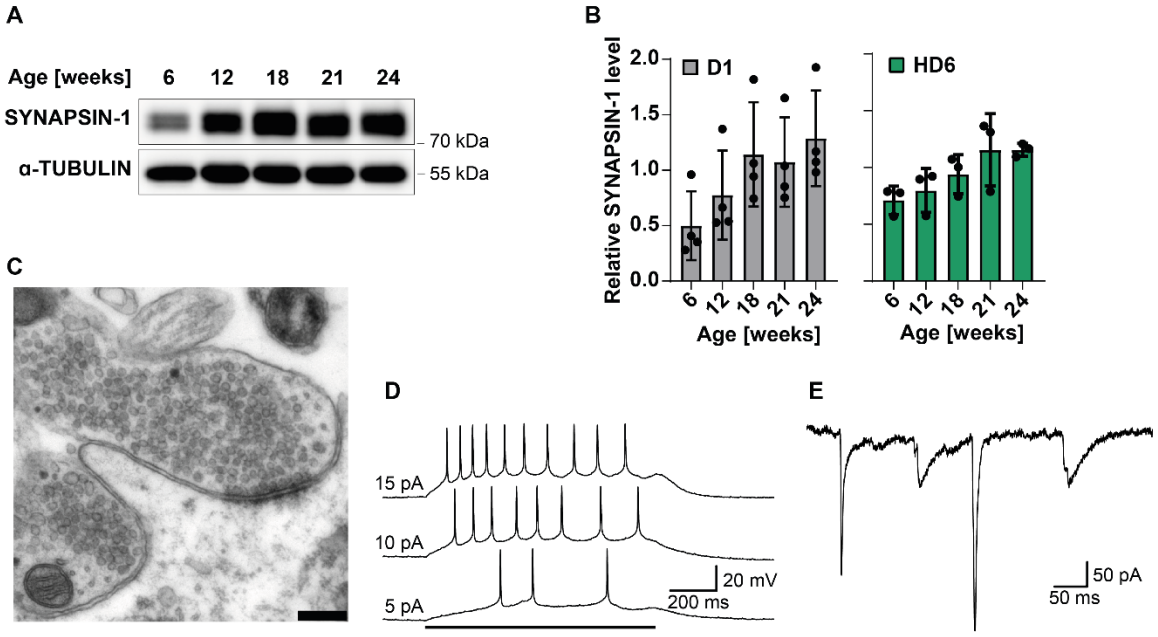

Figure 9: Forebrain organoids contain functional neurons
(**A**) Representative immunoblot of SYNAPSIN-1 and α-TUBULIN expression during development in D1 organoids. Immunoblots performed by U. Weiss (**B**) Quantification of **A** and similar data obtained from HD6 organoids. SYNAPSIN-1 levels were normalized to α-TUBULIN. D1: n = 4 batches, HD6: n = 3 batches. (**C**) Representative TEM image of a synapse in a 23 weeks old D1 organoid. Scale bar = 250 nm. Image acquired by A. Hellwig (**D**) Representative whole cell patch clamp recording from a 23 week old D1 organoid showing voltage traces recorded in current clamp with action potentials induced by a 1 s current injection (black line) at the levels indicated next to each trace. (**E**) Representative voltage clamp recording (Vhold = -70 mV) of postsynaptic currents with rapid (AMPA receptor-mediated) and slow ($GABA_A$ receptor-mediated) decay kinetics. Electrophysiology performed by C. P. Bengtson.

(**Figure 9D** and **9E** are presented in a similar way as in Bauersachs et al. (in submission). Figure legends for **Figure 9** were obtained and modified from Bauersachs et al. (in submission) and had been originally written by myself.)

Parameter	units	Neurons	Glia
Membrane capacitance	pF	40.9 ± 23.7 (42)	43.5 ± 66.8 (35)
Membrane resistance	MΩ	962 ± 925 (42)	249 ± 264 (35)
Vrest	mV	-50.0 ± 12.0 (3)	-87.3 ± 6.0 (35)
AP threshold	mV	-44.2 ± 3.2 (18)	
AP amplitude	mV	38.0 ± 11.8 (18)	
AP half width	ms	2.80 ± 0.98 (18)	
AMPA sEPSC amplitude	pA	-16.7 ± 10.6 (15)	
AMPA sEPSC decay wtau	ms	5.38 ± 0.83 (15)	
$GABA_A$ sIPSC amplitude	pA	-17.89 ± 9.04 (15)	
$GABA_A$ sIPSC decay wtau	ms	54.80 ± 13.90 (15)	

Table 2: Electrophysiological properties of neurons and glia cells within forebrain organoids
Quantification of electrophysiological parameters from whole cell blind patch clamp recordings in 22-25 week old organoids. Vrest: resting membrane potential; AP: action potential; sEPSC: spontaneous excitatory postsynaptic current; sIPSC: spontaneous inhibitory postsynaptic current; wtau: weighted tau. All data is represented as mean ± SD. Measurements were performed in at least 3 batches and exact cell numbers are shown in brackets.

(Legends for **Table 2** were obtained and modified from Bauersachs et al. (in submission) and had been originally written by myself.)

Next, since our aim was to generate a model for excitotoxicity in human neurons, we wanted to determine if cells within the organoids contain the predominant NMDAR subunits expressed in the forebrain *in vivo*, GluN1, GluN2A and GluN2B (146). Western blot analysis showed that organoids expressed all three NMDAR subunits already at 6 weeks in culture (**Figure 10A**). Thereafter, we detected relatively constant increases in the levels of GluN1 and GluN2A, while the expression levels of GluN2B reached a plateau after 12 weeks (**Figure 10B-D**). The developmental expression patterns of GluN2A and GluN2B in the human organoids are in line with NMDAR subunit expression observed *in vivo*. In both, human and rodent, GluN2B expression is strong during embryonic development and sustained in adulthood, whereas GluN2A expression has a relatively delayed onset (16, 111, 112, 147).

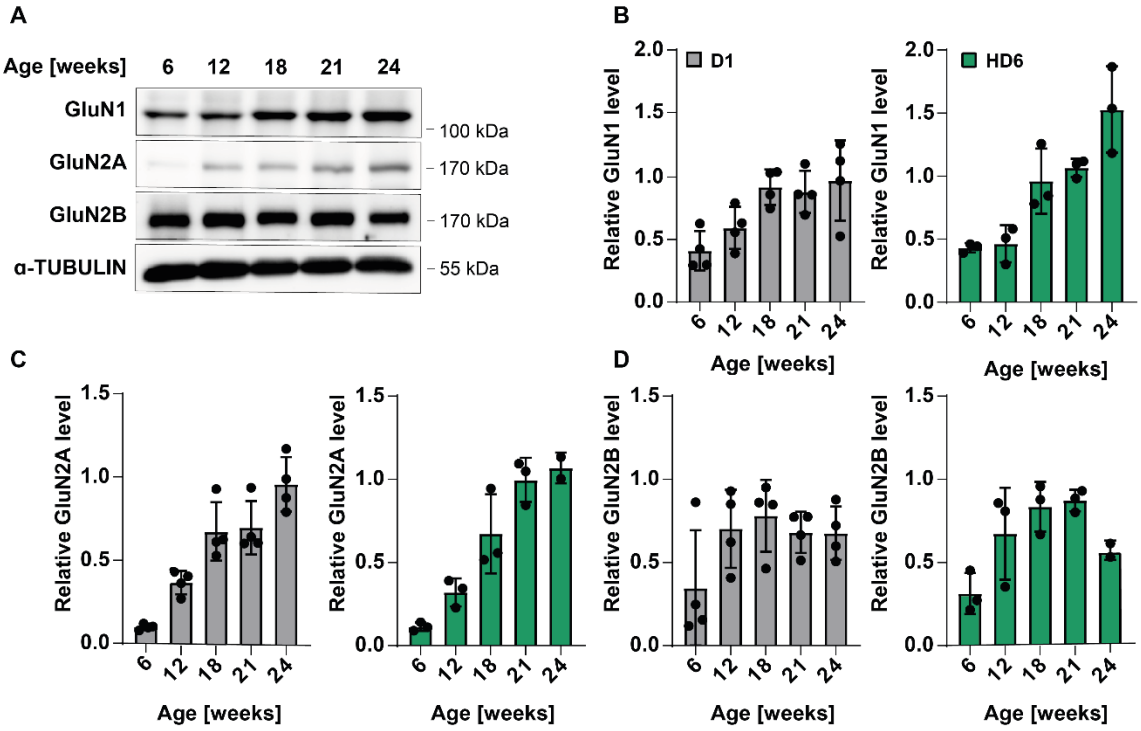

Figure 10: Brain organoids contain all major NMDAR subunits expressed in the forebrain *in vivo*
(**A**) Representative immunoblot of GluN1, GluN2A, GluN2B and α-TUBULIN expression during development in D1 organoids. (**B-D**) Quantification of **A** and similar data obtained from HD6 organoids. GluN1 (**B**), GluN2A (**C**) and GluN2B (**C**) levels were normalized to α-TUBULIN. D1: n = 4 batches, HD6: n = 3 batches. All data is represented as mean ± SD. Immunoblots performed by U. Weiss.

(Figure legends for **Figure 10** were obtained and modified from Bauersachs et al. (in submission) and had been originally written by myself.)

Taken together, our protocol allows for robust and reproducible generation of forebrain organoids from two different hiPSC lines. These organoids contain different cell types, including neural stem cells, glial cells and NMDAR-expressing neurons, the latter forming a synaptically connected network. For subsequent experiments, organoids between 18 and 24 weeks were used.

2.2. Human forebrain organoids are sensitive to glutamate- and NMDA-mediated neurotoxicity

In order to evaluate cell death within organoids in a fast, practical and easily quantifiable way, we investigated the potential of LDH release assays to serve this purpose. To determine the range of LDH that can be released upon a well-established, massive cell death-evoking stimulus (148), we challenged organoids with 10 mM H_2O_2 for 1 hour and assessed LDH release after 24 hours. To normalize for size differences between individual organoids, data is presented as the percentage of LDH released relative to total LDH present after complete lysis. Exposure to H_2O_2 markedly increased levels of LDH in the supernatant from 0.53 ± 0.19 % in untreated organoids to 11.85 ± 5.37 % (**Figure 11A**). This LDH response to a highly toxic, oxidative stress-inducing treatment provided the approximate range of LDH release for determining relative cell death in the organoids. To examine the sensitivity of human forebrain organoids to excitotoxicity, organoids were treated with different concentrations of glutamate for 1 hour. The resulting dose response in LDH release, determined after 24 hours, suggests that organoids generated from both iPSC lines indeed are susceptible to graded concentrations of glutamate (**Figure 11B** and **C**). Exposure to the NMDAR antagonist MK-801 before and during treatment with 200 μM glutamate completely abolished LDH release (**Figure 11D**). In contrast, application of the AMPA and kainate receptor antagonist 2,3-dioxo-6-nitro-7-sulfamoyl-benzo[f]quinoxaline (NBQX) or the L-type Ca^{2+} channel antagonists nifedipine and verapamil did not significantly reduce the LDH release induced by glutamate (**Figure 11E**). These results indicate that neurotoxicity in human forebrain organoids is predominantly mediated through NMDARs. Indeed, similarly to treatment with glutamate, exposure to increasing concentrations of NMDA caused relative LDH release in a dose dependent manner (**Figure 11F** and **G**). Together, these results demonstrate that NMDAR activation is both sufficient and necessary for excitotoxicity in hiPSC-derived neurons. Since relative levels of LDH release were consistently higher in D1 iPSC-derived organoids in response to toxic stimuli, we chose to employ these for a more detailed characterization. Further, to selectively activate NMDARs, NMDA instead of glutamate was used for subsequent experiments.

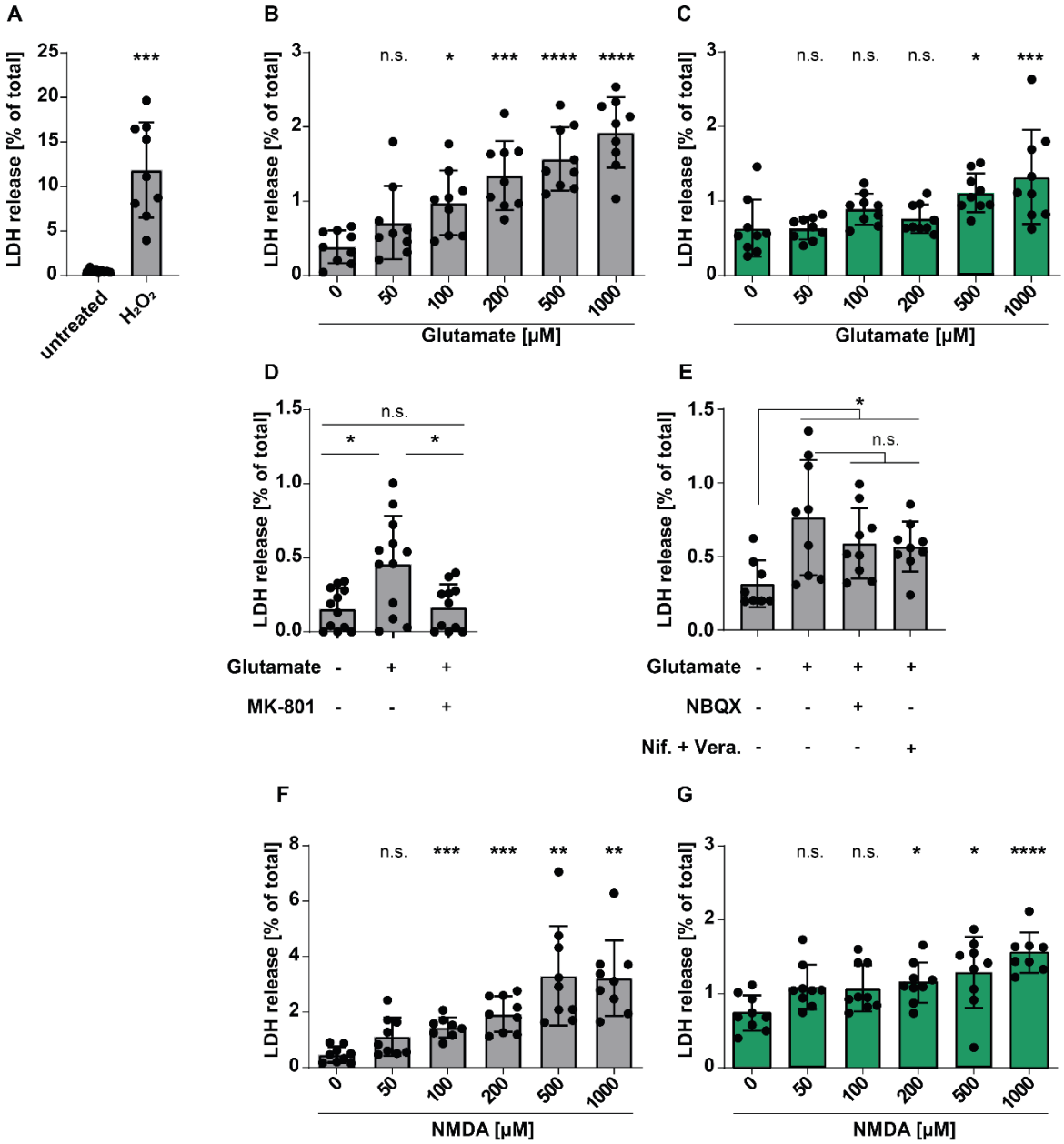

Figure 11: Exposure of forebrain organoids to high concentrations of glutamate or NMDA results in cell death

Quantification of LDH release from organoids as a measure of cell death. Organoids were treated with H_2O_2 (**A**), glutamate (**B**-**E**) or NMDA (**F**, **G**) for 1 h and LDH release was assessed after 24 h. Data is shown as % of LDH release relative to total LDH present in respective organoids as determined by complete lysis. (**A**) D1 organoids treated with 10 mM H_2O_2. n = 9 organoids from 3 batches. (**B**) D1 organoids treated with indicated concentrations of glutamate. n = 9 organoids from 3 batches. (**C**) HD6 organoids treated with indicated concentrations of glutamate. n = 9 organoids from 3 batches. (**D**) D1 organoids treated with 200 µM glutamate. MK-801 (10 µM) was present 1 h before and during the toxic insult. n = 12 organoids from 3 batches. (**E**) D1 orgaoids treated with 200 µM glutamate. NBQX (5 µM) or Nifedipine (Nif., 5 µM) and Verapamil (Vera., 30 µM) were present 1 h before and during the toxic insult. (**F**) D1 organoids treated with indicated concentrations of NMDA. n = 9 organoids from 3 batches. (**G**) HD6 organoids treated with indicated concentrations of NMDA. n = 9 organoids from 3 batches. All data is represented as mean ± SD. n.s. : not significant, *p < 0.05, **p < 0.01, ***p < 0.001, ****p < 0.0001. (**A**) Welch´s t-test. (**B**, **C**, **F**, **G**) Brown Forsythe and Welch ANOVA with Dunnett´s T-3 multiple comparison test. (**D**, **E**) Brown Forsythe and Welch ANOVA with Games Howell´s multiple comparison test.

(Figure legends for **Figure 11** were obtained and modified from Bauersachs et al. (in submission) and had been originally written by myself.)

To confirm that elevated LDH release is associated with an increase in cell death, cell viability states in control and NMDA treated organoids were quantified using TEM. On that account, organoids were treated with 200 µM NMDA for 1 hour and fixed after 2 or 24 hours to monitor early and late phases of excitotoxicity, respectively. For quantification, cells were categorized according to morphological characteristics into 1) Viable cells (equally distributed chromatin, intact membranes and organelles), 2) Type 1 cell death (highly condensed chromatin, cell swelling and / or loss of membrane integrity) and 3) Type 2 cell death (highly condensed chromatin, cell shrinkage, loss of intact organelles) (**Figure 12A**).

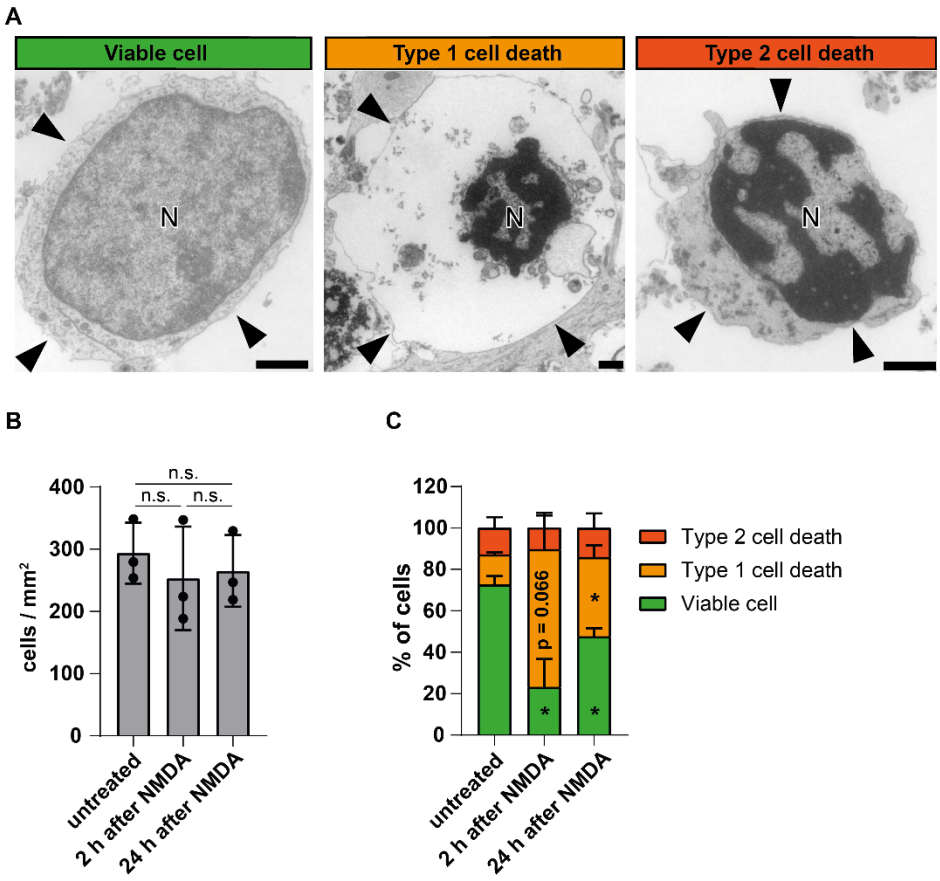

Figure 12: Exposure of forebrain organoids to NMDA results in morphologically distinct forms of cell death

(**A**) Representative TEM images of cell viability states in organoids treated with 200 µM NMDA. Type 1 cell death is characterized by chromatin condensation, cell swelling and / or loss of membrane integrity. Type 2 cell death is characterized by chromatin condensation, cell shrinkage and lack of intact organelles. N: nucleus; arrowheads indicate plasma membranes. Scale bar = 1 µm. Images acquired by A. Hellwig. (**B**) Quantification of cell density (cells / mm²) in ultrathin sections. Organoids were either left untreated of exposed to 200 µM NMDA for 1 h and fixed 2 or 24 h after onset of the treatment. n = 3 organoids from 3 batches. For each organoid and condition, 158 - 396 cells were analyzed. (**C**) Quantification of cell viability states in organoids treated as in (**B**) Statistical analysis is shown compared to untreated organoids. No statistical differences between NMDA-treated conditions were detected. All data is represented as mean ± SD. n.s. : not significant, *p < 0.05. (**B** and **C**) Brown Forsythe and Welch ANOVA with Games Howell´s multiple comparison test.

(Figure legends for **Figure 12** were obtained and modified from Bauersachs et al. (in submission) and had been originally written by myself.)

Analysis of the TEM images showed that cell density was unaltered between conditions, suggesting that cell counts were not distorted by cell loss due to complete structural disintegration (**Figure 12B**). As expected, the number of viable cells was decreased after NMDA treatment. Further, exposure to NMDA induced Type 1 but not Type 2 cell death (**Figure 12C**). These results show that exposure to high concentrations of NMDA induce cell death within organoids, thereby confirming the findings obtained from LDH assays.

Besides changes in soma morphology, NMDA exposure was also reported to affect neurite architecture (149). To investigate if this hallmark of excitotoxicity can is also featured in forebrain organoids as well, we performed scanning electron microscopy (SEM) of either untreated organoids or organoids exposed to 200 µM NMDA for 1 hour followed by fixation 12 or 24 hours after the onset of the treatment. Whereas untreated organoids exhibited uniformly shaped extensions on their surface, organoids fixed 12 and 24 hours after NMDA treatment revealed irregular neurite morphology (**Figure 13**). The here observed blebbing and thinning of protrusions are characteristic features of ongoing neurodegeneration in different pathological conditions such as traumatic brain injury or β-amyloid induced neurotoxicity (150, 151).

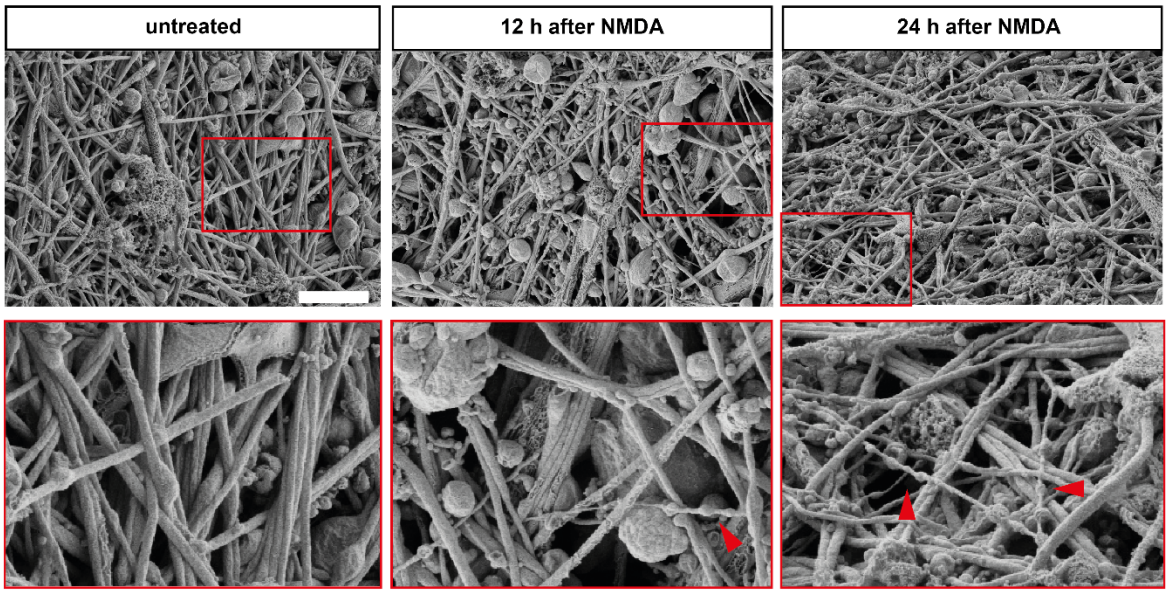

Figure 13: Exposure of forebrain organoids to high concentrations of NMDA results in neurite blebbing
Representative SEM images of the surface of untreated organoids or organoids 12 and 24 h after treatment with 200 µM NMDA for 1 h. Magnifications of framed areas are shown below. Arrowheads indicate neurites that exhibit blebbing. Scale bar = 5 µm. Images acquired by A. Hellwig.

(Figure legends for **Figure 13** were obtained and modified from Bauersachs et al. (in submission) and had been originally written by myself.)

Finally, since forebrain organoids contain various cell types such as neurons, glial and neural stem cells (**Figure 4-7**), we wanted to determine which cells within the organoids are affected by NMDA toxicity. Assuming that the loss of a certain cell type results in a reduction of cell type specific transcripts, we performed RT-qPCR analysis in control and NMDA treated organoids. Whereas mRNAs of marker genes for neural stem cells (*SOX1*, *NESTIN*) and glial cells (*GFAP*, *AQP4*) were either unaltered or even increased, neuronal markers were markedly decreased in NMDA-treated organoids (*NEUN*: 47.3 %; *MYT1L*: 54.1 % of control organoids) (**Figure 14A**). To confirm that excitotoxicity results in a loss of neurons, we further quantified the proportion of MYT1L positive nuclei 24 hours after NMDA exposure. In line with our RT-qPCR data, we found that there is a clear reduction of MYT1L positive cells in NMDA treated organoids (17.07 %) compared to untreated controls (49.38 %) (**Figure 14B and C**), verifying that excitotoxicity is indeed predominantly affecting neurons.

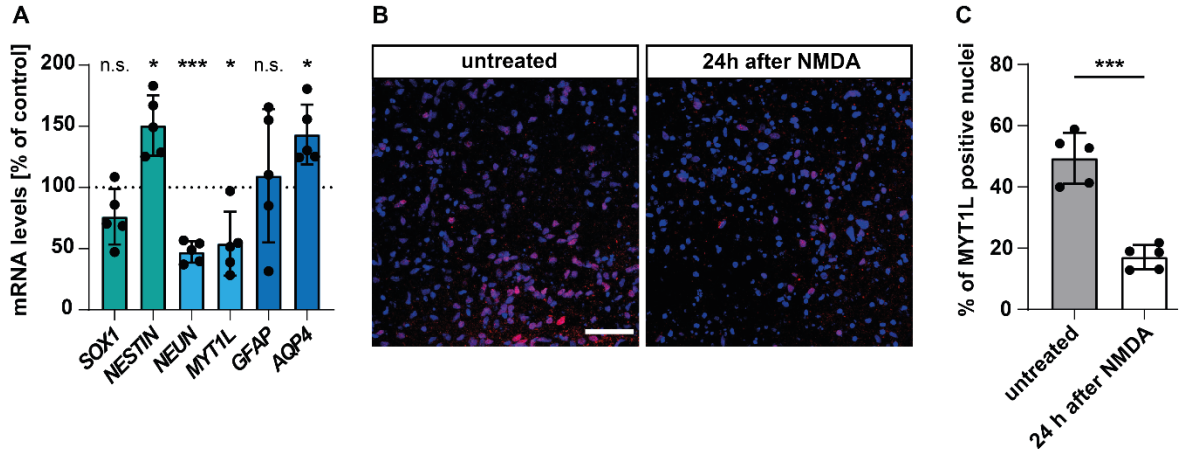

Figure 14: Exposure of forebrain organoids to high concentrations of NMDA results in neuronal cell death
(**A**) RT-qPCR analysis of relative mRNA expression levels of *SOX1*, *NESTIN* (neural stem cells), *MYT1L*, *NEUN* (post-mitotic neurons), *GFAP* and *AQP4* (glial cells) in organoids 24 h after treatment with 200 µM NMDA for 1 h. n = 5 batches. (**B**) Representative immunofluorescence images of MYT1L (red) in untreated organoids and organoids 24 h after treatment with 200 µM NMDA for 1 h. Nuclei are visualized with Hoechst (blue). Scale bar = 50 µm. (**C**) Quantification of MYT1L positive nuclei in untreated and NMDA-treated organoids For each condition, the average from 6 - 7 images is shown. n = 5 organoids from 3 batches.. All data is represented as mean ± SD. n.s. : not significant, *p < 0.05, ***p < 0.001. (**A** and **C**) Welch´s t-test.

(Figure legends for **Figure 14** were obtained and modified from Bauersachs et al. (in submission) and had been originally written by myself.)

Taken together, we demonstrated that excitotoxicity mediated by NMDAR activation results in morphological alterations and ultimately cell death of neurons in human forebrain organoids.

2.3. High and low doses of NMDA lead to opposing physiological outcomes in human forebrain organoids

We next focused on probing acquired neuroprotection in the human forebrain organoids. Acquired neuroprotection has been repeatedly described in mouse cultured primary neurons where action potential bursting and synaptic NMDAR activation mediate CREB-dependent gene expression, thereby ameliorating cell death in response to toxic concentrations of NMDA (83, 152, 153). Various pharmacological protocols have been used to induce acquired neuroprotection, including preconditioning of cultures with a low dose of NMDA (95).

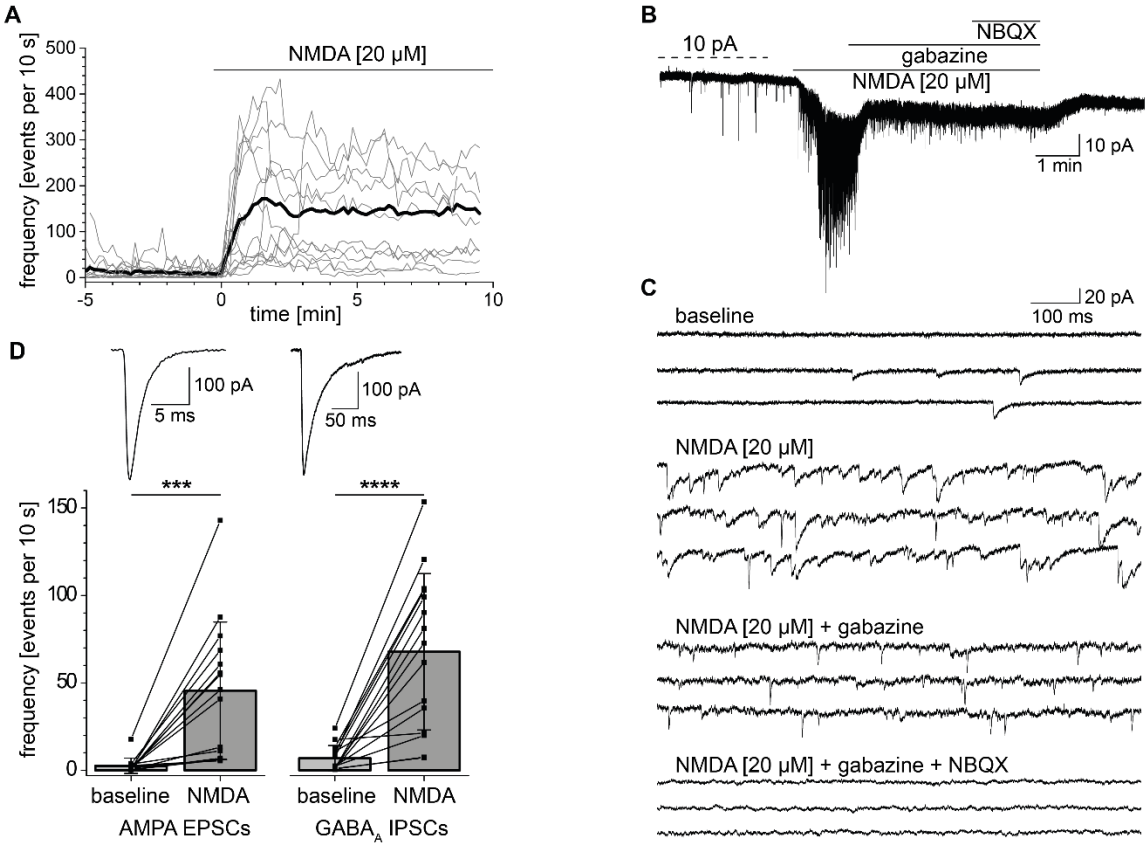

Figure 15: Low concentrations of NMDA increase excitatory and inhibitory synaptic activity within forebrain organoids
(**A**-**D**) Synaptic activity induced by 20 µM NMDA. (**A**) Time series plot of sPSC counts in 10 s bins over 5 min baseline and 10 min NMDA treatment in individual cells (thin traces) and their mean (thick trace). n = 15 cells (of 13 organoids from 3 batches) (**B**) Representative voltage clamp recording (Vhold = -70 mV) of the inward current and increase in synaptic activity evoked by 20 µM NMDA. Organoids were exposed at indicated times to GABA$_A$ receptor blocker (gabazine; 5 µM) and AMPA receptor blocker (NBQX; 5 µM). (**C**) Expanded traces showing spontaneous postsynaptic currents (sPSCs) in baseline and after addition of NMDA (**D**) Examples of sPSCs segregated according to their decay kinetics into rapid AMPA receptor-mediated sEPSCs (left) and slower GABA$_A$ receptor-mediated sIPSCs (right). Line series plots below show the average event frequencies during baseline and NMDA exposure for individual cells and histograms show their means ± SD. n = 15 cells (of 13 organoids from 3 batches). ***p < 0.0005, ****p < 0.00001. Paired t-tests. Experiments performed by C. P. Bengtson and C. García-Vilela.

(Figure legends for **Figure 15** were obtained and modified from Bauersachs et al. (in submission) and had been originally written by myself.)

It is, however, unknown if acquired neuroprotection and the dose-dependent dual action of NMDAR-signalling are conserved in human neurons. In order to investigate if low doses of NMDA are able to induce synaptic activity in our organoids, we performed blind whole cell patch clamp recordings. Previous experiments in cultured primary rodent neurons have shown that tolerated doses of NMDA are neuroprotective (95). Based on our observations from the LDH toxicity assays (**Figure 11G**), we decided to test a concentration of 20 µM, since exposure to 50 µM NMDA still increased LDH release, although not significant. Indeed, bath application of 20 µM NMDA was able to strongly increase synaptic activity and caused a small inward current (**Figure 15A** and **B**). Subsequent exposure to the $GABA_A$ receptor blocker, gabazine, and the AMPA receptor blocker, NBQX, completely blocked postsynaptic currents (PSCs) with slow and fast decay time constants respectively. This demonstrates that 20 µM NMDA induces both, GABAergic and glutamatergic synaptic signalling (**Figure 15B** and **C**). Segregation of PSCs according to their decay kinetics revealed that in the majority of neurons (10/15) both AMPA and $GABA_A$ receptor mediated currents were strongly induced, whereas only a minor increase could be detected in the remaining neurons (5/15) (**Figure 15D**).

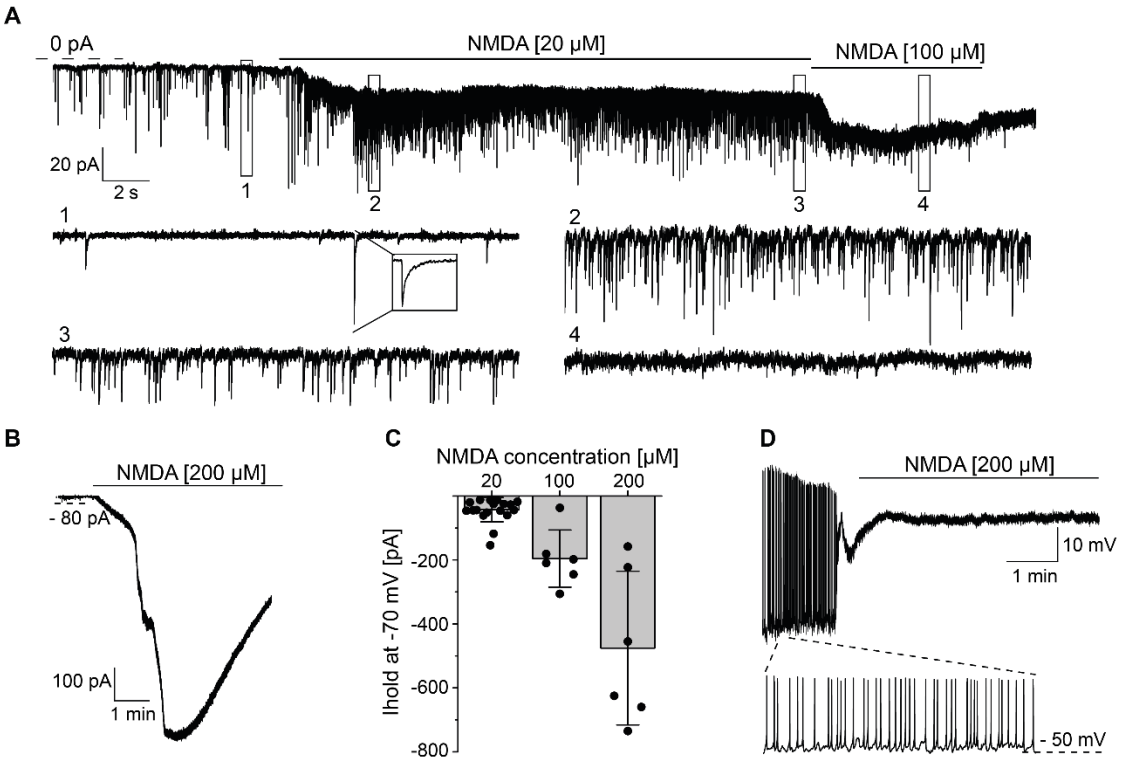

Figure 16: High and low doses of NMDA lead to opposing electrophysiological responses in forebrain organoids

(**A**) Recording of current responses to 20 µM and 100 µM NMDA. Traces 1 to 4 below show expanded views of the boxed regions in the upper trace. (**B**) Representative recording of a current response to 200 µM NMDA application. (**C**) Summary statistics of the change in holding current induced by 20, 100 and 200 µM NMDA at a holding potential of -70 mV. 20 µM: n = 19 cells (of 17 organoids from 3 batches), 100 µM: n = 6 cells (of 6 organoids from 3 batches), 200 µM: n = 6 cells (of 6 organoids from 3 batches). Data is represented as mean ± SD. (**D**) Representative recording of membrane potential response to 200 µM NMDA application. Inset shows spontaneous action potentials in baseline. C. P. Bengtson and C. García-Vilela performed the experiments.

(Figure legends for **Figure 16** were obtained and modified from Bauersachs et al. (in submission) and had been originally written by myself.)

After verifying that low doses of NMDA were able to induce synaptic activity, we investigated if the concentration-dependent dual action of NMDAR-signalling is conserved in human neurons. Therefore, organoids were exposed to 20 µM NMDA, followed by bath application of a toxic NMDA dose (100 or 200 µM). As expected, low NMDA concentrations greatly elevated synaptic activity. This increase, however, was immediately abolished by treatment with 100 µM NMDA (**Figure 16A**). Application of 200 µM NMDA caused membrane instability in voltage clamp due to the large currents induced (**Figure 16B** and **D**). In current clamp, exposure to 200 µM NMDA caused chronic depolarization of neurons and blocked spontaneous action potentials (**Figure 16C**). Taken together, as previously shown in rodents (95), application of low doses of NMDA results in a strong induction of synaptic activity within organoid networks, whereas exposure to high NMDA concentrations causes termination of activity.

Next, we wanted to evaluate if the opposing effects of high and low doses of NMDA on neuronal activity are also reflected in the phosphorylation status of CREB, which was shown to be a central mediator of activity-induced neuroprotection (91). Phosphorylation at Ser133 enables CREB to recruit co-activators like CBP and thereby initiate transcription of target genes (154). In rodent cell culture models, exposure to low concentrations of NMDA was reported to induce sustained CREB phosphorylation, whereas high doses of NMDA result in initial CREB activation, followed by fast dephosphorylation and hence, shut-off (105, 155). To determine if these CREB phosphorylation patterns in response to high and low doses of NMDA are preserved in human neurons, organoids were treated with 20 or 200 µM NMDA for 10 or 30 minutes followed by immunoblot analysis. Indeed, exposure of organoids to 20 µM NMDA for 10 minutes led to an increased CREB phosphorylation that was still sustained after 30 minutes. In contrast, treatment with 200 µM NMDA for 10 minutes resulted in lower CREB activation. Further, the increase in CREB phosphorylation was of transient nature and already decreased after 30 minutes (**Figure 17A** and **B**).

Since CREB is known to be a potent regulator of gene transcription, we further investigated differential effects of high and low NMDA doses on activity-regulated genes. Specifically, we wanted to evaluate if activity-induced neuroprotective genes identified in rodents (83) were upregulated in response to treatment with 20 µM NMDA in human neurons. Organoids were treated with 20 µM NMDA for 1 hour and either collected immediately or 3 hours after the treatment (t = 4 hours). These time points were chosen to investigate immediate and late response genes, respectively. Considering the observed differential effects of high and low NMDA doses on CREB phosphorylation levels, we also included a treatment with 200 µM

NMDA. 1 hour after application of 20 µM NMDA, the immediate-early genes *NPAS4*, *FOS* and *JUNB* were strongly induced (**Figure 17C**).

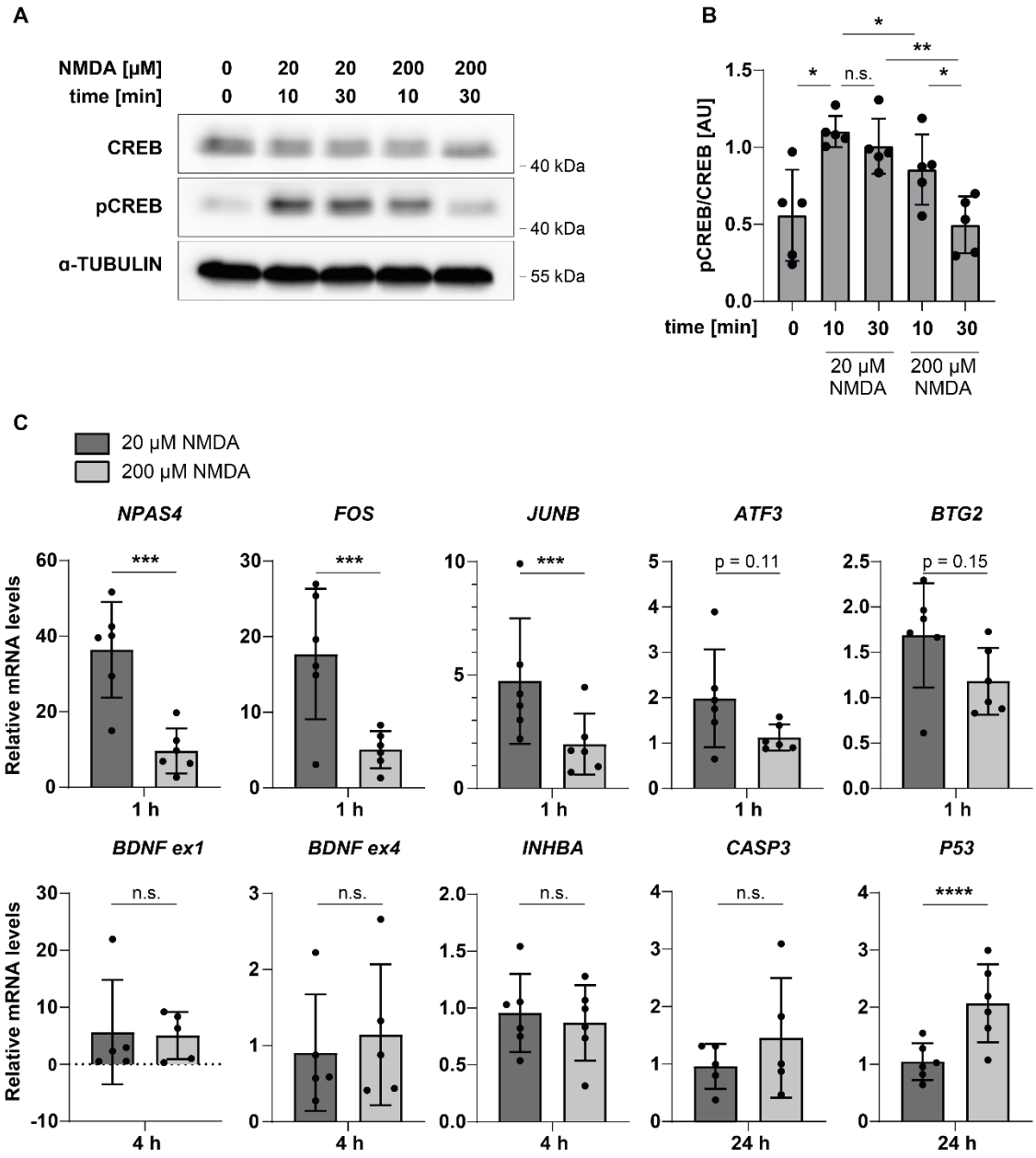

Figure 17: High and low doses of NMDA lead to different transcriptional outcomes in forebrain organoids
A) Representative immunoblot of pCREB, CREB and α-TUBULIN in D1 organoids left untreated or treated with 20 or 200 µM NMDA for 10 or 30 min. Immunoblots performed by U. Weiss. (**B**) Quantification of **A**. CREB and pCREB levels were normalized to α-TUBULIN. AU = arbitrary unit. n = 5 batches. (**C**) RT-qPCR analysis of relative mRNA expression levels of indicated genes in forebrain organoids exposed to 20 or 200 µM NMDA for 1 h and either collected immediately (*NPAS4*, *FOS*, *JUNB*, *ATF3*, *BTG2*), after 4 h (*BNDF ex1* and *ex4*, *INHBA*) or after 24 h (*CASP3* and *P53*). Fold changes are calculated relative to an untreated control. n = 5 - 6 batches. All data is represented as mean ± SD. n.s. = not significant, *p < 0.05, **p < 0.01, ***p < 0.001, ****p < 0.0001. (**B** and **C**) Ratio paired t-test.

(Figure legends for **Figure 17** were obtained and modified from Bauersachs et al. (in submission) and had been originally written by myself.)

This effect, however, was markedly attenuated in organoids treated with 200 µM NMDA. Similar differential responses were observed in the transcriptional upregulation of the previously demonstrated neuroprotective genes *ATF3* and *BTG2* (83). Interestingly, we did not detect altered mRNA levels for *BDNF* exon 1 or 4 (*BDNF* ex1 and *BDNF* ex4) or *INHIBIN β A* (*INHBA*) in human neurons despite previous reports of the upregulation in rodent neurons of *Bdnf* and *Inhba* after 4 hours of synaptic activity (83, 105).

Similar to acquired neuroprotection, also excitotoxic stress is associated with transcriptional changes. To test whether treatments with high or low concentrations of NMDA causes differential upregulation of pro-death genes, organoids were exposed to 20 µM or 200 µM NMDA for 1 hour and collected after 24 hours for gene expression analysis. At this time point, the potent cell death mediators *P53* and *Caspase-3* (*Casp3*) were previously shown to be robustly upregulated in response to excitotoxic insults (156, 157). Whereas *CASP3* mRNA levels remained unaltered amongst the different conditions, *P53* mRNA levels were increased upon treatment with 200 µM NMDA (**Figure 17C**). The upregulation of *P53* was previously observed in both, necrotic and apoptotic cell death, while *Caspase-3* induction and activation is mainly associated with apoptosis (158). Thus, the results from our RT-qPCR analysis indicate that 24 hours after excitotoxic insults predominantly necrotic cell death occurs.

In summary, we showed that the concentration-dependent dual action of NMDAR-signalling is preserved in human iPSC-derived neurons. Exposure to high concentrations of NMDA resulted in cessation of synaptic activity, CREB shut-off and upregulation of the pro-death gene *P53*. In contrast, treatment with low doses of NMDA triggers action potential bursting, sustained induction of CREB and strong upregulation of activity-regulated genes, including neuroprotective genes.

2.4. Pre-treatment with a subtoxic NMDA dose protects cells within forebrain organoids against excitotoxic insults

In the previous section, we demonstrated that exposure to a low concentration of NMDA initiates electrophysiological and transcriptional changes that are implicated in acquired neuroprotection in rodent neurons (83, 95). Accordingly, we hypothesized that pre-treatment with low doses of NMDA could protect cells within the organoids against excitotoxic cell death. To test this hypothesis, organoids were pre-treated with 20 µM NMDA for 1 hour, followed by a medium change. 24 hours later, organoids were challenged with 200 µM NMDA and LDH release was assessed after another 24 hours (see treatment scheme **Figure 18A**). Indeed, the NMDA pre-treatment significantly reduced LDH release in response to toxic NMDA insults (**Figure 18A**). Next, we wanted to determine if varying pre-treatment durations influence the

protective effect. Thus, we applied 20 µM NMDA for 5 minutes, 30 minutes, 1 hour, 2 hours or 4 hours. An optimal protective effect was achieved by pre-treatments for 30 minutes or 1 hour, whereas shorter or longer durations had no effect on LDH release compared to the non-pre-treated condition (**Figure 18B**).

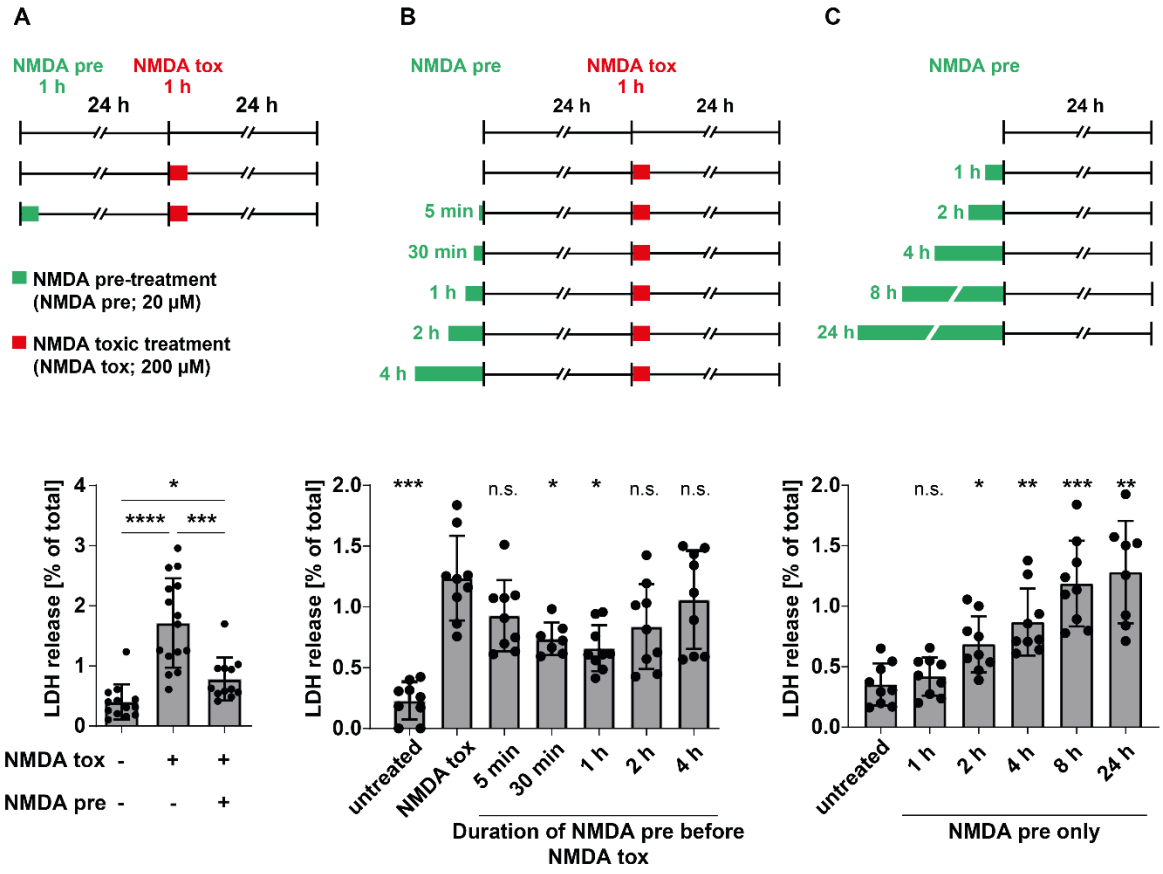

Figure 18: Pre-treatment with subtoxic concentrations of NMDA protects organoids against excitotoxic cell death in a duration dependent manner
(**A**-**C**) Quantification of LDH release from organoids as a measure of cell death. The schematics above the bar graphs outline the experimental settings of each assay. Organoids were either pre-treated with a subtoxic concentration of NMDA (NMDA pre, 20 µM) for and at the times indicated, or left untreated before exposure to a toxic concentration of NMDA (NMDA tox, 200 µM) for 1 h. LDH release was assessed 24 h after the onset of NMDA tox. Data are shown as % of LDH release relative to total LDH present in respective organoids as determined by complete lysis. (**A**) Effect of NMDA pre. n = 12 organoids from 4 batches. (**B**) Effect of the duration of NMDA pre before NMDA tox. n = 9 organoids from 3 batches. Statistical analysis is shown compared to NMDA tox. (**C**) Effect of the duration of NMDA pre only. n = 9 organoids from 3 batches. Statistical analysis is shown compared to NMDA tox. All data is represented as mean ± SD. n.s. : not significant, *p < 0.05, **p < 0.01, ***p < 0.001, ****p < 0.0001. Brown-Forsythe and Welch ANOVA, Games-Howell´s multiple comparisons test.

(Figure legends for **Figure 18** were obtained and modified from Bauersachs et al. (in submission) and had been originally written by myself.)

Presumably, pre-treatment for 5 minutes is not sufficient to trigger sustained pro-survival signalling. On the other hand, preconditioning periods exceeding 1 hour do not protect against subsequent application to high NMDA doses, which may be caused by toxicity evoked through the pre-treatment itself. It has been previously demonstrated that neuroprotection and excitotoxicity can be triggered by similar concentrations of NMDA in a time-dependent manner (159). Thus, to evaluate if longer exposure to low NMDA doses can have toxic effects, forebrain organoids were treated with 20 µM NMDA for 1, 2, 4, 8 and 24 hours and LDH release was measured another 24 hours later. In line with the protection observed in the 1 hour-treatment (**Figure 18B**), exposure to 20 µM NMDA for this time period did not alter LDH level (**Figure 18C**). Longer treatments, however, resulted in increased LDH release in a duration dependent manner. Taken together, these results suggest that exposure to low concentrations of NMDA for a short time period (30 minutes to 1 hour) is non-toxic and evokes long-lasting neuroprotection. In contrast, during prolonged treatments (2 hours or more) the toxic signalling prevails and annihilates the protective effect.

Next, we evaluated if changing the time between NMDA pre-treatment and toxic NMDA application affects the protection by performing pre-treatments 24, 6, 4, 2, 1 or 0.5 hours before the excitotoxic insult. For these experimental settings, a protective effect was only observed when pre-treatments were performed at least 4 hours before the toxic insult (**Figure 19**), indicating that the built-up of a neuroprotective shield is not immediate, but instead requires a certain amount of time.

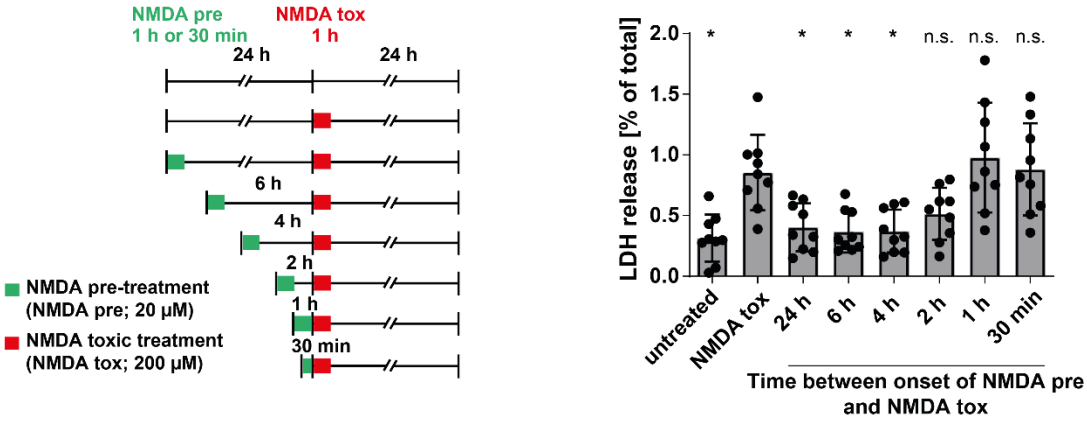

Figure 19: Pre-treatment with subtoxic concentrations of NMDA protects organoids against excitotoxic cell death in a time dependent manner
Quantification of LDH release from organoids as a measure of cell death. The schematics on the left outline the experimental settings of each assay. Organoids were either pre-treated with a subtoxic concentration of NMDA (NMDA pre, 20 µM) for and at the times indicated, or left untreated before exposure to a toxic concentration of NMDA (NMDA tox, 200 µM) for 1 h. LDH release was assessed 24 h after the onset of NMDA tox. Data are shown as % of LDH release relative to total LDH present in respective organoids as determined by complete lysis. n = 9 organoids from 3 batches. Statistical analysis is shown compared to NMDA tox. Data is represented as mean ± SD. n.s. : not significant, *p < 0.05. Brown-Forsythe and Welch ANOVA, Games-Howell´s multiple comparisons test.

(Figure legends for **Figure 19** were obtained and modified from Bauersachs et al. (in submission) and had been originally written by myself.)

In monolayer cultures of rodent primary neurons, NMDA-induced neuroprotection is dependent on an increase in synaptic activity (95). To evaluate if this is also the case in human forebrain organoids, we repeated the pre-treatment with 20 µM NMDA 4 hours before the toxic insult in the presence of NBQX and / or gabazine. Previously, we showed that these blockers of AMPA and kainate or $GABA_A$ receptors, respectively, interfered with the NMDA-induced increase in synaptic activity (**Figure 13C**). Surprisingly, the protective effect of the pre-treatment was unaltered by the presence of NBQX and / or gabazine (**Figure 20A**). To verify this observation, we next performed the pre-treatment together with tetrodotoxin (TTX), which potently blocks voltage gated Na^+ channels and thereby inhibits action potential firing (160). To exclude the possibility that any residual NMDA, which is not removed through the medium change after the pre-treatment, triggers synaptic activity as soon as the Na^+ channel block is relieved, TTX remained present throughout the entire course of the treatment (**Figure 20B**). Due to high variability between experiments, we could not detect a statistically

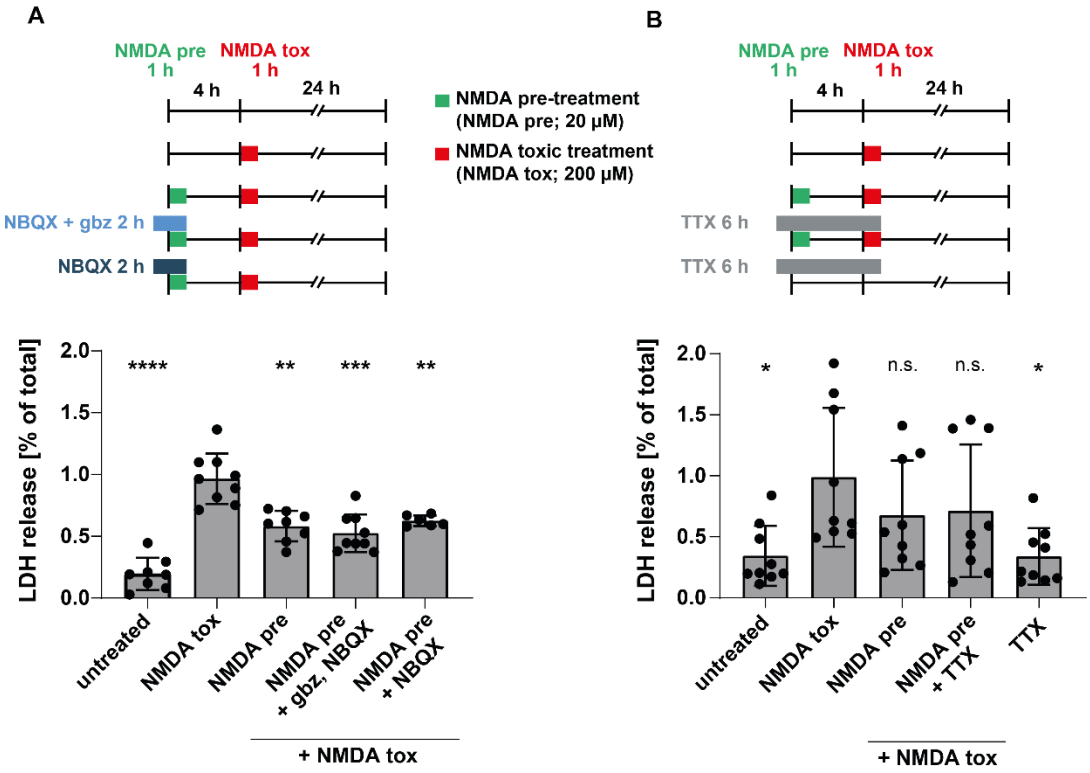

Figure 20: Pre-treatment with subtoxic concentrations of NMDA protects organoids against excitotoxic cell death independent of synaptic activity
Quantification of LDH release from organoids as a measure of cell death. The schematics above the bar graphs outline the experimental settings of each assay. Organoids were either pre-treated with a subtoxic concentration of NMDA (NMDA pre, 20 µM) for 1h or left untreated. Synaptic activity was blocked by application of NBQX (5 µM), gabazine (gbz, 5 µM) or TTX (1 µM) 1 h before and during the pre-treatment. 4 h after the onset of the pre-treatment organoids were exposed to a toxic concentration of NMDA (NMDA tox, 200 µM) for 1 h. LDH release was assessed 24 h after the onset of NMDA tox. Data are shown as % of LDH release relative to total LDH present in respective organoids as determined by complete lysis. (**A**) NMDA pre in the presence of gbz and NBQX or NBQX alone. n = 9 organoids from 3 batches or 6 organoids from 2 batches (NMDA pre + NBQX). (**B**) NMDA pre in the presence of TTX. n = 9 organoids from 3 batches. Statistical analysis is shown compared to NMDA tox. Data is represented as mean ± SD. n.s. : not significant, *p < 0.05, **p < 0.01, ***p < 0.005, ****p < 0.001. Brown-Forsythe and Welch ANOVA, Games-Howell´s multiple comparisons test.

significant protection mediated by the NMDA pre-treatment. Nevertheless, LDH release level seemed not to be increased by the presence of TTX during the NMDA pre-treatment. These results suggest that NMDA-mediated neuroprotection in human forebrain organoids is independent of the synaptic activity induced by pre-treatment with low doses of NMDA.

If the protective effect of NMDA pre-treatment is mediated by the induction of pro-survival genes, which are markedly upregulated by stimulation with low concentrations of NMDA (**Figure 17C**) then gene expression in response to NMDA exposure should be unaffected by blockers of synaptic activity. To test this, organoids were exposed to TTX or NBQX and gabazine 1 hour before and during the 1-hour-lasting 20 µM NMDA treatment. Subsequent

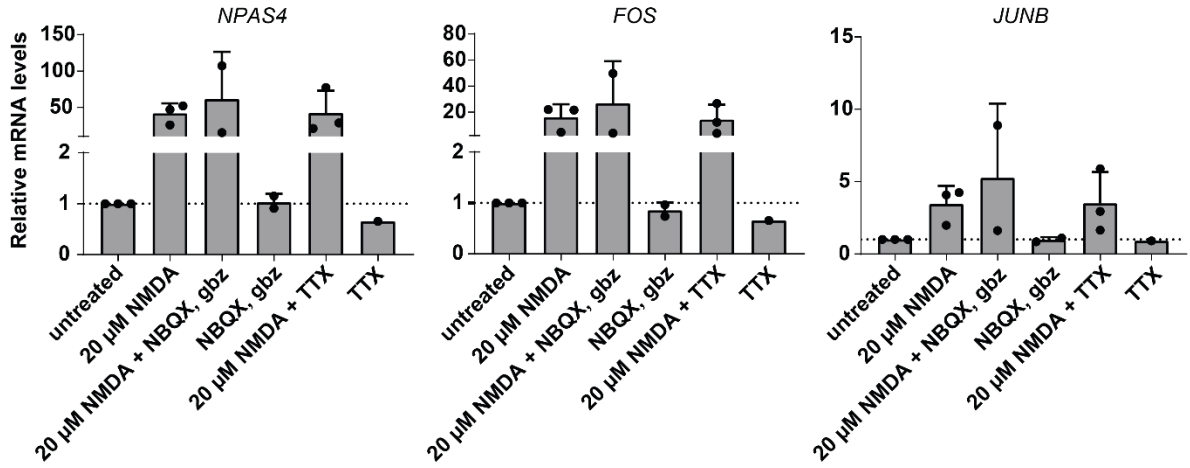

Figure 21: Low doses of NMDA induce transcription independent of synaptic activity
RT-qPCR analysis of relative mRNA expression levels of indicated genes in forebrain organoids treated with 20 µM NMDA for 1 h. To block synaptic activity, organoids were exposed to NBQX (5 µM), gabazine (gbz, 5 µM) or TTX (1 µM) for 2 h, or 1 h before and during the NMDA treatment. Fold changes are calculated relative to an untreated control. n = 1 - 3 batches. Data is represented as mean + SD.

RT-qPCR analysis for *NPAS4*, *FOS* and *JUNB* mRNA levels (**Figure 17C**) revealed an induction in response to NMDA, which was unaltered by the presence gabazine, NBQX or TTX (**Figure 21**). In organoids solely exposed to TTX or NBQX and gabazine, gene expression levels were either unchanged or even decreased compared to baseline, indicative of reduced basal activity. However, due to the small sample size in these two conditions, data is just preliminary and further experiments are required to make a conclusive statement.

Taken together, the results suggest that pre-treatment with a low dose of NMDA protects human neurons against excitotoxicity in a time- and duration-dependent manner. Further, the protective effect of NMDA pre-treatment and its induction of neuroprotective gene expression is not influenced by blockers of synaptic activity. Thus, low level activation of the NMDAR *per se* rather than the associated increase in synaptic activity mediates the upregulation of neuroprotective genes which protect against subsequent excitotoxic stimuli.

2.5. Memantine and C801 protect forebrain organoids against excitotoxic insults

We next explored weather forebrain organoids could serve as a model system for drug testing in human neurons, thereby potentially helping to bridge the gap between animal models and clinical trials critical for translational pharmacology. To begin with, we evaluated the neuroprotective effect of memantine, an uncompetitive antagonist of NMDARs and one of the few FDA-approved therapeutics to treat moderate-to-severe AD (76). Indeed, the presence of memantine 1 hour before and during a toxic NMDA treatment markedly ameliorated the amount of released LDH 24 hours later, indicative of reduced cell death and a protective effect of memantine (**Figure 22A**). Further, we tested the potential of two recently identified small molecule compounds, named C801 and C19 (107), to interfere with excitotoxic cell death. These compounds, or derivates, were previously demonstrated to hinder the interaction between NMDARs and TRPM4, thereby preventing NMDAR-induced cell death (107).

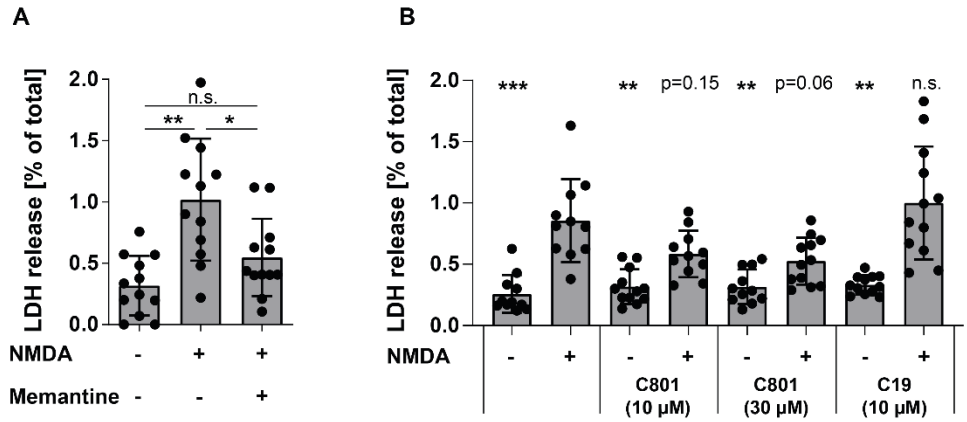

Figure 22: Memantine and C801 protect organoids against excitotoxic cell death
(**A**-**B**) Quantification of LDH release from organoids as a measure of cell death. Organoids were treated with 200 µM NMDA for 1 h and LDH release was assessed after 24 h . Data are shown as % of LDH release relative to total LDH present in respective organoids as determined by complete lysis. (**A**) D1 organoids treated with NMDA. Memantine (10 µM) was present 1 h before and during the toxic insult. n = 12 organoids from 4 batches.
(**B**) D1 organoids treated with NMDA. C801 (10, 30 µM) or C19 (10 µM) were present 1h before and during the toxic insult. n = 12 organoids from 6 batches. Statistical analysis is shown compared to organoids treated with 200 µM NMDA. All data is represented as mean ± SD. n.s. : not significant, *p < 0.05, **p < 0.005, ***p < 0.001. Brown-Forsythe and Welch ANOVA with Games-Howell´s multiple comparisons test (**A**) or Dunnett´s T3 multiple comparisons test (**B**).

Exposure to 10 or 30 µM C801 reduced cell death (10 µM: p = 0.15, 30 µM: p = 0.06) in forebrain organoids in response to toxic NMDA application (**Figure 22B**). In contrast, treatment with 10 µM C19 did not have any effect on relative LDH release, although a similar concentration was demonstrated to interfere with NMDA-induced cell death in rodent cultures (107).

In summary, we demonstrated that forebrain organoids can be used as a screening system to evaluate the effect of both, well-established and newly identified drugs in human neurons.

3. Discussion

This thesis aimed at investigating NMDAR-mediated excitotoxicity and acquired neuroprotection in human iPSC-derived forebrain organoids. Thorough characterization showed that many aspects of human brain development can be modelled in the forebrain organoids generated in the course of this study. Further, the presence of synaptically connected, functional NMDAR-expressing neurons renders our organoids as a suitable tool to investigate the dual action of NMDAR-signalling in human neurons. Using this model system, we revealed that NMDAR activation with high doses of glutamate or NMDA in human neurons is both required and sufficient to induce the typical excitotoxic pathology comprising induction of pro-death signalling, termination of synaptic activity and pro-survival signalling, structural disintegration and ultimately cell death. On the other hand, exposure of organoids to low concentrations of NMDA markedly increased synaptic activity and induced a signalling cascade that was previously identified to promote neuronal survival in rodents. Similarly, pre-treatment with low doses of NMDA protected organoids against excitotoxic insults in a duration- and time-dependent manner. Surprisingly and in contrast to studies in rodents, this NMDA-mediated protection was independent of synaptic activity. Taken together, this study uncovered that the dual action of NMDAR-signalling is preserved in human neurons. The here presented forebrain organoid model represents a suitable system to further consolidate our knowledge about excitotoxicity and acquired neuroprotection in human. Finally, we demonstrated that the organoids may serve as a platform for developing and testing drugs counteracting excitotoxic cell death in human neurons.

3.1. Validation of iPSC-derived forebrain organoids as a model to study NMDAR signalling in human neurons

The first aim of this study was to establish and characterize an iPSC-derived brain organoid system that allows investigating NMDAR signalling in human neurons. So far, a large variety of protocols for the generation of brain organoids has been published. In general, these protocols can be divided into two groups; (a) unguided methods, which rely on intrinsic differentiation mechanisms and result in organoids containing diverse brain regions or (b) guided methods that employ extrinsic application of small molecules or growth factors to generate organoids with defined regional identities (137). Inherently, each system has advantages and disadvantages and the choice of a suitable model system depends on the scientific question. Organoids containing various brain regions (cerebral organoids) are often used to study communication between brain regions (161) or neurodevelopmental disorders with pronounced phenotypes, such as micro- and macroencephaly (162, 163). However, with growing complexity also the degree of variability increases. Hence, for quantitative analysis of

cellular and molecular mechanisms, organoids with a defined regional identity are better suited due to a higher level of reproducibility (164).

To investigate the dual action of NMDAR signalling in human neurons, we intended to utilize a highly reproducible organoid system. Thus, we made use of a human forebrain organoid model, which I had established during my Master's Thesis. The here used method is based on a previously published protocol (129) and further modified to increase reproducibility between organoids through starting with a defined cell number and addition of Wnt- and Shh-inhibitors to promote forebrain fate adoption. Indeed, forebrain organoids generated from two different hiPSC lines were highly comparable in terms of their size and marker gene expression during development (**Figure 4**). Using immunohistochemistry, we confirmed the presence of various cell types within 5 months old organoids, such as neural stem cells, inhibitory and excitatory neurons and glial cells (**Figure 5**). To our surprise, very few excitatory neurons could be detected by sn- and scRNAseq (**Figure 6**), which is in contradiction with other results. However, since the preparation of organoids for sn- or scRNAseq analysis involves dissociation and, in the case of snRNAseq, a fluorescence activated cell sorting (FACS) step, it is more likely that immunohistochemical and electrophysiological results obtained from intact organoids reflect the true estimate for their cellular composition. Indeed, RT-qPCR analysis of intact and dissociated organoids revealed the loss of glutamatergic neurons during dissociation, which was prevented by addition of KyMg. A modified dissociation protocol might enable the acquisition of scRNAseq data sets comprising information about the entirety of cell types within the intact organoids. The phenomenon of cell type composition biases in sn- or scRNAseq data has been described before for rodent kidney tissue. A systematic comparison of various RNA sequencing methods revealed differences in cell type composition between protocols, ranging from underrepresentation to complete loss of cell populations (142). This thorough comparison highlights the importance of a diligent choice of the sequencing method and protocol.

In addition to neurons, our organoid differentiation protocol allows for the generation of astrocytes whose temporal development is consistent with astrogenesis patterns observed in other organoid protocols (129). This development is of particular interest since astrocytes are implicated in controlling proper neuronal development, synapse formation and maturation (165). Indeed, expression of the astrocytic marker GFAP and the pre-synaptic marker SYNAPSIN-1 followed similar induction patterns in forebrain organoids (**Figure 4** and **9**), suggesting that, comparable to what has been reported in rodents, most synapses are generated simultaneously with the emergence of glial cells (165). Electrophysiological measurements revealed excitatory and inhibitory network activity, thereby confirming the presence of functional synapses (**Figure 9**). Analysis of NMDAR subunit profiles revealed

dynamic changes during organoid development. While expression of GluN2B was moderately increased until it plateaued after 18 weeks in culture, GluN2A levels continued to increase (**Figure 10**). These findings suggest that, similar to what has been observed in human post-mortem tissue (111, 112), neuronal maturation in organoids is accompanied by a developmental shift in NMDAR subunit composition from GluN2B- to GluN2A-containing NMDARs. Interestingly, in another study evaluating receptor subunit expression switches during human brain organoid development, GluN2B expression peaks at 200 – 250 days (corresponding to 29 – 35 weeks) (166). In the organoid model presented here, GluN2B expression seems to peak at earlier time points (18-21 weeks), which may be an indication for faster neuronal maturation. The major difference between the two protocols is the forebrain patterning performed in this study and the use of Brainphys medium at later developmental stages. Indeed, BrainPhys medium was demonstrated to accelerate neuronal and synaptic maturation in iPSC-derived neurons (167). However, to confirm that the NMDAR subunit switch occurs earlier in our forebrain organoid model, analysis of later developmental stages would be required.

Taken together, we have established a human iPSC-derived forebrain organoid system containing functional NMDAR-expressing, synaptically connected neurons, thereby fulfilling the qualifications to serve as a model for studying the dual action of NMDAR activation in human neurons. Several features of (human) brain development were reflected during organoid maturation, such as delayed gliogenesis and NMDAR subunit expression patterns, indicating that an intrinsic program regulating development is preserved in our forebrain organoids.

3.2. Forebrain organoids as a model to study excitotoxicity in human neurons

Even though extensively characterized in rodents, glutamate toxicity has been vastly understudied in human neurons. By determining LDH release from forebrain organoids as a measure of toxicity, we observed an increase in cell death upon NMDA- or glutamate exposure in a dose-dependent manner. Pharmacological blockade of NMDARs, but not AMPA or kainate receptors, completely abolished glutamate induced cell death (**Figure 11**), highlighting the predominant role of NMDARs in glutamate toxicity in human neurons. These results are in line with observations in a monolayer culture of 2-3 months old human embryonic stem cell (hESC)-derived cortical neurons (125). Interestingly, in another study using 6-8 week old hESC-derived neurons, NMDAR blockade did not completely abolish glutamate-induced cell death (124). However, in these cultures, an NMDA exposure for 24

hours was required to induce neuronal death. Since immature neurons are intrinsically less sensitive towards excitotoxic insults (168, 169), the requirement of NMDA application for such a long time is likely indicative of low NMDAR expression levels and immature NMDAR subunit expression and localization patterns. Indeed, NMDARs in these cultures were mainly composed of GluN1 and GluN2B subunits, which represent a relatively immature form of the receptor (16). Thus, due to different developmental stages of neurons, the results from this study cannot be directly compared to our findings presented here.

In rodents, excitotoxicity can result in both, apoptotic or necrotic cell death, depending on the strengths of the stimulus (170, 171). Additionally, in the past years, many other forms of cell death have been described in response to excitotoxic insults, such as autophagic cell death, necroptosis and parthanatos (172-174). Our analysis with TEM (**Figure 12**) showed that exposure to NMDA did not change the proportion of cells revealing features of type 2 cell death, which, based on its morphological characteristics, likely represents apoptotic cells (175). However, the fraction of cells resembling type 1 cell death, presumably corresponding to primary or secondary necrosis (176, 177), was strongly increased at early and late stages of NMDA toxicity. By pharmacological interference with known cell death signals, a previous study on excitotoxicity in human neurons identified parthanatos as the main type of cell death induced by NMDA treatment (125). Parthanatos is a form of cell death induced by DNA damage and subsequent poly (ADP-ribose) polymerase (PARP) activation (178). PARP activation, however, is also frequently described in a type of regulated necrosis in different cell types, including human brain (179-181). Thus, it remains to be elucidated if NMDA induced cell death occurs via distinct mechanisms in 2D and 3D human neuron cultures or if the necrotic cell death observed in our organoids is indeed also mediated by PARP activation. This could, however, be addressed through application of NMDA stimuli in the presence of PARP inhibitors.

Interestingly, we observed more viable cells 24 hours after NMDA exposure than in the early stage of excitotoxicity (**Figure 12**). Since cells revealing the necrotic morphology observed here are very unlikely to recover, an increased number of viable cells suggests enhanced proliferative activity. Indeed, several studies in rodents showed increased proliferation of glial and neural stem cells in response to excitotoxic insults (182, 183), suggesting that a similar mechanism might occur in human forebrain organoids. In line with this hypothesis, we observed an increase in relative mRNA levels of *AQP4* and *NESTIN*, which are frequently used marker genes for glia cells and neural stem cells, respectively, after NMDA treatment for 24 hours (**Figure 14**). To elucidate if the increased number of viable cells 24 hours after NMDA treatment indeed is a result of increased proliferation in human forebrain organoids, it would be interesting to perform an immunohistochemical or (flow) cytometrical analysis of

proliferation markers, such as KI67. Additionally, such an approach could be combined with cell type specific antibodies, thereby potentially revealing the identity of the proliferating population(s).

In summary, we demonstrated that many hallmarks of excitotoxicity described in rodents are preserved in human neurons. Thus, the here presented forebrain organoid model provides a suitable system to further investigate human excitotoxic processes.

3.3. The dual action of NMDAR signalling is preserved in human neurons

In rodents, exposure to NMDA induces opposing cellular outcomes depending on the concentration: high doses trigger an excitotoxic pathway, which ultimately results in cell death, whereas treatment with low NMDA doses promotes neuroprotection (95). The reason for these opposing effects is thought to be based on the differential activation of downstream signalling cascades (13, 184). Thereby, exposure to low NMDA concentrations triggers synaptic activity accompanied by CREB-dependent transcription of pro-survival genes and AKT-mediated suppression of death-promoting genes (95). Application of high NMDA doses, in contrast, causes termination of synaptic activity and shut-off of pro-survival signalling via CREB and AKT (87, 159). It was, however, not known if these dual, dose-dependent effects of NMDAR activation are preserved in human neurons. In human forebrain organoids, we showed that application of high and low NMDA doses also results in opposing cellular responses. Treatment with 20 µM NMDA caused a strong increase in inhibitory and excitatory synaptic activity, which was completely abolished by subsequent exposure to high NMDA concentrations (**Figure 16**). We further also detected dose-dependent opposing effects of NMDAR signalling on CREB phosphorylation patterns, with low NMDA doses triggering sustained CREB activation whereas high doses caused a transient pCREB increase followed by fast dephosphorylation (**Figure 17**). Similar kinetics have previously been observed in cultured rodent neurons in response to high and low NMDA doses (155). In these cultures, however, phosphorylation levels of CREB dropped below baseline after treatment with 100 µM NMDA, whereas in forebrain organoids pCREB decreased to levels comparable to untreated conditions. This divergence might be caused by higher basal activity in rodent monolayer cultures compared to forebrain organoids. Alternatively, the effects of NMDAR signalling on CREB phosphorylation might be diluted by the presence of non-neuronal cell types. Besides neurons that account for approximately half of the cells, forebrain organoids further contain glia cells and neural stem cells (**Figure 4 - 6**), which were previously shown to express CREB (185-187). Additionally, the distinct pCREB level after toxic NMDA exposure in rodent monolayer and human forebrain organoids could be caused by differences in dephosphorylation patterns. In rodents, several candidates involved in CREB

dephosphorylation have been identified, including protein phosphatase 1 (PP1) (188, 189) and phosphatase and tensin homolog (PTEN) (190). To investigate if these phosphatases also mediate CREB dephosphorylation in the human forebrain excitotoxicity model, treatment with toxic NMDA concentrations in the presence of specific phosphatase inhibitors and subsequent analysis of pCREB levels would be required.

In rodents, stimulation of NMDARs, either via induction of synaptic activity or application of low doses of NMDA, exerts a neuroprotective effect via CREB-mediated transcription of pro-survival genes (83). In line with our data on synaptic activity and CREB phosphorylation, application of low concentration NMDA resulted in a robust upregulation of immediate early and pro-survival genes in forebrain organoids compared to organoids exposed to high NMDA concentrations (**Figure 17**). Even though not significant, we also observed an differential response in the previously demonstrated neuroprotective genes *ATF3* and *BTG2* (83), indicating that treatment with low concentrations of NMDA might have a survival-promoting effect. Surprisingly, we could not detect an increase in the mRNA expression levels of *BNDF* and *INHBA* in response to low concentration NMDA treatment. This is in contrast to results obtained from rodent primary culture, in which a robust induction of these genes can be observed in response to increased synaptic activity or NMDA application (83, 191). Further, neuronal activity in rodent monolayer cultures was shown to promote the release of BDNF, which then binds to the tyrosine receptor kinase B (TrkB) receptor, thereby initiating neuroprotective signalling cascades (192). One important mediator of this protective mechanism is *inhba*, which is transcriptionally upregulated in response to BDNF stimulation (193). In contrast to rodent monolayer cultures, it appears that *BDNF* and *INHBA* are not induced in human organoids in response to NMDA. Alternatively, it could be that these genes are upregulated, but with different kinetics than observed in rodent monolayer cultures. To answer this question, it would be interesting to repeat the NMDA treatments followed by gene expression analysis at various additional time points.

Of note, even though *BDNF* and *INHBA* are not induced in the forebrain organoids 4 hours after NMDA exposure, pre-treatment with a low dose of NMDA provided a protective effect against excitotoxic cell death at this time point (**Figure 19**). Thus, it may be that NMDA-induced neuroprotection in human organoids works independent of these genes. This assumption could be easily tested by performing the NMDA pre-treatment in the presence of BDNF-signalling blockers, for example via TrkB-IgG, followed by subsequent analysis of excitotoxicity-induced cell death. On the other hand, it would be interesting to evaluate if application of exogenous BDNF is able to promote neuroprotection in forebrain organoids, similar to what has been described in rodents (193-195).

3.4. Pre-treatment with low doses of NMDA protects human forebrain organoids against excitotoxic insults

In this study, we demonstrated that a pre-treatment with a subtoxic concentration of NMDA is able to protect human forebrain organoids against excitotoxic insults (**Figure 18),** similar to what has been shown in rodents (95). We further revealed that this protection is highly dependent on the duration of the NMDA pre-treatment: only the exposure to low NMDA doses for 30 minutes or 1 hour provided neuroprotection, whereas shorter or longer treatments did not ameliorate excitotoxic cell death. Supposedly, application of NMDA for 5 minutes is not sufficient to induce long-lasting protective effects. It has been previously reported that brief or sustained periods of neuronal activity elicit different gene expression programs (196). According to this study, sustained activity for several hours induces three distinct waves of gene expression: rapid primary response genes, delayed primary response genes and secondary response genes. Brief neuronal stimulation, in contrast, selectively induced the first, but not the second or third wave of gene induction. Thus, in our human organoids, it may be that genes responsible for NMDA-mediated neuroprotection are upregulated in one of the latter waves and thus not induced by the short stimulation. Indeed, *Atf3*, a gene with neuroprotective properties (84) that is upregulated in the forebrain organoids upon NMDA exposure (**Figure 17**), belongs to the delayed primary response genes (196). Further, also the amplitude and duration of the first wave differ between brief and sustained neuronal activity. Whereas rapid primary response genes are still upregulated after 6 hours with the sustained stimulation, these genes are almost back to baseline levels after 4 hours with the brief activity protocol. Hence, the lack of protection after a 5-minute–NMDA exposure could also be a result of weaker activation of genes representing the first wave. In order to evaluate the potential reason for the duration-dependent NMDA-mediated protection, it would be interesting to compare gene expression patterns after either a 5 minute or 1 hour NMDA exposure.

This difference in gene expression patterns, however, does not explain why prolonged exposure to low NMDA concentrations did not ameliorate excitotoxic cell death. The reason for this phenomenon is the low dose NMDA-induced toxicity itself. Exposure to 20 µM NMDA for periods extending 1 hour caused an increase in LDH release in a time-dependent manner (**Figure 18**). A similar response has been described before in murine neurons, where the same concentration of NMDA caused pro-survival signalling after brief simulation and cell death after prolonged exposure (159). Presumably, bath application of NMDA activates both, protective and toxic signalling. During short-term treatment with low NMDA doses, the pro-survival signalling is able to combat the negative effects. In contrast, after extensive NMDAR activation caused by high agonist concentrations or prolonged exposure, the toxic signalling prevails. Intriguingly, a previous study from our group observed a neuroprotective effect after

pre-treatment of rodent neurons with 10 μM NMDA for 24 hours (95). Thus, it may be that a very low concentration of NMDA does either not activate toxic signalling at all or that the pro-survival program continuously supresses the toxic aspects of NMDAR activation. It would be interesting to see if this phenomenon can also be observed in human neurons. For this, forebrain organoids could be treated with NMDA concentrations lower than 20 μM for 24 hours followed by LDH release analysis.

We further also investigated if the time period between NMDA pre-treatment and the toxic insult affects the protective effect and found that an interval of at least 4 hours between the different stimuli is required to significantly reduce cell death (**Figure 19**). In rodent cultured neurons, NMDA-mediated protection was shown to require RNA and protein synthesis (197). It is very likely that acquired neuroprotection in human neurons depends on transcription and translation, too, and thus, a certain period of time is needed to build up the protective shield. Our preliminary attempts to test this hypothesis, however, were not successful since the transcriptional blocker Actinomycin D induced toxicity itself (data not shown). Thus, to verify this assumption, a more thorough titration of the treatment interfering with transcription is necessary. Additionally, the effect of protein synthesis inhibition on NMDA-mediated protection needs to be clarified by, for example, exposure to cycloheximide.

In rodent primary neurons, acquired neuroprotection was shown to be dependent on enhanced synaptic activity, either induced by removal of inhibitory inputs or application of low concentrations of NMDA (83, 95). In this model, inhibition of action potential firing by TTX during NMDA exposure completely abolished the protective effect (95). To our surprise, the low dose NMDA-mediated protection was unaltered by blocking synaptic activity either via NBQX and gabazine or TTX in human forebrain organoids (**Figure 20**). Furthermore, these synaptic activity blockers did also not affect the NMDA-induced upregulation of *NPAS4*, *FOS* or *JUNB* (**Figure 21**). These results again are in contrast with data from the previous study in rat hippocampal neurons, in which CRE-dependent gene expression induced by exposure to 10 μM NMDA for 6 hours was markedly impaired by co-application of TTX (95). Interestingly, in another study using rat cortical neurons, treatment with 1 or 5 μM NMDA for 10 minutes triggered sustained CREB phosphorylation even in the presence of TTX (87). Hence, even though this effect of NMDAR-mediated signalling was not evaluated in this study, one could assume that the observed CREB activation may induce the induction of neuroprotective genes, as previously reported (152, 198). If this assumption is correct, it would imply that NMDAR-mediated neuroprotection may also occur independently of synaptic activity in rodent neurons, similar to what we have observed in human forebrain organoids. Due to differences in the magnitude and duration of the NMDA treatment, however, it is impossible to compare the different studies in rodent and human neurons. For a systematic

analysis, one should repeat the prolonged exposure to 10 µM NMDA in the presence and absence of TTX in forebrain organoids. Additionally, it should be evaluated if a brief NMDA treatment mediates neuroprotection in rodent neurons and if this potential protective effect is sensitive to TTX application.

3.5. Forebrain organoids as a model for drug testing in human neurons

To date, pharmacological interference with excitotoxic cell death in pathological conditions of the human brain is limited. Although numerous drugs with demonstrated efficiency in rodents have been developed, the vast majority failed in clinical trials with human probands (78, 199). The causes for these translational failures are manifold and include inadequate animal models, inapplicable time windows, lack of functional evidence of efficiency or unforeseen adverse effects (200). Several of the aforementioned problems can be circumvented by improving study designs, however, genetic species differences still remain. These differences between human and mouse brains include the presence of certain cell types, protein and gene abundance as well as transcriptional and functional dissimilarities (201-204). Further, even conserved cell types were shown to markedly differ in their gene expression patterns between mouse and human, including those for neurotransmitter receptors (205). Thus, it is not surprising that many drugs, whose safety and efficiency were evaluated in rodents, fail in human patients. In order to bridge the gap between animal studies and clinical trials, human iPSC-derived organoids could serve as an intermediate platform for drug testing. We showed that application of memantine, a drug used to treat certain cases of AD, provided protection against excitotoxic insults (**Figure 22**), thereby demonstrating the suitability of the here presented forebrain organoids for testing the efficacy of pharmaceuticals.

Another reason for the past failures of therapeutics against excitotoxic cell death may be the choice of the drug targets. Traditionally, a vast number of compounds have been developed to interfere with NMDAR activation by antagonizing the ion channel-, glutamate or glycine binding site (206-208). These drugs, however, not only interfere with pathological but also with physiological NMDAR signalling. Hence, treatment of patients with these NMDAR antagonists led to severe side effects such as hallucinations, sensory disturbances or hypertension and in some cases even increased mortality (78, 209). Because of these detrimental effects of general NMDAR antagonism, current pharmaceutical development aims at specifically blockade of toxic NMDAR signalling. Different concepts are currently under investigation such as blockade of the excitotoxicity-activated protease calpain (210) or interference with the activation of the pro-death gene *P53* (211). Another approach from our group focused on hindering the interaction between NMDARs and TRPM4, which protects

neurons against excitotoxic cell death via an unknown mechanism (107). Strikingly, a derivate of a small-molecule compound, named C801, which disrupts the NMDAR/TRPM4 complex, was able to also reduce cell death in response to excitotoxic insults in the forebrain organoids (**Figure 22**). C19, however, did not ameliorate NMDA-toxicity in the organoids, although a similar concentration was demonstrated to provide neuroprotection in rodent primary cultures (107). These results highlight the need for evaluating drug efficiency in human neurons before starting clinical trials. Aside from their neuroprotective potential, neither C801 nor C19 induced toxicity themselves for the given exposure time. To exclude side effects on human neurons after prolonged drug exposure, forebrain organoids can further be used to assess the safety of long-term treatments.

Besides generating forebrain organoids from healthy donor-derived iPSCs, it is also possible to employ iPSCs from patients with neurodegenerative disorders as starting material. The resulting organoids may enable drug screening on human neurons in the full genetic context of a particular disease. Thereby, patient iPSC-derived organoids represent a superior tool for drug testing compared to rodents, in which disease phenotypes are artificially induced.

4. Materials and Methods

4.1. hiPSC culture

hiPSC lines

The human D1 and HD6 iPSC lines were obtained from Dr. Jochen Utikal (DKFZ). They were generated from healthy human fibroblasts with an inducible polycistronic lentiviral reprogramming vector encoding for KLF4, MYC, POU5F1 and SOX2 (212, 213).

Matrigel coating

Matrigel (Corning) was diluted according to the manufacturer in ice cold DMEM/F-12 (Thermo Fisher Scientific). Immediately after mixing, the coating solution was added to culture ware placed on ice. Plates were incubated for at least 1 hour at room temperature (RT). If not used the same day, coated plates were sealed with Parafilm and stored at 4 °C for up to 2 weeks. Before usage coating solution was removed and stem cell culture medium was added.

Culture of human iPSCs

Human D1 and HD6 iPSCs were cultured on Matrigel-coated 6-well plates in mTeSR Plus (STEMCELL Technologies) including Normocin (1:1000, Invivogen). Medium change was performed every 2 to 3 days with RT-warmed medium. Areas of spontaneous differentiation characterized by irregular cell morphology within a colony were removed mechanically. Human iPSCs were passaged when confluency reached 50-70 %. 15 to 20 minutes before passaging, 10 µM ROCK inhibitor (Y-27632 dihydrochloride, Tocris) was added to the cells. Cells were washed once with warm DMEM/F-12 followed by an incubation with Dispase (Thermo Fisher Scientific) for 5 to 7 minutes at 37 °C. When detachment of colonies was visible, Dispase was removed and cells were washed two times with DMEM/F-12. Colonies were collected in DMEM/F-12 by gentle mechanical detaching and centrifuged for 5 minutes at 75 x g. Subsequently, cells were taken up in stem cell culture medium and carefully triturated 2 to 3 times to break up bigger aggregates. Cells were plated onto Matrigel coated 6-well plates, placed in a 37 °C incubator and not disturbed for the next 24 hours to improve attachment.

4.2. Generation and maintenance of forebrain organoids

For the formation of forebrain organoids human D1 iPSCs from P49-P57 and HD6 iPSCs from P26-P27 were used. 15 to 20 minutes before starting, 10 µM ROCK inhibitor was added to the cells and differentiated regions were removed mechanically. Cells were washed once with warm DMEM/F-12 and incubated for 6 to 10 minutes in Accutase (STEMCELL Technologies) at 37 °C. When dissociation of colonies became visible, Accutase was stopped with warm DMEM/F-12. Cells were collected and centrifuged for 5 minutes at 75 x g. Subsequently, cells were resuspended in mTeSR containing 30 µM ROCK inhibitor. For organoid formation, 10^4 cells in a total volume of 100 µl medium were transferred into each well of a 96-well plate (Thermo Fisher Scientific). Plates were centrifuged for 5 minutes at 75 x g to aggregate iPSCs and placed in a 37 °C incubator overnight. The next day, hiPSC aggregates were collected, taken up in neural induction medium (DMEM/F-12, GlutaMax (1:100), 2x B27 supplement without Vitamin A, 1x N2 supplement, ß-Mercaptoethanol (1:1000 (all Thermo Fisher Scientific), 500 nM Dorsomorphin dihydrochloride (Tocris), 5 ng/ml recombinant Noggin (R&D Systems), 10 µM SB 431542 (Tocris), Normocin (1:1000)) and transferred into non-coated 35 mm dishes. Medium was changed daily and from day 2 on FGF-2 (10 ng/ml, Peprotech) was added. After 7 days in neural induction medium, free-floating organoids were moved to neural medium (Neurobasal (Thermo Fisher Scientific), GlutaMax (1:100), 1x B27 supplement without Vitamin A, Normocin) supplemented with FGF-2 (10 ng/ml) and EGF (10 ng/ml, Peprotech) to promote proliferation. For the first 7 days, medium was changed daily followed by medium changes every other day for another week. To support survival and differentiation of neural precursor cells within the organoids, FGF-2 and EGF were replaced by BDNF (10 ng/ml, Peprotech) and NT-3 (10 ng/ml Peprotech) from day 21 on. After additional 2 weeks, organoids were transferred into a maintenance medium (BrainPhys (STEMCELL Technologies), GlutaMax (1:100), 1x B27 supplement without Vitamin A, Normocin) which was changed 2 times a week. To ensure forebrain fate adoption, IWP-2 (2 µM, Sigma Aldrich) and Cyclopamine (1 µM, Merck) were added to the medium for the first 21 days. Every week images of 2-8 individual organoids per batch and age were acquired using an Axio Vert.A1 microscope (Zeiss). For size measurements, an ellipse was placed on the images in a way that it covers the whole organoid and Feret´s diameter was measured (ImageJ).

4.3. Immunohistochemistry

To prepare organoids for cryosectioning, they were washed once with PBS followed by fixation for 1 hour in Histofix (Carl Roth). For cryopreservation, organoids were washed 2 times with PBS and stored in 30 % sucrose solution for 24 to 48 hours at 4°C. Following, forebrain organoids were transferred into embedding medium (NEG-50, Thermo Fisher Scientific), snap-frozen on dry ice and stored at -20 °C. For immunohistochemistry, 20 µM thick sections were obtained using a cryostat (CM1950, Leica) and transferred onto histological slides (SUPERFROST PLUS, Thermo Fisher Scientific). If not used immediately, cryosections were stored at -20 °C. Cryosections were thawed at RT for 10 to 20 minutes. For permeabilization, sections were incubated in 0.25 % Triton X-100 (in PBS) for 20 minutes if not stated otherwise. For certain antibodies, antigen-retrieval instead of permeabilization was performed as indicated in **Table 3**. For this, cryosections were incubated for 30 minutes in a Sodium Citrate Buffer (10 mM Sodium Citrate, 0.05 % Tween 20, pH 6) at 95 °C. After permeabilization or antigen retrieval, sections were washed with PBS and incubated in blocking solution (2% bovine serum albumin diluted in PBS+0.1 %) for 1 to 4 hours. Then, sections were incubated overnight at 4 °C with primary antibodies (listed in **Table 3**) diluted in respective blocking solution. The next day, sections were washed with PBS + 0.1 % Tween and secondary antibodies diluted in blocking solution were applied for 1 hour. After additional washes with PBS + 0.1 % Tween cryosections were mounted for microscopy on glass coverslips using Mowiol containing Hoechst 33258 (Serva Biochemica) for visualization of nuclei. Slices were imaged using a TCS SP8 microscope (Leica).

Antibody	Company	Number	Dilution	Protocol modifications
Doublecortin (DCX)	Santa Cruz	#sc-8066	1:100	-
FOXG1	Abcam	#ab18259	1:400	Antigen retrieval: 20 min at 95°C in Sodium-Citrate buffer
GAD67	Millipore	#MAB5406	1:500	-
GFAP	Cell Signalling	#3670	1:500	-
MAP2	Millipore	#MAB3418	1:500	-
MYT1L	Sigma Aldrich	#ABE2915	1:1000	Blocking solution: 3 % BSA+0.5 % Triton, antibodies diluted in 3 % BSA+0.2% Triton
NESTIN	Millipore	#MAB5326	1:400	-
SOX2	Santa Cruz	#sc-17320	1:100	Permeabilization: 0.25 % Triton for 60 minutes
VGLUT2	Synaptic Systems	#135 402	1:400	-
VGLUT2-Alexa488	Sigma Aldrich	#MAB5504A4	1:250	No secondary antibody used

Table 3: Antibodies used for immunohistochemistry and respective protocol modifications

4.4. RNA extraction, cDNA synthesis and RT-qPCR

For RT-qPCR analysis, three organoids per condition were transferred into 1.5 ml Eppendorf tubes and snap-frozen on dry ice or in liquid nitrogen after removal of residual medium. RNA from forebrain organoids was isolated under RNAse free conditions through TRIzol extraction. For this, 1 ml TRIzol (Thermo Fisher Scientific) was added per sample and organoids were lysed by vigorous pipetting. The resulting homogenate was incubated for 5 minutes at RT. Then, 0.2 ml chloroform was added and tubes were shaken vigorously for 15 seconds followed by a 2 to 3 minutes incubation. Samples were centrifuged at 12.000 g for 15 minutes at 4° C and the upper, aqueous phases were transferred into new tubes. After addition of 0.5 ml isopropanol, samples were vortexed thoroughly, incubated for 10 minutes at RT and centrifuged at 12.000 g for 10 minutes at 4 °C. Supernatant was carefully discarded and the remaining RNA was washed by addition of 1 ml 75 % ethanol. After another centrifugation at 12.000 g for 5 minutes at 4 °C, supernatant was removed completely and the RNA pellet was dried for 10 to 15 minutes at RT. Then, the pellet was redissolved by addition of 30 µl RNAse-free water and incubation for 20 minutes at RT. cDNA was synthesized using the SuperScript III Reverse Transcriptase Kit (Thermo Fisher Scientific) according to the manufacturer´s protocols. After synthesis, 30 µl Tris-EDTA buffer per reaction was added and cDNA was stored at -20 °C. RT-qPCRs were run on a StepOnePlus Real-Time PCR System (Applied Biosciences), using 96-well microtiter plates, the Power SYBR Green PCR Master Mix (Thermo Fisher Scientific) and 250 nM of each primer of a desired primer pair (**Table 4**). TBP (TATA box binding protein) mRNA served as internal standard to determine relative mRNA levels.

Primer	**Sequence**	
AQP4	Fwd.	GAG AGT CGT CAC ACC AGT G
	Rev.	TCC CAG CCA GGA AGT AAC TA
ATF3	Fwd.	CGC TGG AAT CAG TCA CTG TCA G
	Rev.	CTT GTT TCG GCA CTT TGC AGC TG
BTG2	Fwd.	GCA GAG GCT TAA GGT CTT CAG C
	Rev.	TGG TTG ATG CGA ATG CAG CGG T
FOS	Fwd.	TGC AGC CAA ATG CCG CAA C
	Rev.	TCG GTG AGC TGC CAG GAT G
FOXG1	Fwd.	ACC CTC TTT GCC AAG TTT TAC GAC
	Rev.	ACG TTC ACT TAC AGT CTG GTC C
GFAP	Fwd.	CCA CTT GCA GGA GTA CCA GGA
	Rev.	GGT CTG CAC GGG AAT GGT GAT
JUNB	Fwd.	CAA GGG ACA CGC CTT CTG AAC
	Rev.	AAG CGA GGG GGT GTC CGT AAA
MYT1L	Fwd.	TCC AAT TCC CAG ATG GAA GCC
	Rev.	TTC GCC AGC TCG TGG AGG AGA
NESTIN	Fwd.	TCA AGA TGT CCC TCA GCC TGG A
	Rev.	AAG CTG AGG GAA GTC TTG GAG C

NEUN	Fwd.	CAA GCG GCT ACA CGT CTC CAA CAT
	Rev.	GCT CGG TCA GCA TCT GAG CTA GT
NPAS4	Fwd.	GTG AGG CTA CAG GCC AAG AC
	Rev.	AGG GCA GCA TGG TCG GAG TG
OCT4	Fwd.	GGG AAG GTA TTC AGC CAA AC
	Rev.	CTT TCT CTT TCG GGC CTG CAC
P53	Fwd.	GCC CAA CAA CAC CAG CTC CT
	Rev.	CCT GGG CAT CCT TGA GTT CC
PAX6	Fwd.	GCA CCA GTG TCT ACC AAC CAA
	Rev.	CCC AAC ATG GAG CCA GAT GTG AA
SOX1	Fwd.	CGC TGA CAC CAG ACT TGG GTT
	Rev.	ACA AAA GTG GGC TTC GCC TCT
TBP	Fwd.	GCC TTG TGC TCA CCC ACC AAC AAT TT
	Rev.	GGT ACA TGA GAG CCA TTA CGT C

Table 4: Forward (Fwd.) and reverse (Rev.) primers used for RT-qPCR analysis

4.5. Single nuclei and single cell RNA sequencing

Single nuclei sequencing

"Nuclei were isolated from frozen organoids according to a protocol adapted from (214). Briefly, organoids were homogenized by trituration on ice in 250 mM sucrose, 25 mM KCl, 5 mM MgCl2, 10 mM Tris-HCl [pH 8], 0.1 % IGEPAL, 1 µM DTT, 0.4 U/µl, Murine RNase Inhibitor (New England Biolabs), 0.2 U/µl SUPERas-In (Thermo Fisher Scientific) and Hoechst 33258. After 5 min of incubation, remaining tissue debris was pelleted and removed by centrifugation at 100 x g for 1 min. Nuclei in the collected supernatant were pelleted at 400 x g for 5 min. Then, nuclei were washed once in homogenization buffer before they were resuspended in 1x PBS. Fluorescence activated cell sorting (BD FACSAria ii, 70 µm nozzle, BD Biosciences) was used to separate single nuclei from remaining debris and aggregates according to forward and sideward scatter properties, as well as DNA content based on Hoechst signal. Following sorting, nuclei were counted on Countess II FL Automated Cell Counter (Thermo Fisher Scientific) and 15 000 nuclei were employed for the single nuclei RNA sequencing experiment using the 10x Chromium Single Cell 3' v3.1 Gene Expression Kit (10x Genomics) following the manufacturer's instructions. Quantification and quality control of libraries was performed using a Qubit Fluorometer and the High Sensitivity NGS Fragment Kit for Agilent's Fragment Analyzer (Agilent). The library was sequenced on an Illumina NextSeq500/550 (Illumina) using the High Output Kit v2.5 (75 Cycles) with paired-end sequencing and 26 cycles for Read 1, 57 cycles for Read 2 and 8 cycles for i7 index to a depth of ca. 300 million reads." (Bauersachs et al., in submission)

Single cell RNA sequencing

"Dissociation of organoids was performed using the Papain Dissociation System (Worthington Biochem) and components were prepared according to manufacturer´s instructions. If dissociation was performed in presence of kynurenic acid and magnesium, 10% KyMg (10 mM kynurenic acid, 100 mM MgCl2, 5 mM HEPES, 0.5 % v/v Phenol red, 12.5 mM NaOH) was included in all components. 12 – 14 organoids per condition were transferred into papain solution and incubated for 15 minutes at 37 °C on a shaker. Subsequently, organoids were carefully titrated 10 – 15 times with 10 – 200 µl pipette tips. After a centrifugation step at 300 x g for 1 minute, supernatant was removed and the papain incubation and titration step were repeated. To remove debris, the cell solution was transferred into a new tube and centrifuged at 200 x g for 5 minutes. From this time point on, the following steps were performed on ice. To remove small debris, the resulting cell pellet was resuspended in 400 µl medium (1080 µl Earle´s Balanced Salt Solution (EBSS), 120 µl albumin-ovomucoid solution, 60 µl DNAse) and transferred onto 600 µl ovomucoid solution. After a centrifugation at 70 x g for 6 minutes, the supernatant was discarded and the density gradient step was repeated. Subsequently, cells were either placed on ice and consigned for single cell RNA sequencing (similar to single nucleus RNA sequencing, see above) or frozen on dry ice for RT-qPCR analysis." (Bauersachs et al., in submission)

Single nucleus RNA sequencing data processing

"10x CellRanger (v 4.0.0) was used to demultiplex the raw sequencing data, align the extracted FASTQ files to the reference genome (assembly GRCh38.p13, annotation GRCh38.91) and count the reads mapping to exons and introns as the number of unique molecular identifiers (UMIs) per gene per droplet. The resulting count matrix was analyzed using the Seurat package (v 3.2.1) (215). Nuclei-containing droplets determined by CellRanger were further filtered using the parameters UMI>1100 and pct.mito <2.5, resulting in a dataset of 3333 nuclei. For clustering and to generate the UMAP, the dataset was normalized and scaled using the function SCTransform (216) and clustered at a resolution of 0.03. Resulting clusters were annotated according to expression of known marker genes." (Bauersachs et al., in submission)

Correlation analysis

"For the human organoid dataset the raw UMI counts were normalized and scaled using the NormalizeData() and ScaleData() functions in Seurat. The normalized and scaled counts were then summed up per cluster per gene. For the developing mouse brain dataset (145) the summed counts per cluster from single cell RNA sequencing data were downloaded from http://mousebrain.org/downloads.html (downloaded April 1st 2021). Clusters belonging to classes annotated as Undefined, Bad cells or Blood were removed. The two datasets were

correlated (Spearman's correlation) based on the expression of 15396 one-to-one orthologous genes obtained using the R package biomaRt (217). In the heatmap, rows and columns are hierarchically clustered. Clusters from the developing mouse brain belonging to the classes Neuron, Neuroblast, Radial Glia and Glioblast contained the clusters with the highest correlations to the organoid dataset. To avoid overcrowding, the class and the likely region of origin of only clusters belonging to these four classes are annotated in the heatmap." (Bauersachs et al., in submission)

4.6. Immunoblotting

Three organoids per condition were collected in 1.5 ml Eppendorf tubes and residual medium was removed. Samples were snap frozen in liquid nitrogen and stored at -80 °C. For lysis, RIPA buffer (150 mM sodium chloride, 1 % Triton X-100, 0.5 % sodium deoxycholate, 0.1 % SDS, and 50 mM Tris-HCl, pH 8) supplemented with 1 % cOmplete Protease Inhibitor Cocktail (Merck) was added and organoids were lysed by vigorous pipetting. Protein content was determined via Bradford Assay (Bio-Rad Laboratories) and 20 µg protein per sample were resolved on 6.5 or 9 % SDS-PAGE gels. Then, proteins were transferred onto 0.45 µm nitrocellulose membranes (Thermo Fisher Scientific for 1 hour 50 minutes at 20 V using a wet blot system. Membranes were blocked with 5 % non-fat dry milk (in PBST) for at least 1 hour. Blocked membranes were incubated with primary antibodies (**Table 5**) diluted in 5 % non-fat dry milk (in PBST) or 5 % BSA (in PBST) over night at 4 °C. The next day, membranes were washed 4 times for 5 minutes with PBST and incubated with secondary antibodies diluted in 5 % non-fat dry milk (in PBST) for 45 minutes. Membranes were then again washed four times with TBST for 5 minutes and bound antibodies were visualized by ECL. Acquired images were quantified and processed in ImageJ.

Antibody	Supplier	Catalogue no.	Dilution	Dilutant
CREB	Cell Signalling	#4820	1:2000	BSA
pCREB	Millipore	#06-519	1:1000	BSA
GluN1	Cell Signalling	#5704	1:1000	BSA
GluN2A	Abcam	#ab17345	1:500	BSA
GluN2B	Cell Signalling	#4205	1:500	non-fat dry milk
SYNAPSIN-1	Synaptic Systems	#106011C5	1:1000	
α-TUBULIN	Sigma Aldrich	#T9026	1:400.000	non-fat dry milk

Table 5: Antibodies and respective blocking reagents used for immunoblotting

4.7. Lactate dehydrogenase (LDH) assay

One day before the experiment, three organoids per condition were transferred into single wells of a 4-well plate containing 0.5 ml maintenance medium. Treatments were performed as indicated. At indicated time points, 5 µl of medium from each well were collected and transferred into 95 µl LDH storage buffer (200 mM Tris-HCl pH 7.3, 10 % Glycerol, 1 % BSA). At the end of each experiment, 10 µl 10 % Triton X-100 was added to each well for lysis. After one hour of incubation, organoids were mechanically lysed via thorough pipetting and 5 µl lysate was collected and diluted as described before. Collected samples were stored at -20 °C in LDH storage buffer until use. To perform the LDH assay (LDH-Glo™ Cytotoxicity Assay, Promega), samples were placed on the bench until they reached RT. After vortexing, 10 µl of each sample was transferred into a well of a white, flat bottom 96-well plate (Corning). Then, the components of the LDH assay (Detection Enzyme and Reductase Substrate) were mixed according to the manufacturer and 10 µl were added to each sample. After an incubation time of 30 minutes, luciferase activity was measured via a luminometer (Glomax 96 Microplate luminometer, Promega). For normalization, relative light units (RLUs) obtained from a well containing only medium were subtracted (with the minimum at 0 indicating no detected release of LDH) and percentage of sample RLUs relative to the respective lysate was calculated using following formula:

$$normalized\ RLU = \frac{(RLU\ sample - RLU\ background)}{RLU\ lysate} * 100$$

4.8. Electron microscopy

Transmission electron microscopy (TEM)

"Organoids were prepared for transmission electron microscopy as previously described (218). Ultrathin sections were examined with an electron microscope (EM 10 CR, Zeiss) at an acceleration voltage of 60 kV. To investigate cell viability states images of all cells within one ultrathin section per organoid and condition were acquired. For quantification blind scoring was performed (Blinder, Solibyte Solutions) using following criteria: Healthy cells (equally distributed chromatin, presence of organelles, intact membranes), Type 1 cell death (condensed chromatin, cell swelling and/or disturbed membrane integrity), Type 2 cell death (condensed chromatin, cell shrinkage, no or few organelles, presence of clear vacuoles), Other (no clear definition possible). For quality control, 10% of all images were shown repeatedly and 89.9% of these images obtained similar scoring. Images of the category "Other" were excluded from analysis." (Bauersachs et al., in submission)

Scanning electron microscopy (SEM)

"Scanning electron microscopy (SEM) was performed as previously described (219). Briefly, the samples were fixed with 2% glutaraldehyde in 0.1 M sodium phosphate buffer. After washing and postfixation with 2% osmium tetroxide/ 1.5% potassium ferrocyanide for 1 h, they were washed and dehydrated with an ascending series of ethanol and pure acetone before critical point drying. The samples were then sputter-coated with an 80% gold, 20% palladium alloy and examined with a ULTRA 55 field-emission scanning electron microscope (ZEISS)." (Bauersachs et al., in submission)

4.9. Electrophysiology

"Blind whole-cell patch-clamp recordings were made from 22 to 23-week old organoids secured with gentle suction in a fire polished glass pipette (exit diameter ~150 µm) in a recording chamber (OAC-1, Science Products) on a wide field upright microscope (BX51WI, Olympus). Organoids were continuously perfused (3 ml/min) with extracellular solution (artificial cerebrospinal fluid, aCSF: NaCl 125 mM, KCl 3.5 mM, MgCl2 1.3 mM, NaH2PO4 1.2 mM, CaCl2 2.4 mM, glucose 25 mM, NaHCO3 26 mM, gassed with 95 % O2 and 5 % CO2) heated to 32 °C (TC324B, Warner Instruments). Patch electrodes (4-6 MΩ) were made from 1.5 mm borosilicate glass and filled with a potassium-based solution (K-methylsulphate 122 mM, HEPES 10 mM, NaCl 8 mM, KCl 12 mM, EGTA 5 mM, CaCl2 0.25 mM, Na3-GTP 0.5 mM, Mg-ATP 4 mM, K2-phosphocreatine 10 mM). Whole-cell patch clamp recordings were made with a MultiClamp 700A amplifier, digitized through a Digidata 1322A (Axon Instruments) and acquired using pClamp 10 software (Molecular Devices). Recordings were established without cell visualization at depths of 50 to 250 µm from the organoid surface. Passive electrical properties, resting membrane potential and action potential generation were assessed to determine a neuronal or putative glial phenotype. All voltages have been corrected for a calculated junction potential of -10 mV. Spontaneous postsynaptic currents (sPSCs) were recorded in voltage clamp at a holding potential of -70 mV. Due to the more positive chloride reversal potential (-49 mV), both $GABA_A$ receptor-mediated inhibitory sPSCs (sIPSCs) and AMPA receptor-mediated excitatory sPSCs (sEPSCs) were inward and were distinguished pharmacologically and by their decay kinetics. Events were detected and their decay kinetics were determined from biexponential fits using Mini Analysis software (Synaptosoft). Decay kinetics were calculated from standard biexponential fits with the formula:

$$I_{decay} = A_1\left(e^{-\frac{t}{\tau_1}}\right) + A_2\left(e^{-\frac{t}{\tau_2}}\right)$$

where A1 and A2 are the amplitudes of the fast and slow components of the curves fit to the decay currents (peak to end) with the time constants, τ_1 and τ_2, respectively. The weighted decay τ (wtaudecay) was calculated as the sum of the relative proportions of the total amplitude for each τ with the formula:

$$\text{wtau}_{decay} = \tau_1 \left(\frac{A_1}{A_1 + A_2}\right) + \tau_2 \left(\frac{A_2}{A_1 + A_2}\right)$$

Events whose decay kinetics could not be satisfactorily fit were excluded from analysis. The remaining events were classified as AMPA sEPSCs (wtaudecay < 10 ms) and $GABA_A$ sIPSCs (wtaudecay > 20 ms) and visually verified in baseline conditions. In the presence of 20 µM NMDA, however, many events were superimposed due to the barrage of synaptic activity and thus could not be successfully fit leading to an underestimate of their frequency in our analysis." (Bauersachs et al., in submission)

4.10. Drugs and chemical compounds used in this thesis

Drug / Compound	**Source**	**Catalogue no.**	**Stock concentration**	**Concentration used**
C19	Fundamental Pharma	-	10 mM in DMSO	10 µM
C801	Fundamental Pharma	-	10 mM in DMSO	10 – 30 µM
Gabazine	Biotrend	BN0507	10 mM in water	5 µM
Glutamate	Sigma Aldrich	G-8415	100 mM in 1M HCl	50 – 1000 µM
Hydrogen Peroxide	Sigma Aldrich	31642-M	9.8 M	10 mM
Memantine	Biotrend	BG0374	100 mM in water	10 µM
MK-801	Biotrend	BN0338	50 mM in water	10 µM
NBQX	Hellobio.	HB0443	10 mM in water	5 µM
Nifedipine	Sigma Aldrich	N7634	100 mM in DMSO	5 µM
NMDA	Hellobio.	HB0454	100 mM in water	20 – 1000 µM
TTX (Tetrodotoxin Citrate)	Hellobio.	HB1035	1 mM in water	1 µM
Verapamil	Biotrend	BG0353	100 mM in water	30 µM

4.11. Statistical analyses

All Data is represented as mean ± standard deviation (SD). Image analysis of TEM images and quantification of MYT1L positive cells was performed blindly with respect to the treatment condition. Statistical analyses of electrophysiology data were performed with OriginPro (OriginLab). Outlier identification and statistical analyses of all other data was performed using Prism software version 8.0 (GraphPad). Outliers were identified using the ROUT method (Q = 1%) and removed before analysis. Statistical tests used for each experiment are specified in the figure legends.

(Obtained and modified from Bauersachs et al., in submission)

Acknowledgements

First of all, I would like to thank Hilmar Bading not only for the opportunity to do my PhD in his laboratory but also for his support and the elaborate discussions. Furthermore, I want to thank my TAC members Christoph Schuster, Sidney Cambridge and Carlos Bas Orth for their critical questions, input and support during the years.

A special thanks goes to Priit Pruunsild! Thank you for your intellectual and mental support in all kind of occasions, the stimulating discussions and for your constant help during this thesis (and the cheese!).

I would also like to deeply thank all the people that contributed to this project: Peter – you´re the best! Thank you so much for generating the ephys data but also for your great friendship and all the wonderful time that we spend together – looking forward to celebrate my 50th birthday in your garden! Many thanks also to Celia for producing a big part of the recordings! Thank you, Ursula, not only for the great help with the immunoblots but also for all the amazing conversations and for constantly cheering me up. Thank you, Andrea, for all the wonderful EM images! I also want to thank Hendrik Kaessmann and especially Bastienne Zaremba for generating and analysing the sequencing data.

Many thanks also to all the people that keep the lab running and always helped in case of smaller or bigger problems: Otto, thank you so much for your help, the incredibly fast ordering of everything I needed for this project and most importantly for constantly encouraging me. Olli, thank you for all your work behind the scenes – without you everything would have been much more difficult!

Of course, I also want to thank all the amazing people that I´ve met in the lab. Thank you for your friendship, your support, your encouragement and all the great moments that we shared together. I´ll always remember the parties, yoga sessions, after-work beers, barbeques and all the big or small adventures we experienced together.

Lastly, but most importantly, I want to thank my family and friends for their endless support, their continuous help, their understanding and for always being there for me in all stages of my PhD. I am extremely grateful to be surrounded by so many wonderful people and without you, I would not be where and who I am. Especially, I want to thank Rolf for always being there for me and believing in me, even in times when I struggled. Everything is better together!

References

1. Riedel G, Platt B, Micheau J. Glutamate receptor function in learning and memory. Behav Brain Res. 2003;140(1-2):1-47

2. Reiner A, Levitz J. Glutamatergic Signaling in the Central Nervous System: Ionotropic and Metabotropic Receptors in Concert. Neuron. 2018;98(6):1080-98

3. Blanke ML, VanDongen AMJ. Activation Mechanisms of the NMDA Receptor. In: Van Dongen AM, editor. Biology of the NMDA Receptor. Boca Raton (FL): CRC Press/Taylor & Francis; 2009. Chapter 13. PMID: 21204408.

4. Willard SS, Koochekpour S. Glutamate, glutamate receptors, and downstream signaling pathways. Int J Biol Sci. 2013;9(9):948-59

5. Zhu S, Gouaux E. Structure and symmetry inform gating principles of ionotropic glutamate receptors. Neuropharmacology. 2017;112(Pt A):11-5

6. Clapham DE. Calcium signaling. Cell. 2007;131(6):1047-58

7. Mahmoud S, Gharagozloo M, Simard C, Gris D. Astrocytes Maintain Glutamate Homeostasis in the CNS by Controlling the Balance between Glutamate Uptake and Release. Cells. 2019;8(2)

8. Sanderson DJ, Hindley E, Smeaton E, Denny N, Taylor A, Barkus C, et al. Deletion of the GluA1 AMPA receptor subunit impairs recency-dependent object recognition memory. Learn Mem. 2011;18(3):181-90

9. Sanderson DJ, Sprengel R, Seeburg PH, Bannerman DM. Deletion of the GluA1 AMPA receptor subunit alters the expression of short-term memory. Learn Mem. 2011;18(3):128-31

10. Iida I, Konno K, Natsume R, Abe M, Watanabe M, Sakimura K, et al. A comparative analysis of kainate receptor GluK2 and GluK5 knockout mice in a pure genetic background. Behav Brain Res. 2021;405:113194

11. Single FN, Rozov A, Burnashev N, Zimmermann F, Hanley DF, Forrest D, et al. Dysfunctions in mice by NMDA receptor point mutations NR1(N598Q) and NR1(N598R). J Neurosci. 2000;20(7):2558-66

12. Armada-Moreira A, Gomes JI, Pina CC, Savchak OK, Gonçalves-Ribeiro J, Rei N, et al. Going the Extra (Synaptic) Mile: Excitotoxicity as the Road Toward Neurodegenerative Diseases. Front Cell Neurosci. 2020;14:90

13. Ge Y, Chen W, Axerio-Cilies P, Wang YT. NMDARs in cell survival and death: implications in stroke pathogenesis and treatment. Trends in Molecular Medicine. 2020;26(6):533-51

14. Vyklicky V, Korinek M, Smejkalova T, Balik A, Krausova B, Kaniakova M, et al. Structure, function, and pharmacology of NMDA receptor channels. Physiol Res. 2014;63(Suppl 1):S191-203

15. Sheng M, Cummings J, Roldan LA, Jan YN, Jan LY. Changing subunit composition of heteromeric NMDA receptors during development of rat cortex. Nature. 1994;368(6467):144-7

16. Monyer H, Burnashev N, Laurie DJ, Sakmann B, Seeburg PH. Developmental and regional expression in the rat brain and functional properties of four NMDA receptors. Neuron. 1994;12(3):529-40

17. Traynelis SF, Wollmuth LP, McBain CJ, Menniti FS, Vance KM, Ogden KK, et al. Glutamate receptor ion channels: structure, regulation, and function. Pharmacol Rev. 2010;62(3):405-96

18. Lussier MP, Sanz-Clemente A, Roche KW. Dynamic Regulation of N-Methyl-d-aspartate (NMDA) and α-Amino-3-hydroxy-5-methyl-4-isoxazolepropionic Acid (AMPA) Receptors by Posttranslational Modifications. J Biol Chem. 2015;290(48):28596-603

19. Gardoni F, Di Luca M. Protein-protein interactions at the NMDA receptor complex: From synaptic retention to synaptonuclear protein messengers. Neuropharmacology. 2021;190:108551

20. Hardingham GE, Bading H. Synaptic versus extrasynaptic NMDA receptor signalling: implications for neurodegenerative disorders. Nat Rev Neurosci. 2010;11(10):682-96

21. Furukawa H, Singh SK, Mancusso R, Gouaux E. Subunit arrangement and function in NMDA receptors. Nature. 2005;438(7065):185-92

22. Mayer ML, Westbrook GL, Guthrie PB. Voltage-dependent block by Mg2+ of NMDA responses in spinal cord neurones. Nature. 1984;309(5965):261-3

23. Durand GM, Kovalchuk Y, Konnerth A. Long-term potentiation and functional synapse induction in developing hippocampus. Nature. 1996;381(6577):71-5

24. Wu G, Malinow R, Cline HT. Maturation of a central glutamatergic synapse. Science. 1996;274(5289):972-6

25. Lee LJ, Lo FS, Erzurumlu RS. NMDA receptor-dependent regulation of axonal and dendritic branching. J Neurosci. 2005;25(9):2304-11

26. Rajan I, Cline HT. Glutamate receptor activity is required for normal development of tectal cell dendrites in vivo. J Neurosci. 1998;18(19):7836-46

27. Forrest D, Yuzaki M, Soares HD, Ng L, Luk DC, Sheng M, et al. Targeted disruption of NMDA receptor 1 gene abolishes NMDA response and results in neonatal death. Neuron. 1994;13(2):325-38

28. Kutsuwada T, Sakimura K, Manabe T, Takayama C, Katakura N, Kushiya E, et al. Impairment of suckling response, trigeminal neuronal pattern formation, and hippocampal LTD in NMDA receptor epsilon 2 subunit mutant mice. Neuron. 1996;16(2):333-44

29. Volianskis A, France G, Jensen MS, Bortolotto ZA, Jane DE, Collingridge GL. Long-term potentiation and the role of N-methyl-D-aspartate receptors. Brain Res. 2015;1621:5-16

30. Hunt DL, Castillo PE. Synaptic plasticity of NMDA receptors: mechanisms and functional implications. Current Opinion in Neurobiology. 2012;22(3):496-508

31. Rebola N, Srikumar BN, Mulle C. Activity-dependent synaptic plasticity of NMDA receptors. J Physiol. 2010;588(Pt 1):93-9

32. Sakimura K, Kutsuwada T, Ito I, Manabe T, Takayama C, Kushiya E, et al. Reduced hippocampal LTP and spatial learning in mice lacking NMDA receptor epsilon 1 subunit. Nature. 1995;373(6510):151-5

33. Chen PE, Errington ML, Kneussel M, Chen G, Annala AJ, Rudhard YH, et al. Behavioral deficits and subregion-specific suppression of LTP in mice expressing a population of mutant NMDA receptors throughout the hippocampus. Learn Mem. 2009;16(10):635-44

34. Segev A, Yanagi M, Scott D, Southcott SA, Lister JM, Tan C, et al. Reduced GluN1 in mouse dentate gyrus is associated with CA3 hyperactivity and psychosis-like behaviors. Molecular Psychiatry. 2020;25(11):2832-43

35. de Lima MNM, Laranja DC, Bromberg E, Roesler R, Schröder N. Pre- or post-training administration of the NMDA receptor blocker MK-801 impairs object recognition memory in rats. Behavioural Brain Research. 2005;156(1):139-43

36. Lucas DR, Newhouse JP. The toxic effect of sodium L-glutamate on the inner layers of the retina. AMA Arch Ophthalmol. 1957;58(2):193-201

37. Olney JW. Brain lesions, obesity, and other disturbances in mice treated with monosodium glutamate. Science. 1969;164(3880):719-21

38. Dong X-x, Wang Y, Qin Z-h. Molecular mechanisms of excitotoxicity and their relevance to pathogenesis of neurodegenerative diseases. Acta Pharmacologica Sinica. 2009;30(4):379-87

39. Wang Y, Qin Z-h. Molecular and cellular mechanisms of excitotoxic neuronal death. Apoptosis. 2010;15(11):1382-402

40. Mehta A, Prabhakar M, Kumar P, Deshmukh R, Sharma PL. Excitotoxicity: bridge to various triggers in neurodegenerative disorders. Eur J Pharmacol. 2013;698(1-3):6-18

41. Bano D, Ankarcrona M. Beyond the critical point: An overview of excitotoxicity, calcium overload and the downstream consequences. Neuroscience Letters. 2018;663:79-85

42. Sun D, Murali SG. Stimulation of Na+-K+-2Cl- cotransporter in neuronal cells by excitatory neurotransmitter glutamate. Am J Physiol. 1998;275(3):C772-9

43. Liang D, Bhatta S, Gerzanich V, Simard JM. Cytotoxic edema: mechanisms of pathological cell swelling. Neurosurg Focus. 2007;22(5):E2

44. Choi DW. Glutamate neurotoxicity in cortical cell culture is calcium dependent. Neuroscience Letters. 1985;58(3):293-7

45. Du Y, Bales KR, Dodel RC, Hamilton-Byrd E, Horn JW, Czilli DL, et al. Activation of a caspase 3-related cysteine protease is required for glutamate-mediated apoptosis of cultured cerebellar granule neurons. Proceedings of the National Academy of Sciences. 1997;94(21):11657-62

46. Hashimoto R, Hough C, Nakazawa T, Yamamoto T, Chuang DM. Lithium protection against glutamate excitotoxicity in rat cerebral cortical neurons: involvement of NMDA receptor inhibition possibly by decreasing NR2B tyrosine phosphorylation. J Neurochem. 2002;80(4):589-97

47. Kumar A, Dejanovic B, Hetsch F, Semtner M, Fusca D, Arjune S, et al. S-sulfocysteine/NMDA receptor-dependent signaling underlies neurodegeneration in molybdenum cofactor deficiency. J Clin Invest. 2017;127(12):4365-78

48. Connor JA, Wadman WJ, Hockberger PE, Wong RK. Sustained dendritic gradients of Ca2+ induced by excitatory amino acids in CA1 hippocampal neurons. Science. 1988;240(4852):649-53

49. Farooqui AA, Anderson DK, Horrocks LA. Effect of glutamate and its analogs on diacylglycerol and monoacylglycerol lipase activities of neuron-enriched cultures. Brain Res. 1993;604(1-2):180-4

50. Wang KK, Yuen PW. Calpain inhibition: an overview of its therapeutic potential. Trends Pharmacol Sci. 1994;15(11):412-9

51. Szydlowska K, Tymianski M. Calcium, ischemia and excitotoxicity. Cell Calcium. 2010;47(2):122-9

52. Reynolds IJ. Mitochondrial membrane potential and the permeability transition in excitotoxicity. Ann N Y Acad Sci. 1999;893:33-41

53. Greenwood SM, Connolly CN. Dendritic and mitochondrial changes during glutamate excitotoxicity. Neuropharmacology. 2007;53(8):891-8

54. Lipton SA, Nicotera P. ■ REVIEW : Excitotoxicity, Free Radicals, Necrosis, and Apoptosis. The Neuroscientist. 1998;4(5):345-52

55. Belov Kirdajova D, Kriska J, Tureckova J, Anderova M. Ischemia-Triggered Glutamate Excitotoxicity From the Perspective of Glial Cells. Frontiers in Cellular Neuroscience. 2020;14(51)

56. Drejer J, Benveniste H, Diemer NH, Schousboe A. Cellular origin of ischemia-induced glutamate release from brain tissue in vivo and in vitro. J Neurochem. 1985;45(1):145-51

57. Phillis JW, Ren J, O'Regan MH. Transporter reversal as a mechanism of glutamate release from the ischemic rat cerebral cortex: studies with DL-threo-beta-benzyloxyaspartate. Brain Res. 2000;868(1):105-12

58. Simon RP, Swan JH, Griffiths T, Meldrum BS. Blockade of N-methyl-D-aspartate receptors may protect against ischemic damage in the brain. Science. 1984;226(4676):850-2

59. Gill R, Foster AC, Woodruff GN. Systemic administration of MK-801 protects against ischemia-induced hippocampal neurodegeneration in the gerbil. J Neurosci. 1987;7(10):3343-9

60. Folkersma H, Foster Dingley JC, van Berckel BN, Rozemuller A, Boellaard R, Huisman MC, et al. Increased cerebral (R)-[(11)C]PK11195 uptake and glutamate release in a rat model of traumatic brain injury: a longitudinal pilot study. J Neuroinflammation. 2011;8:67

61. Katayama Y, Becker DP, Tamura T, Hovda DA. Massive increases in extracellular potassium and the indiscriminate release of glutamate following concussive brain injury. J Neurosurg. 1990;73(6):889-900

62. Sönmez A, Sayın O, Gürgen SG, Çalişir M. Neuroprotective effects of MK-801 against traumatic brain injury in immature rats. Neurosci Lett. 2015;597:137-42

63. Lewerenz J, Maher P. Chronic Glutamate Toxicity in Neurodegenerative Diseases—What is the Evidence? Frontiers in Neuroscience. 2015;9(469)

64. Shaw PJ, Forrest V, Ince PG, Richardson JP, Wastell HJ. CSF and plasma amino acid levels in motor neuron disease: elevation of CSF glutamate in a subset of patients. Neurodegeneration. 1995;4(2):209-16

65. Madeira C, Vargas-Lopes C, Brandão CO, Reis T, Laks J, Panizzutti R, et al. Elevated Glutamate and Glutamine Levels in the Cerebrospinal Fluid of Patients With Probable Alzheimer's Disease and Depression. Frontiers in Psychiatry. 2018;9(561)

66. Iwasaki Y, Ikeda K, Shiojima T, Kinoshita M. Increased plasma concentrations of aspartate, glutamate and glycine in Parkinson's disease. Neurosci Lett. 1992;145(2):175-7

67. Howland DS, Liu J, She Y, Goad B, Maragakis NJ, Kim B, et al. Focal loss of the glutamate transporter EAAT2 in a transgenic rat model of SOD1 mutant-mediated amyotrophic lateral sclerosis (ALS). Proc Natl Acad Sci U S A. 2002;99(3):1604-9

68. Schallier A, Smolders I, Van Dam D, Loyens E, De Deyn PP, Michotte A, et al. Region- and age-specific changes in glutamate transport in the AβPP23 mouse model for Alzheimer's disease. J Alzheimers Dis. 2011;24(2):287-300

69. Faideau M, Kim J, Cormier K, Gilmore R, Welch M, Auregan G, et al. In vivo expression of polyglutamine-expanded huntingtin by mouse striatal astrocytes impairs glutamate transport: a correlation with Huntington's disease subjects. Hum Mol Genet. 2010;19(15):3053-67

70. Chung EK, Chen LW, Chan YS, Yung KK. Downregulation of glial glutamate transporters after dopamine denervation in the striatum of 6-hydroxydopamine-lesioned rats. J Comp Neurol. 2008;511(4):421-37

71. Rothstein JD, Van Kammen M, Levey AI, Martin LJ, Kuncl RW. Selective loss of glial glutamate transporter GLT-1 in amyotrophic lateral sclerosis. Ann Neurol. 1995;38(1):73-84

72. Jacob CP, Koutsilieri E, Bartl J, Neuen-Jacob E, Arzberger T, Zander N, et al. Alterations in expression of glutamatergic transporters and receptors in sporadic Alzheimer's disease. J Alzheimers Dis. 2007;11(1):97-116

73. Arzberger T, Krampfl K, Leimgruber S, Weindl A. Changes of NMDA receptor subunit (NR1, NR2B) and glutamate transporter (GLT1) mRNA expression in Huntington's disease--an in situ hybridization study. J Neuropathol Exp Neurol. 1997;56(4):440-54

74. Zhang H, Li Q, Graham RK, Slow E, Hayden MR, Bezprozvanny I. Full length mutant huntingtin is required for altered Ca2+ signaling and apoptosis of striatal neurons in the YAC mouse model of Huntington's disease. Neurobiol Dis. 2008;31(1):80-8

75. Texidó L, Martín-Satué M, Alberdi E, Solsona C, Matute C. Amyloid β peptide oligomers directly activate NMDA receptors. Cell Calcium. 2011;49(3):184-90

76. Thomas SJ, Grossberg GT. Memantine: a review of studies into its safety and efficacy in treating Alzheimer's disease and other dementias. Clin Interv Aging. 2009;4:367-77

77. Ikonomidou C, Turski L. Why did NMDA receptor antagonists fail clinical trials for stroke and traumatic brain injury? The Lancet Neurology. 2002;1(6):383-6

78. Muir KW. Glutamate-based therapeutic approaches: clinical trials with NMDA antagonists. Current Opinion in Pharmacology. 2006;6(1):53-60

79. Xu SY, Pan SY. The failure of animal models of neuroprotection in acute ischemic stroke to translate to clinical efficacy. Med Sci Monit Basic Res. 2013;19:37-45

80. Hardingham GE, Bading H. The Yin and Yang of NMDA receptor signalling. Trends Neurosci. 2003;26(2):81-9

81. Gould E, Cameron HA, McEwen BS. Blockade of NMDA receptors increases cell death and birth in the developing rat dentate gyrus. J Comp Neurol. 1994;340(4):551-65

82. Ikonomidou C, Stefovska V, Turski L. Neuronal death enhanced by N-methyl-D-aspartate antagonists. Proc Natl Acad Sci U S A. 2000;97(23):12885-90

83. Zhang SJ, Zou M, Lu L, Lau D, Ditzel DA, Delucinge-Vivier C, et al. Nuclear calcium signaling controls expression of a large gene pool: identification of a gene program for acquired neuroprotection induced by synaptic activity. PLoS Genet. 2009;5(8):e1000604

84. Zhang SJ, Buchthal B, Lau D, Hayer S, Dick O, Schwaninger M, et al. A signaling cascade of nuclear calcium-CREB-ATF3 activated by synaptic NMDA receptors defines a gene repression module that protects against extrasynaptic NMDA receptor-induced neuronal cell death and ischemic brain damage. J Neurosci. 2011;31(13):4978-90

85. Simms Brett A, Zamponi Gerald W. Neuronal Voltage-Gated Calcium Channels: Structure, Function, and Dysfunction. Neuron. 2014;82(1):24-45

86. Seo MD, Enomoto M, Ishiyama N, Stathopulos PB, Ikura M. Structural insights into endoplasmic reticulum stored calcium regulation by inositol 1,4,5-trisphosphate and ryanodine receptors. Biochim Biophys Acta. 2015;1853(9):1980-91

87. Lee B, Butcher GQ, Hoyt KR, Impey S, Obrietan K. Activity-dependent neuroprotection and cAMP response element-binding protein (CREB): kinase coupling, stimulus intensity, and temporal regulation of CREB phosphorylation at serine 133. J Neurosci. 2005;25(5):1137-48

88. Cruzalegui FH, Bading H. Calcium-regulated protein kinase cascades and their transcription factor targets. Cell Mol Life Sci. 2000;57(3):402-10

89. Kwok RPS, Lundblad JR, Chrivia JC, Richards JP, Bächinger HP, Brennan RG, et al. Nuclear protein CBP is a coactivator for the transcription factor CREB. Nature. 1994;370(6486):223-6

90. Chawla S, Hardingham GE, Quinn DR, Bading H. CBP: a signal-regulated transcriptional coactivator controlled by nuclear calcium and CaM kinase IV. Science. 1998;281(5382):1505-9

91. Sakamoto K, Karelina K, Obrietan K. CREB: a multifaceted regulator of neuronal plasticity and protection. J Neurochem. 2011;116(1):1-9

92. Kowiański P, Lietzau G, Czuba E, Waśkow M, Steliga A, Moryś J. BDNF: A Key Factor with Multipotent Impact on Brain Signaling and Synaptic Plasticity. Cellular and Molecular Neurobiology. 2018;38(3):579-93

93. Liu Z, Ma D, Feng G, Ma Y, Hu H. Recombinant AAV-mediated expression of human BDNF protects neurons against cell apoptosis in Abeta-induced neuronal damage model. J Huazhong Univ Sci Technolog Med Sci. 2007;27(3):233-6

94. Brunet A, Datta SR, Greenberg ME. Transcription-dependent and -independent control of neuronal survival by the PI3K-Akt signaling pathway. Curr Opin Neurobiol. 2001;11(3):297-305

95. Soriano FX, Papadia S, Hofmann F, Hardingham NR, Bading H, Hardingham GE. Preconditioning doses of NMDA promote neuroprotection by enhancing neuronal excitability. J Neurosci. 2006;26(17):4509-18

96. Papadia S, Soriano FX, Léveillé F, Martel MA, Dakin KA, Hansen HH, et al. Synaptic NMDA receptor activity boosts intrinsic antioxidant defenses. Nat Neurosci. 2008;11(4):476-87

97. Liu Y, Wong TP, Aarts M, Rooyakkers A, Liu L, Lai TW, et al. NMDA receptor subunits have differential roles in mediating excitotoxic neuronal death both in vitro and in vivo. The Journal of neuroscience : the official journal of the Society for Neuroscience. 2007;27(11):2846-57

98. Chen M, Lu TJ, Chen XJ, Zhou Y, Chen Q, Feng XY, et al. Differential roles of NMDA receptor subtypes in ischemic neuronal cell death and ischemic tolerance. Stroke. 2008;39(11):3042-8

99. Martel MA, Ryan TJ, Bell KF, Fowler JH, McMahon A, Al-Mubarak B, et al. The subtype of GluN2 C-terminal domain determines the response to excitotoxic insults. Neuron. 2012;74(3):543-56

100. Chung C, Marson JD, Zhang QG, Kim J, Wu WH, Brann DW, et al. Neuroprotection Mediated through GluN2C-Containing N-methyl-D-aspartate (NMDA) Receptors Following Ischemia. Sci Rep. 2016;6:37033

101. Nakanishi N, Tu S, Shin Y, Cui J, Kurokawa T, Zhang D, et al. Neuroprotection by the NR3A subunit of the NMDA receptor. J Neurosci. 2009;29(16):5260-5

102. Baron A, Montagne A, Cassé F, Launay S, Maubert E, Ali C, et al. NR2D-containing NMDA receptors mediate tissue plasminogen activator-promoted neuronal excitotoxicity. Cell Death Differ. 2010;17(5):860-71

103. Rauner C, Köhr G. Triheteromeric NR1/NR2A/NR2B receptors constitute the major N-methyl-D-aspartate receptor population in adult hippocampal synapses. J Biol Chem. 2011;286(9):7558-66

104. Al-Hallaq RA, Conrads TP, Veenstra TD, Wenthold RJ. NMDA di-heteromeric receptor populations and associated proteins in rat hippocampus. J Neurosci. 2007;27(31):8334-43

105. Hardingham GE, Fukunaga Y, Bading H. Extrasynaptic NMDARs oppose synaptic NMDARs by triggering CREB shut-off and cell death pathways. Nat Neurosci. 2002;5(5):405-14

106. Impey S, Fong AL, Wang Y, Cardinaux JR, Fass DM, Obrietan K, et al. Phosphorylation of CBP mediates transcriptional activation by neural activity and CaM kinase IV. Neuron. 2002;34(2):235-44

107. Yan J, Bengtson CP, Buchthal B, Hagenston AM, Bading H. Coupling of NMDA receptors and TRPM4 guides discovery of unconventional neuroprotectants. Science. 2020;370(6513)

108. Aarts M, Liu Y, Liu L, Besshoh S, Arundine M, Gurd JW, et al. Treatment of ischemic brain damage by perturbing NMDA receptor- PSD-95 protein interactions. Science. 2002;298(5594):846-50

109. Küppenbender KD, Standaert DG, Feuerstein TJ, Penney JB, Jr., Young AB, Landwehrmeyer GB. Expression of NMDA receptor subunit mRNAs in neurochemically identified projection and interneurons in the human striatum. J Comp Neurol. 2000;419(4):407-21

110. Jantzie LL, Talos DM, Jackson MC, Park HK, Graham DA, Lechpammer M, et al. Developmental expression of N-methyl-D-aspartate (NMDA) receptor subunits in human white and gray matter: potential mechanism of increased vulnerability in the immature brain. Cereb Cortex. 2015;25(2):482-95

111. Bar-Shira O, Maor R, Chechik G. Gene Expression Switching of Receptor Subunits in Human Brain Development. PLoS Comput Biol. 2015;11(12):e1004559

112. Bagasrawala I, Memi F, N VR, Zecevic N. N-Methyl d-Aspartate receptor expression patterns in the human fetal cerebral cortex. Cereb Cortex. 2017;27(11):5041-53

113. Hedegaard M, Hansen KB, Andersen KT, Bräuner-Osborne H, Traynelis SF. Molecular pharmacology of human NMDA receptors. Neurochem Int. 2012;61(4):601-9

114. Dage JL, Colvin EM, Fouillet A, Langron E, Roell WC, Li J, et al. Pharmacological characterisation of ligand- and voltage-gated ion channels expressed in human iPSC-derived forebrain neurons. Psychopharmacology (Berl). 2014;231(6):1105-24

115. D'Aiuto L, Zhi Y, Kumar Das D, Wilcox MR, Johnson JW, McClain L, et al. Large-scale generation of human iPSC-derived neural stem cells/early neural progenitor cells and their neuronal differentiation. Organogenesis. 2014;10(4):365-77

116. Zhang WB, Ross PJ, Tu Y, Wang Y, Beggs S, Sengar AS, et al. Fyn Kinase regulates GluN2B subunit-dominant NMDA receptors in human induced pluripotent stem cell-derived neurons. Sci Rep. 2016;6:23837

117. Halliwell RF. Electrophysiological properties of neurons derived from human stem cells and iNeurons in vitro. Neurochemistry International. 2017;106:37-47

118. Lam RS, Töpfer FM, Wood PG, Busskamp V, Bamberg E. Functional Maturation of Human Stem Cell-Derived Neurons in Long-Term Cultures. PLoS One. 2017;12(1):e0169506

119. Fenske P, Grauel MK, Brockmann MM, Dorrn AL, Trimbuch T, Rosenmund C. Autaptic cultures of human induced neurons as a versatile platform for studying synaptic function and neuronal morphology. Scientific Reports. 2019;9(1):4890

120. Klima S, Brüll M, Spreng AS, Suciu I, Falt T, Schwamborn JC, et al. A human stem cell-derived test system for agents modifying neuronal N-methyl-D-aspartate-type glutamate receptor Ca(2+)-signalling. Arch Toxicol. 2021;95(5):1703-22

121. McQueen J, Ryan TJ, McKay S, Marwick K, Baxter P, Carpanini SM, et al. Pro-death NMDA receptor signaling is promoted by the GluN2B C-terminus independently of Dapk1. Elife. 2017;6

122. D'Orsi B, Bonner H, Tuffy LP, Düssmann H, Woods I, Courtney MJ, et al. Calpains are downstream effectors of bax-dependent excitotoxic apoptosis. J Neurosci. 2012;32(5):1847-58

123. Peterson C, Neal JH, Cotman CW. Development of N-methyl-d-aspartate excitotoxicity in cultured hippocampal neurons. Developmental Brain Research. 1989;48(2):187-95

124. Gupta K, Hardingham GE, Chandran S. NMDA receptor-dependent glutamate excitotoxicity in human embryonic stem cell-derived neurons. Neurosci Lett. 2013;543:95-100

125. Xu JC, Fan J, Wang X, Eacker SM, Kam TI, Chen L, et al. Cultured networks of excitatory projection neurons and inhibitory interneurons for studying human cortical neurotoxicity. Sci Transl Med. 2016;8(333):333ra48

126. Chambers SM, Fasano CA, Papapetrou EP, Tomishima M, Sadelain M, Studer L. Highly efficient neural conversion of human ES and iPS cells by dual inhibition of SMAD signaling. Nat Biotechnol. 2009;27(3):275-80

127. Zhang Y, Pak C, Han Y, Ahlenius H, Zhang Z, Chanda S, et al. Rapid single-step induction of functional neurons from human pluripotent stem cells. Neuron. 2013;78(5):785-98

128. Lancaster MA, Knoblich JA. Generation of cerebral organoids from human pluripotent stem cells. Nat Protoc. 2014;9(10):2329-40

129. Paşca AM, Sloan SA, Clarke LE, Tian Y, Makinson CD, Huber N, et al. Functional cortical neurons and astrocytes from human pluripotent stem cells in 3D culture. Nat Methods. 2015;12(7):671-8

130. Tieng V, Stoppini L, Villy S, Fathi M, Dubois-Dauphin M, Krause KH. Engineering of midbrain organoids containing long-lived dopaminergic neurons. Stem Cells Dev. 2014;23(13):1535-47

131. Qian X, Nguyen HN, Song MM, Hadiono C, Ogden SC, Hammack C, et al. Brain-Region-Specific Organoids Using Mini-bioreactors for Modeling ZIKV Exposure. Cell. 2016;165(5):1238-54

132. Kathuria A, Lopez-Lengowski K, Watmuff B, Karmacharya R. Comparative Transcriptomic Analysis of Cerebral Organoids and Cortical Neuron Cultures Derived from Human Induced Pluripotent Stem Cells. Stem Cells Dev. 2020;29(21):1370-81

133. Klapper SD, Garg P, Dagar S, Lenk K, Gottmann K, Nieweg K. Astrocyte lineage cells are essential for functional neuronal differentiation and synapse maturation in human iPSC-derived neural networks. Glia. 2019;67(10):1893-909

134. Amin ND, Paşca SP. Building Models of Brain Disorders with Three-Dimensional Organoids. Neuron. 2018;100(2):389-405

135. Terasaki Y, Sasaki T, Yagita Y, Okazaki S, Sugiyama Y, Oyama N, et al. Activation of NR2A receptors induces ischemic tolerance through CREB signaling. J Cereb Blood Flow Metab. 2010;30(8):1441-9

136. Gordon A, Yoon SJ, Tran SS, Makinson CD, Park JY, Andersen J, et al. Long-term maturation of human cortical organoids matches key early postnatal transitions. Nat Neurosci. 2021;24(3):331-42

137. Kim J, Sullivan GJ, Park IH. How well do brain organoids capture your brain? iScience. 2021;24(2):102063

138. Imaizumi K, Sone T, Ibata K, Fujimori K, Yuzaki M, Akamatsu W, et al. Controlling the regional identity of hPSC-derived neurons to uncover neuronal subtype specificity of neurological disease phenotypes. Stem Cell Reports. 2015;5(6):1010-22

139. Imaizumi K, Fujimori K, Ishii S, Otomo A, Hosoi Y, Miyajima H, et al. Rostrocaudal areal patterning of human PSC-derived cortical neurons by FGF8 signaling. eNeuro. 2018;5(2)

140. Yu DX, Di Giorgio FP, Yao J, Marchetto MC, Brennand K, Wright R, et al. Modeling hippocampal neurogenesis using human pluripotent stem cells. Stem Cell Reports. 2014;2(3):295-310

141. Yakoub AM, Sadek M. Development and characterization of human cerebral organoids: An optimized protocol. Cell Transplant. 2018;27(3):393-406

142. Denisenko E, Guo BB, Jones M, Hou R, de Kock L, Lassmann T, et al. Systematic assessment of tissue dissociation and storage biases in single-cell and single-nucleus RNA-seq workflows. Genome Biol. 2020;21(1):130

143. Zhao F, Wu T, Lau A, Jiang T, Huang Z, Wang XJ, et al. Nrf2 promotes neuronal cell differentiation. Free Radic Biol Med. 2009;47(6):867-79

144. Lenoir S, Genoux A, Agasse F, Saudou F, Humbert S. Recreating mouse cortico-hippocampal neuronal circuit in microfluidic devices to study BDNF axonal transport upon glucocorticoid treatment. STAR Protocols. 2021;2(1):100382

145. La Manno G, Siletti K, Furlan A, Gyllborg D, Vinsland E, Langseth CM, et al. Molecular architecture of the developing mouse brain. bioRxiv. 2020:2020.07.02.184051

146. Paoletti P, Bellone C, Zhou Q. NMDA receptor subunit diversity: impact on receptor properties, synaptic plasticity and disease. Nat Rev Neurosci. 2013;14(6):383-400

147. Watanabe M, Inoue Y, Sakimura K, Mishina M. Developmental changes in distribution of NMDA receptor channel subunit mRNAs. Neuroreport. 1992;3(12):1138-40

148. Whittemore ER, Loo DT, Watt JA, Cotman CW. A detailed analysis of hydrogen peroxide-induced cell death in primary neuronal culture. Neuroscience. 1995;67(4):921-32

149. Olney JW, Fuller T, de Gubareff T. Acute dendrotoxic changes in the hippocampus of kainate treated rats. Brain Res. 1979;176(1):91-100

150. Johnson VE, Stewart W, Smith DH. Axonal pathology in traumatic brain injury. Exp Neurol. 2013;246:35-43

151. Suwanna N, Thangnipon W, Soi-ampornkul R. Neuroprotective effects of diarylpropionitrile against β-amyloid peptide-induced neurotoxicity in rat cultured cortical neurons. Neuroscience Letters. 2014;578:44-9

152. Papadia S, Stevenson P, Hardingham NR, Bading H, Hardingham GE. Nuclear Ca2+ and the cAMP response element-binding protein family mediate a late phase of activity-dependent neuroprotection. J Neurosci. 2005;25(17):4279-87

153. Bading H. Nuclear calcium signalling in the regulation of brain function. Nat Rev Neurosci. 2013;14(9):593-608

154. Mayr B, Montminy M. Transcriptional regulation by the phosphorylation-dependent factor CREB. Nature Reviews Molecular Cell Biology. 2001;2(8):599-609

155. Hou H, Chávez AE, Wang CC, Yang H, Gu H, Siddoway BA, et al. The Rac1 inhibitor NSC23766 suppresses CREB signaling by targeting NMDA receptor function. J Neurosci. 2014;34(42):14006-12

156. Chen R-W, Chuang D-M. Long Term Lithium Treatment Suppresses p53 and Bax Expression but Increases Bcl-2 Expression: A PROMINENT ROLE IN NEUROPROTECTION AGAINST EXCITOTOXICITY*. Journal of Biological Chemistry. 1999;274(10):6039-42

157. Girling KD, Demers MJ, Laine J, Zhang S, Wang YT, Graham RK. Activation of caspase-6 and cleavage of caspase-6 substrates is an early event in NMDA receptor-mediated excitotoxicity. J Neurosci Res. 2018;96(3):391-406

158. D'Amelio M, Cavallucci V, Cecconi F. Neuronal caspase-3 signaling: not only cell death. Cell Death Differ. 2010;17(7):1104-14

159. Zhou X, Hollern D, Liao J, Andrechek E, Wang H. NMDA receptor-mediated excitotoxicity depends on the coactivation of synaptic and extrasynaptic receptors. Cell Death & Disease. 2013;4(3):e560-e

160. Narahashi T, Moore JW, Scott WR. TETRODOTOXIN BLOCKAGE OF SODIUM CONDUCTANCE INCREASE IN LOBSTER GIANT AXONS. J Gen Physiol. 1964;47(5):965-74

161. Quadrato G, Nguyen T, Macosko EZ, Sherwood JL, Min Yang S, Berger DR, et al. Cell diversity and network dynamics in photosensitive human brain organoids. Nature. 2017;545(7652):48-53

162. Lancaster MA, Renner M, Martin C-A, Wenzel D, Bicknell LS, Hurles ME, et al. Cerebral organoids model human brain development and microcephaly. Nature. 2013;501(7467):373-9

163. Li Y, Muffat J, Omer A, Bosch I, Lancaster MA, Sur M, et al. Induction of Expansion and Folding in Human Cerebral Organoids. Cell Stem Cell. 2017;20(3):385-96.e3

164. Qian X, Song H, Ming GL. Brain organoids: advances, applications and challenges. Development. 2019;146(8)

165. Ullian EM, Sapperstein SK, Christopherson KS, Barres BA. Control of synapse number by glia. Science. 2001;291(5504):657-61

166. Gordon A, Yoon S-J, Tran SS, Makinson CD, Park JY, Andersen J, et al. Long-term maturation of human cortical organoids matches key early postnatal transitions. Nature Neuroscience. 2021;24(3):331-42

167. Satir TM, Nazir FH, Vizlin-Hodzic D, Hardselius E, Blennow K, Wray S, et al. Accelerated neuronal and synaptic maturation by BrainPhys medium increases Aβ secretion and alters Aβ peptide ratios from iPSC-derived cortical neurons. Scientific Reports. 2020;10(1):601

168. Marks JD, Friedman JE, Haddad GG. Vulnerability of CA1 neurons to glutamate is developmentally regulated. Brain Res Dev Brain Res. 1996;97(2):194-206

169. Liu Z, Stafstrom CE, Sarkisian M, Tandon P, Yang Y, Hori A, et al. Age-dependent effects of glutamate toxicity in the hippocampus. Brain Res Dev Brain Res. 1996;97(2):178-84

170. Bonfoco E, Krainc D, Ankarcrona M, Nicotera P, Lipton SA. Apoptosis and necrosis: two distinct events induced, respectively, by mild and intense insults with N-methyl-D-aspartate or nitric oxide/superoxide in cortical cell cultures. Proc Natl Acad Sci U S A. 1995;92(16):7162-6

171. Ankarcrona M, Dypbukt JM, Bonfoco E, Zhivotovsky B, Orrenius S, Lipton SA, et al. Glutamate-induced neuronal death: a succession of necrosis or apoptosis depending on mitochondrial function. Neuron. 1995;15(4):961-73

172. Puyal J, Ginet V, Clarke PG. Multiple interacting cell death mechanisms in the mediation of excitotoxicity and ischemic brain damage: a challenge for neuroprotection. Prog Neurobiol. 2013;105:24-48

173. Li Y, Yang X, Ma C, Qiao J, Zhang C. Necroptosis contributes to the NMDA-induced excitotoxicity in rat's cultured cortical neurons. Neuroscience Letters. 2008;447(2):120-3

174. Kuzhandaivel A, Nistri A, Mladinic M. Kainate-mediated excitotoxicity induces neuronal death in the rat spinal cord in vitro via a PARP-1 dependent cell death pathway (Parthanatos). Cell Mol Neurobiol. 2010;30(7):1001-12

175. Yan G, Elbadawi M, Efferth T. Multiple cell death modalities and their key features (Review). World Acad Sci J. 2020;2(2):39-48

176. Syntichaki P, Tavernarakis N. The biochemistry of neuronal necrosis: rogue biology? Nat Rev Neurosci. 2003;4(8):672-84

177. Fricker M, Tolkovsky AM, Borutaite V, Coleman M, Brown GC. Neuronal Cell Death. Physiol Rev. 2018;98(2):813-80

178. Koehler RC, Dawson VL, Dawson TM. Targeting Parthanatos in Ischemic Stroke. Frontiers in Neurology. 2021;12(622)

179. Sosna J, Voigt S, Mathieu S, Lange A, Thon L, Davarnia P, et al. TNF-induced necroptosis and PARP-1-mediated necrosis represent distinct routes to programmed necrotic cell death. Cell Mol Life Sci. 2014;71(2):331-48

180. Shin H-J, Kwon H-K, Lee J-H, Gui X, Achek A, Kim J-H, et al. Doxorubicin-induced necrosis is mediated by poly-(ADP-ribose) polymerase 1 (PARP1) but is independent of p53. Scientific Reports. 2015;5(1):15798

181. Sairanen T, Szepesi R, Karjalainen-Lindsberg ML, Saksi J, Paetau A, Lindsberg PJ. Neuronal caspase-3 and PARP-1 correlate differentially with apoptosis and necrosis in ischemic human stroke. Acta Neuropathol. 2009;118(4):541-52

182. Pérez-Capote K, Serratosa J, Solà C. Excitotoxic and apoptotic neuronal death induce different patterns of glial activation in vitro. J Neurochem. 2005;94(1):226-37

183. Aguado T, Romero E, Monory K, Palazuelos J, Sendtner M, Marsicano G, et al. The CB1 cannabinoid receptor mediates excitotoxicity-induced neural progenitor proliferation and neurogenesis. J Biol Chem. 2007;282(33):23892-8

184. Bading H. Therapeutic targeting of the pathological triad of extrasynaptic NMDA receptor signaling in neurodegenerations. J Exp Med. 2017;214(3):569-78

185. Mantamadiotis T, Papalexis N, Dworkin S. CREB signalling in neural stem/progenitor cells: recent developments and the implications for brain tumour biology. Bioessays. 2012;34(4):293-300

186. Kim DW, Lee JH, Park SK, Yang W-M, Jeon GS, Lee YH, et al. Astrocytic Expressions of Phosphorylated Akt, GSK3β and CREB Following an Excitotoxic Lesion in the Mouse Hippocampus. Neurochemical Research. 2007;32(9):1460-8

187. Pardo L, Valor LM, Eraso-Pichot A, Barco A, Golbano A, Hardingham GE, et al. CREB Regulates Distinct Adaptive Transcriptional Programs in Astrocytes and Neurons. Scientific Reports. 2017;7(1):6390

188. Bito H, Deisseroth K, Tsien RW. CREB Phosphorylation and Dephosphorylation: A Ca2+- and Stimulus Duration–Dependent Switch for Hippocampal Gene Expression. Cell. 1996;87(7):1203-14

189. Szatmari E, Habas A, Yang P, Zheng JJ, Hagg T, Hetman M. A positive feedback loop between glycogen synthase kinase 3beta and protein phosphatase 1 after stimulation of NR2B NMDA receptors in forebrain neurons. J Biol Chem. 2005;280(45):37526-35

190. Gu T, Zhang Z, Wang J, Guo J, Shen WH, Yin Y. CREB is a novel nuclear target of PTEN phosphatase. Cancer Res. 2011;71(8):2821-5

191. Tian F, Marini AM, Lipsky RH. NMDA receptor activation induces differential epigenetic modification of Bdnf promoters in hippocampal neurons. Amino Acids. 2010;38(4):1067-74

192. Chen A, Xiong LJ, Tong Y, Mao M. The neuroprotective roles of BDNF in hypoxic ischemic brain injury. Biomed Rep. 2013;1(2):167-76

193. Lau D, Bengtson CP, Buchthal B, Bading H. BDNF Reduces Toxic Extrasynaptic NMDA Receptor Signaling via Synaptic NMDA Receptors and Nuclear-Calcium-Induced Transcription of inhba/Activin A. Cell Rep. 2015;12(8):1353-66

194. Almeida RD, Manadas BJ, Melo CV, Gomes JR, Mendes CS, Grãos MM, et al. Neuroprotection by BDNF against glutamate-induced apoptotic cell death is mediated by ERK and PI3-kinase pathways. Cell Death Differ. 2005;12(10):1329-43

195. Melo CV, Okumoto S, Gomes JR, Baptista MS, Bahr BA, Frommer WB, et al. Spatiotemporal resolution of BDNF neuroprotection against glutamate excitotoxicity in cultured hippocampal neurons. Neuroscience. 2013;237:66-86

196. Tyssowski KM, DeStefino NR, Cho JH, Dunn CJ, Poston RG, Carty CE, et al. Different Neuronal Activity Patterns Induce Different Gene Expression Programs. Neuron. 2018;98(3):530-46.e11

197. Marini AM, Paul SM. N-methyl-D-aspartate receptor-mediated neuroprotection in cerebellar granule cells requires new RNA and protein synthesis. Proc Natl Acad Sci U S A. 1992;89(14):6555-9

198. Zhang SJ, Steijaert MN, Lau D, Schütz G, Delucinge-Vivier C, Descombes P, et al. Decoding NMDA receptor signaling: identification of genomic programs specifying neuronal survival and death. Neuron. 2007;53(4):549-62

199. Hoyte L, Barber PA, Buchan AM, Hill MD. The rise and fall of NMDA antagonists for ischemic stroke. Curr Mol Med. 2004;4(2):131-6

200. Green AR. Why do neuroprotective drugs that are so promising in animals fail in the clinic? An industry perspective. Clin Exp Pharmacol Physiol. 2002;29(11):1030-4

201. Miller DJ, Bhaduri A, Sestan N, Kriegstein A. Shared and derived features of cellular diversity in the human cerebral cortex. Current Opinion in Neurobiology. 2019;56:117-24

202. Bayés A, Collins MO, Croning MD, van de Lagemaat LN, Choudhary JS, Grant SG. Comparative study of human and mouse postsynaptic proteomes finds high compositional conservation and abundance differences for key synaptic proteins. PLoS One. 2012;7(10):e46683

203. Zhang Y, Sloan Steven A, Clarke Laura E, Caneda C, Plaza Colton A, Blumenthal Paul D, et al. Purification and Characterization of Progenitor and Mature Human Astrocytes Reveals Transcriptional and Functional Differences with Mouse. Neuron. 2016;89(1):37-53

204. Hardingham GE, Pruunsild P, Greenberg ME, Bading H. Lineage divergence of activity-driven transcription and evolution of cognitive ability. Nat Rev Neurosci. 2018;19(1):9-15

205. Hodge RD, Bakken TE, Miller JA, Smith KA, Barkan ER, Graybuck LT, et al. Conserved cell types with divergent features in human versus mouse cortex. Nature. 2019;573(7772):61-8

206. McBurney RN. Chapter 8 Development of the NMDA Ion-Channel Blocker, Aptiganel Hydrochloride, as a Neuroprotective Agent for Acute CNS Injury. In: Green AR, Cross AJ, editors. International Review of Neurobiology. 40: Academic Press; 1996. p. 173-95.

207. Pérez-Pinzón MA, Steinberg GK. CGS 19755 (Selfotel): A Novel Neuroprotective Agent Against CNS Injury. CNS Drug Rev. 1996;2(3):257-68

208. Tranquillini ME, Reggiani A. Glycine-site antagonists and stroke. Expert Opin Investig Drugs. 1999;8(11):1837-48

209. Albers GW, Goldstein LB, Hall D, Lesko LM. Aptiganel hydrochloride in acute ischemic stroke: a randomized controlled trial. Jama. 2001;286(21):2673-82

210. Bains M, Cebak JE, Gilmer LK, Barnes CC, Thompson SN, Geddes JW, et al. Pharmacological analysis of the cortical neuronal cytoskeletal protective efficacy of the calpain inhibitor SNJ-1945 in a mouse traumatic brain injury model. J Neurochem. 2013;125(1):125-32

211. Pei L, Shang Y, Jin H, Wang S, Wei N, Yan H, et al. DAPK1-p53 interaction converges necrotic and apoptotic pathways of ischemic neuronal death. J Neurosci. 2014;34(19):6546-56

212. Horschitz S, Matthäus F, Groß A, Rosner J, Galach M, Greffrath W, et al. Impact of preconditioning with retinoic acid during early development on morphological and functional

characteristics of human induced pluripotent stem cell-derived neurons. Stem Cell Res. 2015;15(1):30-41

213. Schrenk-Siemens K, Wende H, Prato V, Song K, Rostock C, Loewer A, et al. PIEZO2 is required for mechanotransduction in human stem cell–derived touch receptors. Nature Neuroscience. 2015;18(1):10-6

214. Krishnaswami SR, Grindberg RV, Novotny M, Venepally P, Lacar B, Bhutani K, et al. Using single nuclei for RNA-seq to capture the transcriptome of postmortem neurons. Nat Protoc. 2016;11(3):499-524

215. Stuart T, Butler A, Hoffman P, Hafemeister C, Papalexi E, Mauck WM, 3rd, et al. Comprehensive Integration of Single-Cell Data. Cell. 2019;177(7):1888-902.e21

216. Hafemeister C, Satija R. Normalization and variance stabilization of single-cell RNA-seq data using regularized negative binomial regression. Genome Biol. 2019;20(1):296

217. Durinck S, Spellman PT, Birney E, Huber W. Mapping identifiers for the integration of genomic datasets with the R/Bioconductor package biomaRt. Nat Protoc. 2009;4(8):1184-91

218. Ahlgren H, Bas-Orth C, Freitag HE, Hellwig A, Ottersen OP, Bading H. The nuclear calcium signaling target, activating transcription factor 3 (ATF3), protects against dendrotoxicity and facilitates the recovery of synaptic transmission after an excitotoxic insult. J Biol Chem. 2014;289(14):9970-82

219. Khatri P, Obernier K, Simeonova IK, Hellwig A, Hölzl-Wenig G, Mandl C, et al. Proliferation and cilia dynamics in neural stem cells prospectively isolated from the SEZ. Scientific Reports. 2014;4(1):3803